# Topology and interactions in Weyl metals and quantum Hall systems

by

Ivan Panfilov

A thesis
presented to the University of Waterloo
in fulfillment of the
thesis requirement for the degree of
Doctor of Philosophy
in
Physics

Waterloo, Ontario, Canada, 2017

Examining Committee Membership

The following served on the Examining Committee for this thesis. The decision of the Examining Committee is by majority vote.

| | |
|---|---|
| **External Examiner** | **Professor Arun Paramekanti** |
| **Supervisor** | **Professor Anton Burkov** |
| **Internal Member** | **Professor David Hawthorn** |
| **Internal Member** | **Professor Roger Melko** |
| **Internal-external Member** | **Professor Pierre-Nicholas Roy** |

This thesis consists of material all of which I authored or co-authored: see Statement of Contributions included in the thesis. This is a true copy of the thesis, including any required final revisions, as accepted by my examiners.

I understand that my thesis may be made electronically available to the public.

## Statement of Contributions

This thesis is based on the results of research which were published in two papers (Refs. [1], [2]). In both these papers I'm the first author. The content of the two papers is presented in the Chapters 5 and 6 respectively. I performed majority of the research presented in the papers. The content of the papers is presented in the corresponding chapters in its published form. The content of the articles is mainly presented as it appears in the publications. The minor alterations were added to enhance the structure of the thesis. All other chapters were written solely by myself.

**Abstract**

In recent years it became clear that in the Condensed Matter physics, the study of the interactions and the topology allows one to find and to describe many new phases of matter. Even more interest was drawn by the systems, where the topology is nontrivial and the interactions are not negligible, such as fractional quantum Hall effect. Therefore, in this thesis we study two examples of the interacting systems that have non-trivial topological properties.

First, we consider the Weyl metals - a class of material that were suggested theoretically few years ago and observed on experiments first time in 2015. We study the behavior of the theoretical model of Weyl metal in the presence of an external magnetic field. Using the random field approximation, we show that the applied field gives the correction to the density response, that is topological in nature and is closely related to the phenomenon of chiral anomaly. This contribution manifests in a nonanalytic nonclassical corrections to the electronic compressibility and the plasmon frequency, proportional to the magnitude of the magnetic field. Such a nonanalytic correction to the electronic compressibility clearly distinguishes Weyl metals from ordinary ferromagnetic metals and hence can be used to identify the Weyl metals.

Next, we study the connection between the bosonic quantum Hall systems and the lattice models. We present a mapping of a two-dimensional system of interacting bosons in a strong perpendicular magnetic field to an equivalent system of interacting bosons on the square lattice in the absence of the field. This mapping utilizes a magnetic Bloch and the corresponding magnetic Wannier single particle bases in the lowest Landau level. We demonstrate that, by construction, the ground states of the resulting model of interacting bosons on the square lattice are gapped fractionalized liquids or gapless Bose metal states with broken time reversal symmetry at specific rational filling fractions.

**Acknowledgements**

First of all, I would like to express my deepest gratitude to my supervisor Professor Anton Burkov for guiding my trough the program and also for spending a lot of time teaching me.

I would also like to thank Professor David Hawthorn, Professor Roger Melko and Professor Pierre-Nicholas Roy for contributing their time to serve in the committee and for providing valuable feedback on my progress in the research.

Finally, I would like to appreciate my family and all my friends who supported me on this journey.

# Table of Contents

# List of Figures

## List of Abbreviations

QHE - quantum Hall effect

- IQHE - integer quantum Hall effect
- FQHE - fractional quantum Hall effect
- 2DEG - two-dimensional electron gas
- BZ - Brillouin zone
- NN - nearest neighbor
- NNN - next nearest neighbor
- TI - topological insulator
- NI - normal insulator
- ARPES - angle-resolved photoemission spectroscopy
- LLL - lowest Landau level
- GMP - Girvin-MacDonald-Platzman

# Chapter 1

# Introduction

In mathematics, topology is a branch that studies the properties of objects, which do not change under the small deformations. The simplest example of such property is the "number of holes", or the "genus" of a closed surface. The two simplest objects that have different genus are the sphere and the torus, Fig. 1.1. It is intuitively clear that no deformation of the sphere can make it into the torus, as long as deformation does not include tearing the surface and gluing it back together.

In recent years in condensed matter physics it became clear that there are some properties of the materials that, as the genus of surfaces, can only take some specific values and hence do not change with the small alterations of the sample. Such properties are called topological. Since such properties were observed in a number of materials, topology became an important tool for distinguishing different phases of matter in physics. At the same time, it is known that interactions between the elementary pieces of material are often crucially important for describing the material. Hence, our goal in this thesis is to study the interplay between the topology and the interactions in various condensed matter systems.

The rest of the thesis is ordered as follows. The original results are presented in the chapters 5 and 6. As it was explained on the page iv, each of these chapters is structured as standalone

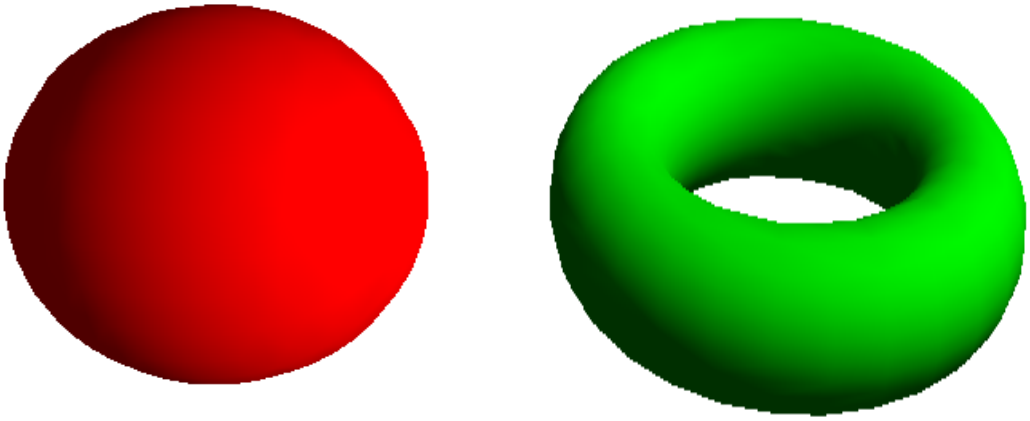

(a) *Genus* = 0 (b) *Genus* = 1

Figure 1.1: Genus of the surfaces

publication and hence can be viewed separately from the rest of the text. However, the place of these result in the bigger picture might be unclear if chapters read separately. Hence we start by providing the wider perspective on the field of condensed matter theory in this chapter. In order to introduce the models and the methods we used, we review the quantum Hall effect in chapter 2, the Haldane model of graphene in chapter 3 and the multilayer model of Weyl semimetal in chapter 4.

## 1.1 Historical overview

With the naked eye observation scientists first distinguished only three phases of matter: solid, liquid and gaseous. Since these three phases had most of their properties very different from each other, they all where studied separately. While the qualitatively accurate theoretical description of gases was built before the beginning of twentieth century, the study of the two other phases showed many subtleties. The properties of various materials in the same phase

were drastically different. This led to division of the initial phases (which where later named fundamental phases in order to avoid confusion) into more separate phases of matter. First such separation appeared with the division of the materials into conductors and insulators depending on their ability to conduct electric current. Then the study of magnetic properties led to the identification of ferromagnets as a phase. Soon after that it became clear that the more properties of the materials are studied, the more separations into different phases will occur. At the same time not all the properties of different phases where significantly different. As example, ferromagnetic conductors behaved alike other conductors in the case of time-independent current. This led to understanding that different phases of matter have to be studied together. A new branch of physics, encompassing all the phases of matter that can not be described by theory of gases, was formed. This branch was named Condensed Matter Physics. Hence the main objectives of the Condensed Matter are to discover new phases of matter, to describe them and to find the connections between the different phases.

All of the goals of Condensed Matter require large contributions from both the experimental and the theoretical sides, but since this thesis is a part of theoretical research, we will focus now on the history of the Condensed Matter theory.

Most of the challenges on Condensed Matter theory arise from a single origin - the fact that each macroscopic system consists of immense amount similar microscopic blocks (which can be elementary particles, atom, molecules, etc.). Their number is so big that even if one knows exactly the laws that govern the behavior of a single block and the laws of interaction between the blocks, it is practically impossible to resolve the systems of so many equations, with the exception of very few special cases.

However, the development of thermodynamics and its success in description of most of the properties of the gases showed a way to describe the many body systems. This way begun with the introduction of macroscopic parameters of the system, such as temperature, pressure, density, etc. These parameters are functions of all the microscopic parameters and hence their values can be found by solving the system of all the microscopic equations, if it can be done. But

the most important part was the formulation of laws of thermodynamics, which include only the macroscopic parameters. Then, solving only the equations that connect the macroscopic parameters one could derive the properties of the system without finding all the microscopic parameters. Naturally, the number of properties that can be captured such description is limited by number of introduced parameters.

The description of many body systems by introducing fewer parameters than system really has and finding the closed set of laws that includes only new parameters was later named the "Effective model". Such name came from the fact that main criteria for choosing the artificial parameters is how effectively they will capture the properties of the system.

Naturally, the number of properties that can be described by effective model is limited by number of parameters in it. But at the same time, with each new parameter effective model gets harder to solve, eventually becoming as unsolvable as original system. Hence, the main challenge of creating the effective models is introducing enough parameters to the model to capture the important properties, while keeping their number small enough for model to be practically solvable.

The first effective model that can be considered the part of Condensed Matter theory was the Drude model of metal [3]. This model suggested that certain amount of electrons can leave their atom in metal. These electrons then could move without interacting with each other and only interacting with atoms through the elastic collisions. The atoms were considered to be solidly fixed in the material. Then the effective parameters - density of electrons $n$ and average time one electron travels between collision $\tau$ were introduced. This way the problem of many electrons moving in the material with the applied external electromagnetic field was simplified to the problem of one electron moving in the external field and being scattered to the random direction every $\tau$ seconds. Despite the fact that this model completely neglected all the motion of atoms and their bound electron, neglected all the interactions between electrons and maximally simplified interaction of electrons with atoms, the Drude model was able to describe not only the currents appearing in the constant external field (Ohm's law), but also the current

in metal in the time-dependent external field.

The first condensed matter theory, that described the two different phases of matter and the transition between them was the Landau theory of phase transitions. This theory assumes that free energy of the system, besides thermodynamic parameters like temperature and pressure, depends also on one more parameter. Such parameter was named "order parameter". This parameter was not fixed by the external factors and hence, for the system in the thermodynamic equilibrium, the order parameter would take the value that minimizes the free energy. The key idea of Landau theory was that dependence of free energy on order parameter has to respect all the symmetries the system possesses. For example, if system is translation invariant, then order parameter should not depend on coordinate, if system, like Ising model, possesses the internal $Z_2$ symmetry, then the Free energy should only contain even powers of order parameter. Then, if a temperature $T_C$ exists such that, the value of order parameter that minimizes the free energy is zero when $T < T_C$ and in non-zero when $T > T_C$, the system would experience the phase transition at $T = T_C$. Landau theory allowed to find the the behavior of the system parameters around the point of phase transition $T = T_C$. While the exact predictions of the Landau theory did not match the experimental observations (it was later shown that Landau theory is strictly valid only for systems with more than four dimensions), the main achievement of the Landau theory was the demonstration that very different systems, if they have same symmetries, would exhibit same behavior around the phase transition.

Landau theory was later developed in few other phenomenological theories such as the Ginsburg-Landau theory of superconductivity and the Fermi liquid theory. The theories allowed to describe many phase transition and classify many phases of matter based on their symmetries. But all these theories needed the knowledge of material's symmetries obtained from experiment in order to describe the behavior of systems around phase transitions. The phenomenological theories could not explain why the symmetry was changing. For example, Landau theory described the paramagnetic-ferromagnetic phase transition with the magnetization being the order parameter, but it could not explain, how non-zero magnetization can be the equilibrium

state. The Ginsburg-Landau theory did not explain why superconducting part of electric current existed.

## 1.2 Interactions and topology

With development of quantum mechanics the microscopic theories were developed for many phases of matter and it became clear that some of the macroscopic properties of materials have purely quantum origins. The examples we used before can only be explained when one takes into account the quantum nature of interactions between the electrons: the existence of the ferromagnets was explained by the Pauli exclusion principle and the origin of superconductivity, found by Bardeen, Cooper and Schrieffer, was in the formation of the electron pairs.

With the discovery of integer quantum Hall (QHE) effect by Klitzing [4] and the theoretical explanation of it by Laughlin [5] the concept of topology was brought into condensed matter physics. As in mathematics topological properties of the object are those that can not be changed by continuous deformations, the topological properties in physics are those that can not be changed by any small (local) changes in the system. While it seems intuitively clear from their name that topological properties can be very useful for the distinguishing different phases of matter, it was not known, before the QHE theory,that physical material possess any. After that a whole new class of materials with the topological properties, the topological insulators, was suggested theoretically [6] and later found in experiments [7].

In recent years it became clear that the study of the interactions and the topology allows us to find and to describe many new phases of matter. Even more interest was drawn by the systems, where the topology is nontrivial and the interactions are not negligible, such as fractional quantum Hall effect. Therefore, in this thesis we study two examples of the interacting systems that have non-trivial topological properties.

First, we consider the Weyl metals - a class of material that were suggested theoretically few years ago [8, 9, 10, 11] and observed on experiments recently [12, 13, 14]. We study the

behavior of the theoretical model of Weyl metal in the presence of the external magnetic field [2]. Using the random field approximation, we show that the applied field gives the correction to the density response, that is topological in nature and is closely related to the phenomenon of chiral anomaly. This contribution manifests in a nonanalytic nonclassical corrections to the electronic compressibility and the plasmon frequency, proportional to the magnitude of the magnetic field. Such a nonanalytic correction to the electronic compressibility clearly distinguishes Weyl metals from ordinary ferromagnetic metals and hence can be used to identify the Weyl metals.

Next, we study the connection between the bosonic quantum Hall systems and the lattice models [1]. We present a mapping of a two-dimensional system of interacting bosons in a strong perpendicular magnetic field to an equivalent system of interacting bosons on the square lattice in the absence of the field. This mapping utilizes a magnetic Bloch and the corresponding magnetic Wannier single particle basis in the lowest Landau level. By construction, the ground states of the resulting model of interacting bosons on the square lattice are gapped fractionalized liquids or gapless Bose metal states with broken time reversal symmetry at specific rational filling fractions.

The rest of the thesis is organized as follows. In chapter 2 we review the phenomena and the theory of quantum Hall effect as the first known example of the topological material. In chapter 3 we review Haldane model of the Graphene, as a 2D predecessor of Weyl metals. In chapter 4 we review the main properties of Weyl metals on the example multilayer model. In chapter 5 we use the model of Weyl metal introduced in chapter 4 and study its properties in the presence of the magnetic field. In chapter 6 we construct the mapping between the quantum Hall systems and the lattice models. In chapter 7 we conclude with brief summary of our results.

# Chapter 2

# Quantum Hall Effect

In this chapter we will review the basic properties of topological insulator on the example of Quantum Hall effect.

## 2.1 Quantum Hall Effect phenomena

Classical Hall effect predicts that in the presence of magnetic field in the sample, applied electric field will cause the current perpendicular to the electric field. Without magnetic field, current is flowing in the direction of the applied electric field and is proportional to the strength of the field

$$\sigma\vec{E} = \vec{J}, \tag{2.1}$$

where $\vec{E}$ is electric field, J is the density of electric current and $\sigma$ is the conductivity.

But if strong perpendicular magnetic field is added, the Lorentz force causes electrons to turn and does not let them travel across the sample in the direction of electric field. Instead of that electrons start drifting in the direction perpendicular to both fields. This current is described by modifying equation (2.1) to the form

$$\hat{\sigma}\vec{E} = \vec{J}, \tag{2.2}$$

where $\sigma$ now is a tensor and hence its off-diagonal terms connect components of electric field with different components of current density.

In the classical case, for the magnetic field B pointing in z direction, we have

$$\sigma_{xx} = \sigma_{yy} = \sigma_D, \qquad \sigma_{xy} = -\sigma_{yx} = \frac{en}{B}, \tag{2.3}$$

where $e$ is the charge of electron and n is the density of electrons. $\sigma_D = \frac{ne^2\tau}{m}$ is the Drude conductivity, defined by the density of free electrons $n$ and average time between collisions of one electron with the ion lattice $\tau$.

It was discovered by Klitzing [4], that at low temperature, in clean samples, conductivity as function of magnetic field, behaves very differently. Namely, the off-diagonal conductivity $\sigma_{xy}$, instead of hyperbolic dependence, shows series of plateaus, with constant value within each plateau. At the same time the diagonal conductivity $\sigma_{xx}$ is zero for values of B corresponding to the plateaus of $\sigma_{xy}$ and is not zero between them. Such behavior could not be explained by classical theory and hence it was named quantum Hall effect.

The most outstanding part in quantum Hall effect observation was the fact that at the plateaus, the off-diagonal conductivity shows same values for different samples with up to nine digits precision. This was unseen before in condensed matter physics due to the fact that it is impossible to fabricate edges of samples with such precision as well as it is impossible to get rid of all impurities in the macroscopic size samples. At the plateaus

$$\sigma_{xy} = \nu\frac{e^2}{h} \tag{2.4}$$

was observed, where h is the Plank constant and $\nu$ is the filling factor of Landau levels, defined by magnetic field and density of electrons. Quantum Hall effect was initially observed at integer values of $\nu$ (later named integer quantum Hall effect, IQHE), later QHE was also observed for certain non-integer, but rational values (referred as fractional quantum Hall effect, FQHE)[15]. Plot of Hall resistance versus the magnetic field is shown on Fig. 2.1. Note that since conductivity and resistance are two by two matrices, if $\sigma_{xx} = \sigma_{yy} = 0$ , then $\rho_{xx} = \rho_{yy} = 0$ and $\rho_{xy} \propto \frac{1}{\sigma_{xy}}$.

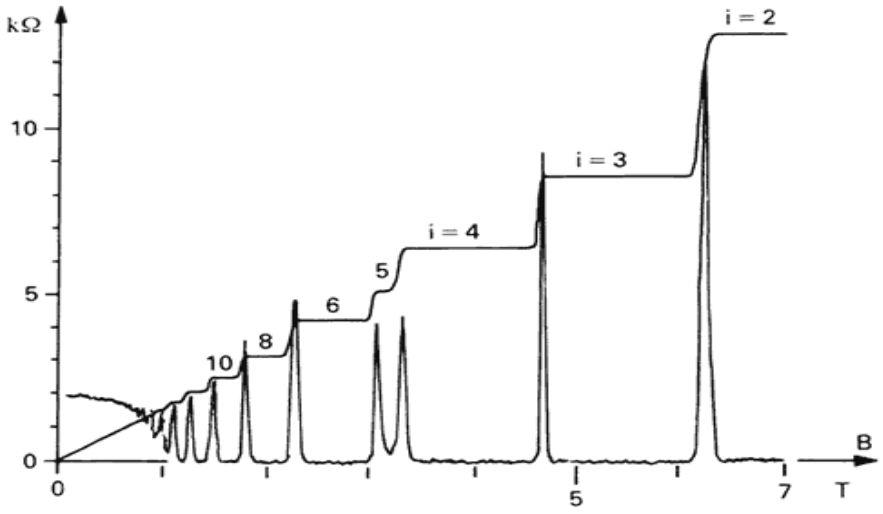


Figure 2.1: Integer Quantum Hall effect. Hall resistance (line starting at zero) and standard resistance (line starting at non-zero) as functions of the magnetic field (Kosmos 1986)

Such precision of the value of conductivity and independence on the sample led to the definition of a new type of materials - Topological Insulators. In mathematics topology studies properties of geometric objects that do not change under small deformations and we will see below how it can be defining some properties of materials in condensed mater physics.

Since our goal in this chapter is only to review the main properties of the material in the quantum Hall state, in the following sections of this chapter we will focus on the simpler case - the IQHE. We will only review the theory of non-interacting electrons. This theory can describe the integer quantum Hall effect, but predicts the complete absence of the FQHE.

## 2.2 Two dimensional electron gas in magnetic field

We can first consider one particle in the magnetic field. For non-charged particle, the Schrödinger equation takes form

$$i\partial_t\psi(x,y,t) = \frac{1}{2m}[(-i\hbar\partial_x)^2 + (-i\hbar\partial_y)^2]\psi(x,y,t). \tag{2.5}$$

For the particle with the charge $-e$, we have to add interaction with electric and magnetic field. This can be done by changing spatial derivatives $-i\partial_j$ to $-i\partial_j + \frac{e}{c}A_j$, where $\vec{A}$ is the vector potential and $i\partial_t$ to $i\partial_t - \frac{e}{c}\Phi$, where $\Phi$ is the scalar electromagnetic potential.

$$(i\partial_t - \frac{e}{c}\Phi)\psi(x,y,t) = \frac{1}{2m}[(-i\hbar\partial_x + \frac{e}{c}A_x)^2 + (-i\hbar\partial_y + \frac{e}{c}A_y)^2]\psi(x,y,t). \tag{2.6}$$

We want to consider electron in constant magnetic field along z direction, without any electric field, but this does not fix $\Phi$ and $A$ uniquely. Hence we have to put some extra restrictions on them. As we know from electrodynamics, they are not an observables, hence we can choose any combination, that gives us desired values of E and B. Obviously, simplest choice for the potential is to put it equal to zero everywhere. For the vector potential there are two useful choices:

$$A_x = 0 \; and \; A_y = Bx \tag{2.7}$$

,

$$A_x = -\frac{B}{2}y \; and \; A_y = \frac{B}{2}x \tag{2.8}$$

called Landau gauge and symmetric gauge respectively. For there rest of this chapter we will use the Landau gauge Eq.(2.7), but in chapter 6 we will need the symmetric gauge as well.

Now we can find the eigenstates of stationary Schrödinger equation. In the Landau gauge, Hamiltonian does not depend explicitly on y coordinate, hence momentum in y direction is conserved and we can write wavefunctions as

$$\psi(x,y) = exp(-ik_y y)f(x). \tag{2.9}$$

Substituting Eq. 2.9 into the Schrödinger equation 2.6 we find that $f(x)$ are the Hermit polynomials an their corresponding energies are

$$\epsilon_{n,k_y} = (n + \frac{1}{2})\frac{eB\hbar}{cm}. \tag{2.10}$$

Hence, we get the set of different energies, distinguished by quantum number n and independent on momentum in y direction. These separate values of energy are called Landau levels. Since our Hamiltonian contained explicit dependence on x, momentum in x direction will not be conserved and $k_x$ can not be used to label eigenstates of Hamiltonian. The Landau levels plot of energy versus momentum can be compared to the energy bands in solids. In this case all bands are simply flat. It is well known, that if the picture of the energy bands has states with energy equal to the Fermi energy $E_F$, then material is a metal, otherwise it is an insulator. For the Landau levels picture, if $E_F$ is between the two levels, then all levels under it will be completely filled and levels above will be completely empty. This will be an insulating quantum Hall state. If $E_F$ matches the energy of one of the levels, this level will be partially filled and the state will be metallic.

Now we can look back to Fig. 2.1. As we change magnetic field, the energy of the levels changes and they one by one cross the value of $E_F$ and our system becomes an insulator, then a metal, then another insulator and another metal and so on.

## 2.3 Berry connection and Berry curvature

We saw in previous section, that as perpendicular magnetic field changes, 2DEG forms series of insulators with different measurable properties (ex.: off-diagonal conductivity). And we saw that these insulators can not directly change one into another, between each pair of insulating states system passes through metallic state. In this section we will see why these insulating states have to be separated.

It is one of the basic principles of quantum mechanics that the phase of the wavefunction

can not be measured. Hence, if one adds constant $\phi$ to the phase off all eigenfunctions of Hamiltonian, these will still be the eigenfunctions. However, if one adds phase that depends on coordinate $\phi(x, y)$, obtained wavefunctions will not be eigenfunctions of Hamiltonian, because Hamiltonian is a differential operator and coordinate-dependent phase shift adds extra term to the derivatives. But this set of functions will still be describing same physical system and to show that we need to adjust the potentials $\Phi$ and $\vec{A}$, which are also not observable, accordingly to $\phi$:

$$\psi(r,t) \to \psi'(r,t) = \psi(r,t)exp(i\phi(r,t)), \tag{2.11}$$

$$\Phi \to \Phi' = \Phi - \frac{\hbar}{e}\partial_t\phi(r,t), \tag{2.12}$$

$$\vec{A} \to \vec{A'} = \vec{A} + \frac{c\hbar}{e}\vec{\nabla}\phi(r,t). \tag{2.13}$$

With such change of potentials, both the wave functions and the Hamiltonian change, but all the measurable variables remain the same, hence these wavefunctions and Hamiltonian describe the same system as the initial Hamiltonian did.

Similarly to this, if we want to change phase of different eigenfunctions of Hamiltonian depending on their momentum $k$ rather than coordinate, we would have to introduce the "momentum space analog" $\vec{\mathcal{A}}$ of the potential $\vec{A}$. Such an object is called Berry connection and is defined as

$$\vec{\mathcal{A}}(k) = -i\langle u_k|\vec{\nabla}_k|u_k\rangle, \tag{2.14}$$

where functions $u_k$ are called Bloch functions. They are defined as

$$u_k(r) = \psi_k(r)exp(-ikr). \tag{2.15}$$

Then, under the momentum-dependent phase transformation we get:

$$|u_k\rangle \to exp(i\phi(k))|u_k\rangle, \tag{2.16}$$

$$\vec{\mathcal{A}} \to \vec{\mathcal{A}}' = \vec{\mathcal{A}} + \vec{\nabla}_k \phi(k). \tag{2.17}$$

Knowing that the curl of vector potential in the real space is an observable quantity - magnetic field, we can define the curl of Berry connection - Berry curvature:

$$\vec{\Omega} = \vec{\nabla} \times \vec{\mathcal{A}}. \tag{2.18}$$

In order to understand how Berry connection and Berry curvature affect the properties of material, we can use the fact that the coordinate space (real space) representation and the momentum space representation can be used to solve Quantum Mechanics problems on equal terms.

In the real space, in the presence of electric and magnetic fields, we have equations of motion (Newtons law):

$$\frac{d\vec{p}}{dt} = e\vec{E} + \frac{e}{c}\vec{v} \times \vec{B} = -e\vec{\nabla}_r \Phi(r) + \frac{e}{c}\frac{d\vec{r}}{dt} \times (\vec{\nabla}_r \times \vec{A}(r)). \tag{2.19}$$

Here we consider only time-independent electromagnetic potential and hence omit all the terms with time derivatives of it.

Then, in the momentum space representation, we can include Berry connection in the same way:

$$\frac{d\vec{r}}{dt} = \vec{\nabla}_p \epsilon(p) + \hbar \frac{d\vec{p}}{dt} \times (\vec{\nabla}_p \times \vec{\mathcal{A}}(p)). \tag{2.20}$$

Now, we can find the transverse conductivity in Quantum Hall effect following the Haldane [16].

Substituting Eq. (2.19) into Eq. (2.20) and switching all $p$ into $\hbar k$ we obtain:

$$\frac{d\vec{r}}{dt} = \frac{1}{\hbar}(\vec{\nabla}_k \epsilon(k) + (\vec{E} + e\vec{v} \times \vec{B}) \times (\vec{\nabla}_k \times \vec{\mathcal{A}}(k)). \tag{2.21}$$

Since we are considering motion in x-y plane, we can rewrite $\vec{\nabla}_k \times \vec{\mathcal{A}}(k) = \Omega(k)\vec{e}_z$, where $\vec{e}_z$ is the unit vector in z direction.

When all particles move with the same velocity, density of current can be written as $j = env = \frac{eNv}{A}$, but since all states have different velocities, we have to sum over all occupied states:

$$j = \frac{e}{A}\sum_{n,k} v_{n,k}, \tag{2.22}$$

where n is the band index and k is the wave vector.

By putting it all together we obtain:

$$j = \frac{e}{A\hbar}\sum_{n,k}(\vec{\nabla}_k\epsilon(k) + (\vec{E}\times\vec{e}_z + e\vec{v}\times\vec{B}\times\vec{e}_z)\Omega(k)) \tag{2.23}$$

The only term that will contribute to the Hall effect is $\vec{E}\times e_z$, because it's the only term perpendicular to the electric field. Hence we can write

$$j_H = \frac{e}{A\hbar}\sum_{n,k} e\vec{E}\times\vec{e}_z\Omega_n(k). \tag{2.24}$$

For each n we can rewrite sum over k as integral over Fermi sea.

$$\frac{1}{A}\sum_k \Omega(k) = \int_{FS}\frac{d^2k}{(2\pi)^2}\Omega(k). \tag{2.25}$$

In general, if integration on the right hand side of Eq. 2.25 is performed over area without boundaries, it will give us an integer value known as Chern number, divided by $2\pi$. In this case, when it is performed over the whole Brillouin zone, it will give us 1. Hence, when the system is in insulating state and we have n completely filled levels with no electrons on higher levels, we get

$$\sigma_{xy} = \frac{j_H}{E} = \frac{e^2}{2\pi\hbar}n = \frac{e^2}{h}n, \tag{2.26}$$

while for metallic states we will have one incompletely filled level and hence conductivity value will be in between two plateaus.

It is important to note, that since Berry curvature $\vec{\Omega}$ is the curl of Berry connection $\vec{\mathcal{A}}$, integral of flux of $\vec{\Omega}$ through some surface can be written as the circulation of $\vec{\mathcal{A}}$ around the

boundary of the surface. In our case, we look at integral over whole Brillouin zone, which has no boundary and that suggests that circulation should be zero. We can argue, that integral of Berry curvature over whole BZ should be zero by drawing a circle "C" in BZ and considering flux through inside and outside:

$$\begin{aligned}\int_{BZ} \frac{d^2k}{(2\pi)^2}\Omega(k) &= \int_{inside\, C} \frac{d^2k}{(2\pi)^2}\Omega(k) + \int_{outside\, C} \frac{d^2k}{(2\pi)^2}\Omega(k) \\ &= \int_{C_{in}} \frac{\vec{\mathcal{A}}\cdot d\vec{k}}{(2\pi)^2} + \int_{C_{out}} \frac{\vec{\mathcal{A}}\cdot d\vec{k}}{(2\pi)^2}.\end{aligned} \tag{2.27}$$

When we go around the circle "clockwise", looking from inside the circle and when we go "clockwise" looking from outside, we go in opposite directions, hence

$$\int_{BZ} \frac{d^2k}{(2\pi)^2}\Omega(k) = \int_{C_{in}} \frac{\vec{\mathcal{A}}\cdot d\vec{k}}{(2\pi)^2} - \int_{C_{in}} \frac{\vec{\mathcal{A}}\cdot d\vec{k}}{(2\pi)^2}. \tag{2.28}$$

And so it seems that Integral is equal to zero and so Hall conductivity would be zero. But, if we do the calculation explicitly for the quantum Hall effect, we obtain non-zero result, then if we look at $\vec{\mathcal{A}}(\vec{k})$, we will see that it has singularity in the BZ. Position of the singularity changes with gauge transformation, hence this singularity itself is not a physical effect, but an artifact of the gauge choice. This means, that for a part of BZ we can find a gauge, in which Berry connection is regular withing the region, but we cannot do so for whole BZ. And in the example with the circle dividing BZ into two regions, we have to use different gauge choices for them. Then

$$\int_{BZ} \frac{d^2k}{(2\pi)^2}\Omega(k) = \int_{C_{in}} \frac{\vec{\mathcal{A}}_1\cdot d\vec{k}}{(2\pi)^2} - \int_{C_{in}} \frac{\vec{\mathcal{A}}_2\cdot d\vec{k}}{(2\pi)^2} \neq 0. \tag{2.29}$$

Reversing the argument, we can say that in order to have the non-trivial Hall conductivity, $\vec{\mathcal{A}}$ has to have some singularity in every gauge.

## 2.4 Edge States

So far we considered translation-invariant system. This implied that our two-dimensional model did not have boundaries. Since it is hard to solve exactly the quantum mechanical problem of electrons in magnetic field on the sample with the boundaries, we will use the semi-classical approach.

In the classical mechanics, electron in magnetic field experiences the Lorentz force, always perpendicular to the direction of motion:

$$\vec{F} = \frac{q}{c}\vec{v} \times \vec{B}. \tag{2.30}$$

In the case of two-dimensional sample in perpendicular magnetic field, all the electrons in the bulk of sample will move in circles, hence

$$a_c = \omega_c^2 r = \frac{F}{m} = \frac{q}{c} vB = \frac{q}{c}\omega_c r B \tag{2.31}$$

and from that we see that angular frequency will be same for all electrons:

$$\omega_C = \frac{qB}{mc}. \tag{2.32}$$

In classical case electrons that are moving in circles with angular frequency $\omega_c$ can have any radius of orbit and hence any energy. But, in quantum mechanics, when we have only one frequency, we expect that energy can only change by increments of $\hbar\omega_c$. This perfectly matches the difference of energy between to consequent Landau levels Eq. 2.10.

In order to study the behavior of electrons near the edge of the sample, we need to clarify, how the edge is made. Most common setup of 2D electron gas in experiments is the surface between two semiconductors( GaAs and AlGaAs for example). Then, in order to limit the electron gas on this 2D surface to some particular area, one adds the negatively charged electrodes around the area. Their potential repels the electrons, not allowing them to leave the area. This means electrodes create the electric field near the edge of 2D electron gas, acting in the plane of 2DEG, perpendicular to the edge.

Continuing the semi-classical consideration, we now see that electrons near the edge move in crossed electric and magnetic fields:

$$m\frac{d\vec{v}}{dt} = \vec{F} = q\vec{E} + \frac{q}{c}\vec{v} \times \vec{B}. \tag{2.33}$$

By the change of reference frame

$$\vec{v} = \frac{\vec{E} \times \vec{B}}{B^2} + \vec{v'} \tag{2.34}$$

we can obtain the equation of circular motion once again:

$$m\frac{d\vec{v'}}{dt} = \vec{F} = \frac{q}{c}\vec{v'} \times \vec{B}. \tag{2.35}$$

Hence, on average, electrons on the edge are moving with velocity

$$\vec{v}_{EB} = \frac{\vec{E} \times \vec{B}}{B^2}. \tag{2.36}$$

Due to the cross product electrons will be moving along the edge of the sample in one fixed direction. At the same time, on the opposite edge of the sample, the electric field has to be pointing in the opposite direction to keep the electrons in the sample, hence the electrons on the edge are moving in the opposite direction. Due to the fact, that for electrons on the edge there is only one possible direction of motion and the reflection symmetry is absent, these states are called Chiral edge states by the analogy to the high energy physics, where chiral anomaly is the phenomena arising from breaking the reflection symmetry.

When the material is in the insulating state, Fermi energy is in between the two Landau levels. However, the electric potential that creates the boundary raises the energy of the electron states near the edge, effectively curving the Landau levels upwards. This means that each Landau level that is filled in the bulk of the system will reach the Fermi energy as it gets closer to the boundary. Hence, the system in quantum Hall insulating state does not have states on the Fermi surface in the bulk, as a normal insulator. But it does have states on the Fermi surface at the boundary and number of such states matches the number of filled Landau levels in the bulk.

# Chapter 3

# Graphene

In this chapter we review another example of the two-dimensional topological insulator - Graphene. We will start by considering a simple model, proposed by Haldane [17]. This model was proposed in 1988, almost 30 year before the graphene was first obtained in laboratory in 2005 Ref [18]. This model does not capture all the properties of the real graphene, because it does not take into account spin of the electrons, but it captures main properties of the material. The more accurate model of graphene was proposed by Kane-Mele [19, 20]. This model is essentially combination of two Haldane models put together due to the fact that for each state of momentum we have two spin states of electron. Since our goal is to review main features of the graphene we will only consider in this chapter the simpler model, proposed by Haldane.

## 3.1 Haldane Model

Model proposed by Haldane [17] in 1988 was initially a theoretical construction, in which quantized transversal conductivity (or Hall conductivity) could appear in the absence of the strong external magnetic field. Haldane considered the two-dimensional honeycomb lattice Fig.

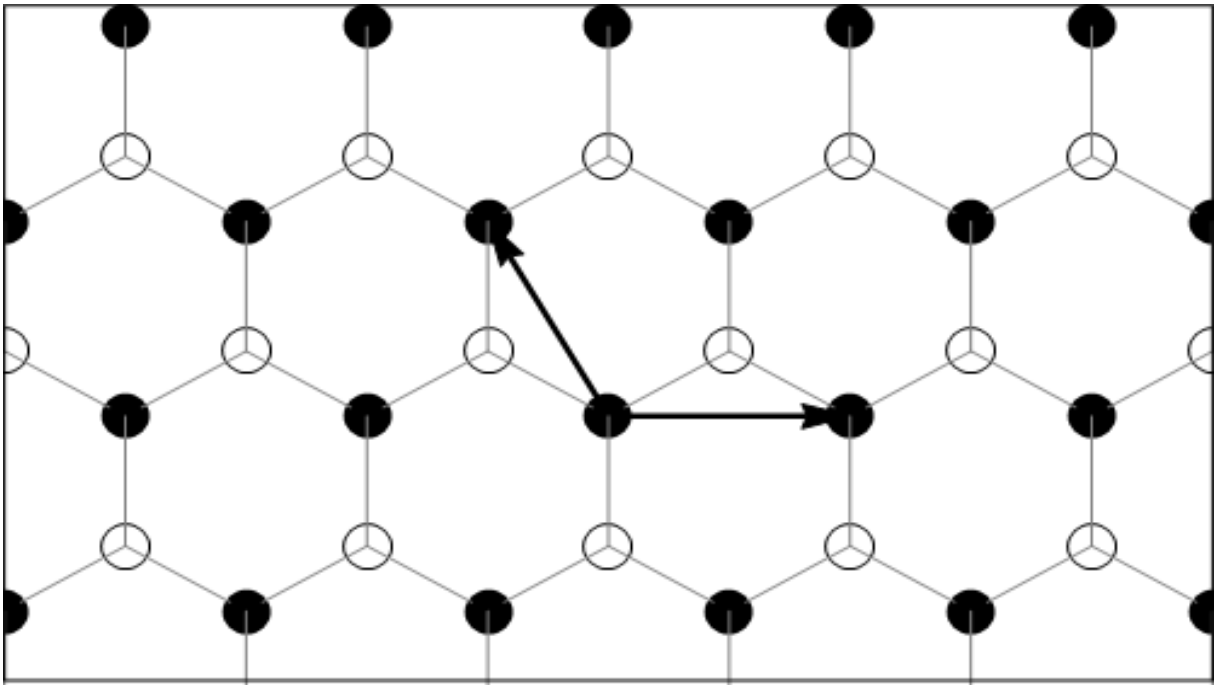

Figure 3.1: Graphene. Honeycomb lattice built of two sublattices A (White) and B (black) with nearest-neighbor bonds shown by thin lines. Two blue arrows show the primitive translation vectors of the lattice.

3.1. Electrons in it are able to hop between the neighboring sites and are interacting with the periodic background potential. In 2005 Novoselov at all [18] obtained such system in the experiment - two dimensional carbon lattice which was named graphene.

As one can see from Fig. 3.1, honeycomb lattice is translation-invariant, but not all the sites can be moved one into another by the translations that leave lattice unchanged. Namely, there are two sublattices "A" and "B" (white and black circles on the figure respectively) such that sites of each lattice only move to other sites of same lattice under arbitrary translation. Hence, in order to use the translation-invariance and switch to momentum representation we have to consider these two sublattices separately. We will use the second quantization notations and name creation operators of electrons on sublattices A and B "$a_i^+$" and "$b_i^+$" respectively.

If we define distance between two nearest neighbor (NN) sites to be a, then the primitive translation vectors of lattice (arrows on Fig. 3.1) will be

$$\vec{v}_1 = (\sqrt{3}a, 0), \tag{3.1}$$

$$\vec{v}_2 = (-\frac{\sqrt{3}}{2}a, \frac{3}{2}a). \tag{3.2}$$

If we consider that electron number does not change, then all the terms in Hamiltonian have to be products of even number of creation and annihilation operators.

## 3.2 Nearest-Neighbor Hamiltonian

We will start from the simplest case, when electrons can only move between the closest sites, then Hamiltonian can be written as

$$H_{NN} = -t \sum_{<i,j>} a_i^+ b_j - t \sum_{<i,j>} b_i^+ a_j. \tag{3.3}$$

Because each site has only the three sites of different sublattice as its nearest neighbors. In this equation t is the hopping amplitude, $< i, j >$ means summation over the nearest neighbors and indexes i and j run over all the sites of lattice.

We can rewrite the nearest neighbor explicitly:

$$H_{NN} = -t \sum_i (a^+_{\vec{r}_i} b_{\vec{r}_i+\vec{e}_1} + a^+_{\vec{r}_i} b_{\vec{r}_i+\vec{e}_2} + a^+_{\vec{r}_i} b_{\vec{r}_i+\vec{e}_3}) + h.c.\ , \tag{3.4}$$

where h.c. means hermitian conjugated terms and

$$\vec{e}_1 = (0, a), \tag{3.5}$$

$$\vec{e}_2 = (-\frac{\sqrt{3}}{2}a, -\frac{a}{2}), \tag{3.6}$$

$$\vec{e}_3 = (\frac{\sqrt{3}}{2}a, -\frac{a}{2}). \tag{3.7}$$

Since our Hamiltonian is translation-invariant, all its eigenstates should have definite the value of momentum, hence it should be diagonal (block-diagonal if we have more than one state for each value of momentum) in the momentum representation.

We can switch to momentum representation using the Fourier transformation

$$a_{\vec{r}} = \frac{1}{\sqrt{N}} \sum_{\vec{k}} a_{\vec{k}}\, e^{-i\vec{k}\cdot\vec{r}}, , \tag{3.8}$$

$$b_{\vec{r}} = \frac{1}{\sqrt{N}} \sum_{\vec{k}} b_{\vec{k}}\, e^{-i\vec{k}\cdot\vec{r}}, \tag{3.9}$$

where $k$ is the wave vector, connected to momentum $p$ as $p = \hbar k$ and N is the total number of sites, included for the normalization.

Then for the Hamiltonian we obtain:

$$H_{NN} = -t \sum_{\vec{k}} a^+_{\vec{k}} b_{\vec{k}} (e^{-i\vec{k}\cdot\vec{e}_1} + e^{-i\vec{k}\cdot\vec{e}_2} + e^{-i\vec{k}\cdot\vec{e}_3}) - t \sum_{\vec{k}} b^+_{\vec{k}} a_{\vec{k}} (e^{i\vec{k}\cdot\vec{e}_1} + e^{i\vec{k}\cdot\vec{e}_2} + e^{i\vec{k}\cdot\vec{e}_3})$$

$$= \sum_{\vec{k}} (a^+_{\vec{k}} \quad b^+_{\vec{k}}) \begin{pmatrix} 0 & \mathcal{H}_{12}(\vec{k}) \\ \mathcal{H}^*_{12}(\vec{k}) & 0 \end{pmatrix} \begin{pmatrix} a_{\vec{k}} \\ b_{\vec{k}} \end{pmatrix}, \tag{3.10}$$

where

$$\mathcal{H}_{12}(\vec{k}) = -t \left( exp(-i\vec{k}\cdot\vec{e}_1) + exp(-i\vec{k}\cdot\vec{e}_2) + exp(-i\vec{k}\cdot\vec{e}_3) \right). \tag{3.11}$$

As we expected, Hamiltonian is diagonal with respect to the momentum, hence we only need to diagonalize blocks corresponding to each value of momentum to finish the diagonalization:

$$\mathcal{H}(\vec{k}) = \begin{pmatrix} 0 & \mathcal{H}_{12}(\vec{k}) \\ \mathcal{H}^*_{12}(\vec{k}) & 0 \end{pmatrix}. \tag{3.12}$$

Then we obtain two opposite values of energy, which we will label "+" and "-" for each $k$:

$$\epsilon_{\pm}(\vec{k}) = \pm \left| \mathcal{H}_{12}(\vec{k}) \right| = |t| \sqrt{3 + 2cos\left(\sqrt{3}k_x a\right) + 4cos\left(\frac{\sqrt{3}}{2}k_x a\right) cos\left(\frac{3}{2}k_y a\right)}. \tag{3.13}$$

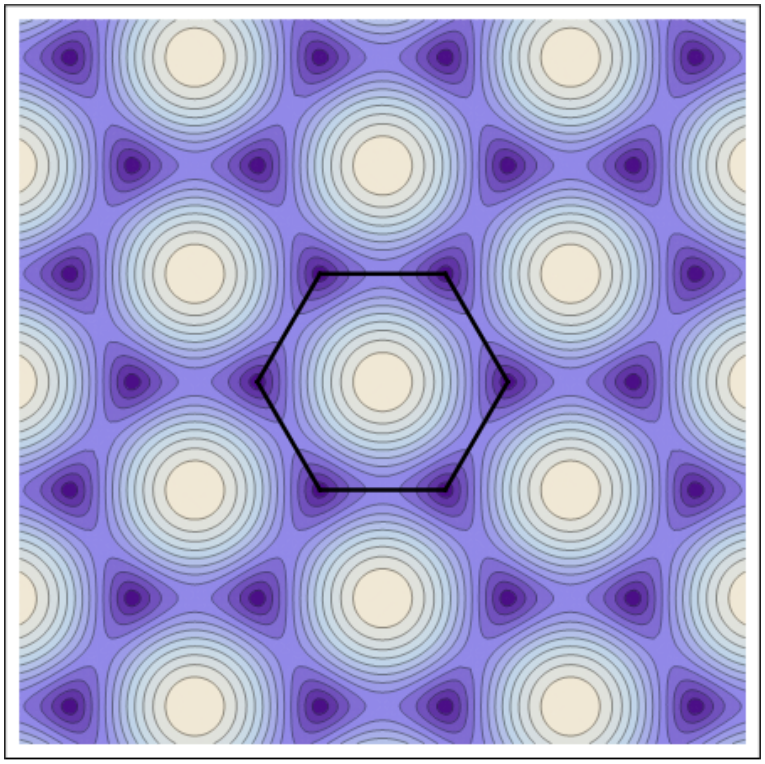

Figure 3.2: Contour plot of the energy versus two components of momentum for positive energy band in nearest-neighbor Haldane model. Hexagon in the center shows the edges of first Brillouin Zone.

Since we have hexagonal lattice in the real space, energy is a periodic function of momentum and on figure above we can see that first Brillouin Zone (hexagon shown) repeats itself. For the positive band $\epsilon_+$ shown on the figure, energy is maximal at the center of first BZ and is reaching minimum at the corners of first BZ. Out of six corners of first BZ three corners with azimuthal coordinates $\theta = 0$, $\theta = \frac{2\pi}{3}$ and $\theta = \frac{4\pi}{3}$ have the momenta that differ by a reciprocal vector, hence they are the same point. In the same way, other three corners are also one point up to a period. Hence, there are only two distinct corner points in the first BZ. We will choose

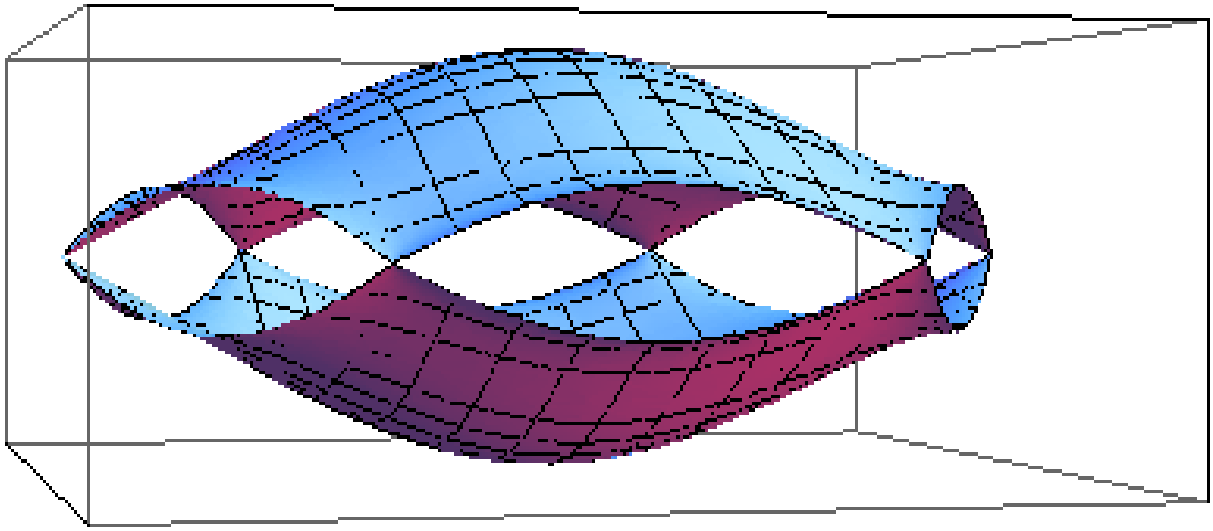

Figure 3.3: Energy as function of $k_x$ and $k_y$ in the first Brillouin Zone for two bands together. Bands are touching in every corner of the first BZ.

to label them by coordinates of two corners of first BZ that are on the x-axis. Since these two points have opposite momenta, we can label them as $\vec{k}_0$ and $-\vec{k}_0$, where

$$\vec{k}_0 = (\frac{4\pi}{3\sqrt{3}a}, 0). \tag{3.14}$$

For all the points in first BZ, except its corners, $\epsilon_+ > 0$ and $\epsilon_- < 0$ and hence two bands have different values of energy. But both bands have $\epsilon = 0$ at the corners of first BZ (see Fig. 3.3).

$$\epsilon_\pm(\vec{k}_0) = \pm\,|t|\,\sqrt{3 + 2cos\left(\sqrt{3}\,\frac{4\pi}{3\sqrt{3}a}\,a\right) + 4cos\left(\frac{\sqrt{3}}{2}\,\frac{4\pi}{3\sqrt{3}\,a}a\right)cos\left(\frac{3}{2}\,0\,a\right)} = 0. \tag{3.15}$$

Because of unusual structure of the bands at the corners of the first BZ, we will now focus our attention at the neighborhood of the corners. In the neighborhood of $\vec{k}_0$ (and $-\vec{k}_0$), we can expand energy in Taylor series of the momentum, measured from the corner $\vec{k} - \vec{k}_0$ (and $\vec{k} + \vec{k}_0$).

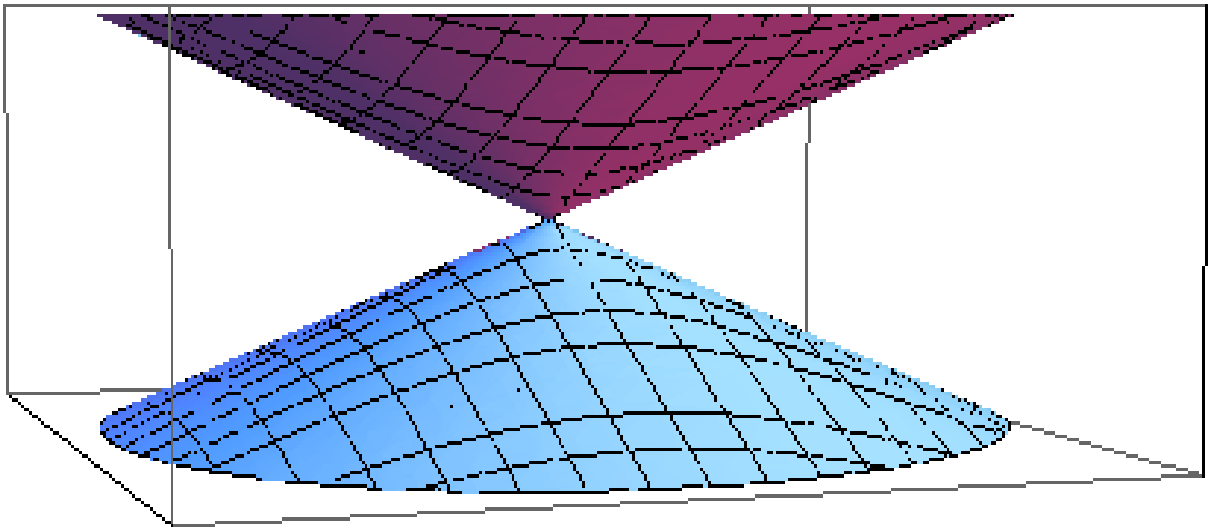

Figure 3.4: Energy as function of $k_x$ and $k_y$ in the neighborhood of the corner of first BZ plotted for two bands together.

For the $\vec{k}_0$ corner we can define $\vec{q} = \vec{k} - \vec{k}_0$. Then we get:

$$\begin{aligned} & \epsilon_{\pm}(\vec{k}) = \epsilon_{\pm}(\vec{k}_0 + \vec{q}) \\ = \; & \pm |t| \sqrt{3 + 2cos\left(\sqrt{3}\left(\frac{4\pi}{3\sqrt{3}a} + q_x\right)a\right) + 4cos\left(\frac{\sqrt{3}}{2}\left(\frac{4\pi}{3\sqrt{3}a} + q_x\right)a\right) cos\left(\frac{3}{2}\, q_y\, a\right)} \\ = \; & \pm|t|\, a\sqrt{q_x^2 + q_y^2} + O(q^2) = \pm\, \frac{3}{2}\, |t|\, a\, |\vec{q}| + O(q^2). \end{aligned} \tag{3.16}$$

The dispersion in the proximity of band touching point is linear. This resembles Dirac fermions with one significant difference: in case of Dirac fermions momentum has three components, while in our case $q$ has only two components.

The Hamiltonian from Eq. (3.12) will take form

$$\begin{aligned} & \mathcal{H}(\vec{k}) = \mathcal{H}(\vec{k}_0 + \vec{q}) = \frac{3ta}{2} \begin{pmatrix} 0 & q_x - iq_y \\ q_x + iq_y & 0 \end{pmatrix} + O(q^2) \\ \approx \; & \frac{3ta}{2}(q_x\sigma^x + q_y\sigma^y) = v\vec{q}\cdot\vec{\sigma} \end{aligned} \tag{3.17}$$

in the neighborhood of $\vec{k}_0$ and

$$\mathcal{H}(\vec{k}) = \mathcal{H}(-\vec{k}_0 + \vec{q}) = \frac{3ta}{2}\begin{pmatrix} 0 & q_x + iq_y \\ q_x - iq_y & 0 \end{pmatrix} + O(q^2)$$

$$\approx \; -\frac{3ta}{2}(q_x\sigma^x - q_y\sigma^y) = -v\vec{q}\cdot(\sigma^x\vec{\sigma}\sigma^x) \tag{3.18}$$

around $-\vec{k}_0$. Here $v$ is the constant with units of velocity that is the analog of speed of light for Dirac fermions and $\sigma^i$ are Pauli matrices:

$$\sigma^x = \begin{pmatrix} 0 & 1 \\ 1 & 0 \end{pmatrix}, \quad \sigma^y = \begin{pmatrix} 0 & -i \\ i & 0 \end{pmatrix}, \quad \sigma^z = \begin{pmatrix} 1 & 0 \\ 0 & -1 \end{pmatrix}, \quad \sigma^0 = \begin{pmatrix} 1 & 0 \\ 0 & 1 \end{pmatrix}. \tag{3.19}$$

Now, if are only interested in low energy excitations, we can construct an effective Hamiltonian that includes excitations around both nodes $\pm\vec{k}_0$ by putting the blocks from Eqs. 3.17 and 3.18 together:

$$\mathcal{H}(\vec{q}) = \begin{pmatrix} -v\vec{q}\cdot(\sigma^x\vec{\sigma}\sigma^x) & 0 \\ 0 & v\vec{q}\cdot\vec{\sigma} \end{pmatrix}. \tag{3.20}$$

This Hamiltonian resembles the Hamiltonian of massless Dirac fermions in three-dimensional space.

In fact, the Dirac Hamiltonian in 3D in it's original representation has form

$$\mathcal{H}_D = \begin{pmatrix} m & c\,\vec{q}\cdot\vec{\sigma} \\ c\,\vec{q}\cdot\vec{\sigma} & -m \end{pmatrix}. \tag{3.21}$$

where $c$ is the speed of light and $m$ is the mass of the fermion.

In the case when $m = 0$, this Hamiltonian can be made block-diagonal by unitary transformation

$$\psi' = \frac{1}{\sqrt{2}}\begin{pmatrix} 0 & 1 & 1 & 0 \\ 1 & 0 & 0 & 1 \\ 0 & -1 & 1 & 0 \\ -1 & 0 & 0 & 1 \end{pmatrix}\psi. \tag{3.22}$$

It will then be constructed of two 2 by 2 blocks:

$$\mathcal{H}_D = \begin{pmatrix} -c\vec{q}\cdot(\sigma^x\vec{\sigma}\sigma^x) & 0 \\ 0 & c\vec{q}\cdot\vec{\sigma} \end{pmatrix}. \tag{3.23}$$

Such basis is called Weyl's basis and two fermions (independent of each other in the massless case) that together make one Dirac fermion, are called Weyl fermions. The Hamiltonian Eq. 3.20 has exactly same form as the 3D Dirac Hamiltonian Eq. 3.23 with substitution $q_z = 0$. However, the Dirac fermions in two 2D have different representation. Since there are only two components of momentum and 1 mass term their Hamiltonian can be represented by 3 Pauli matrices of size 2 by 2. Since the product $\sigma^x\sigma^y\sigma^z = i\sigma^0$ is the trivial operator, the 2D Dirac Hamiltonian can not be made block-diagonal. Therefore, our effective Hamiltonian 3.20 is equivalent to the 3D Dirac Hamiltonian with substitution $q_z = 0$ but it is not a 2D Dirac Hamiltonian.

## 3.3 Next-nearest-neighbor hopping in Haldane model

Now we will see how the model changes, when we include to the Hamiltonian next-nearest-neighbor (NNN) hopping term. We will consider general case, when NNN hopping is a complex number, with magnitude $t_1$ and phase $\phi$. For Hamiltonian to be Hermitian operator we have to have hopping in opposite direction with same magnitude and opposite phase. We also want to preserve the translation and rotational symmetries of Hamiltonian, hence we will have same hopping magnitude $t_1$ and same phase $\pm\phi$ for all NNN. Furthermore we will define phase of hopping to be $\phi$, if it represents hopping clockwise around common neighbor and $-\phi$ otherwise (see Fig. 3.5).

Haldane suggested in Ref [17] that such complex hopping can be realized by applying staggered external magnetic field, positive at the centers of hexagons, negative near the edges and averaging to zero. NNN hopping always connects points of same sublattice (A or B), hence

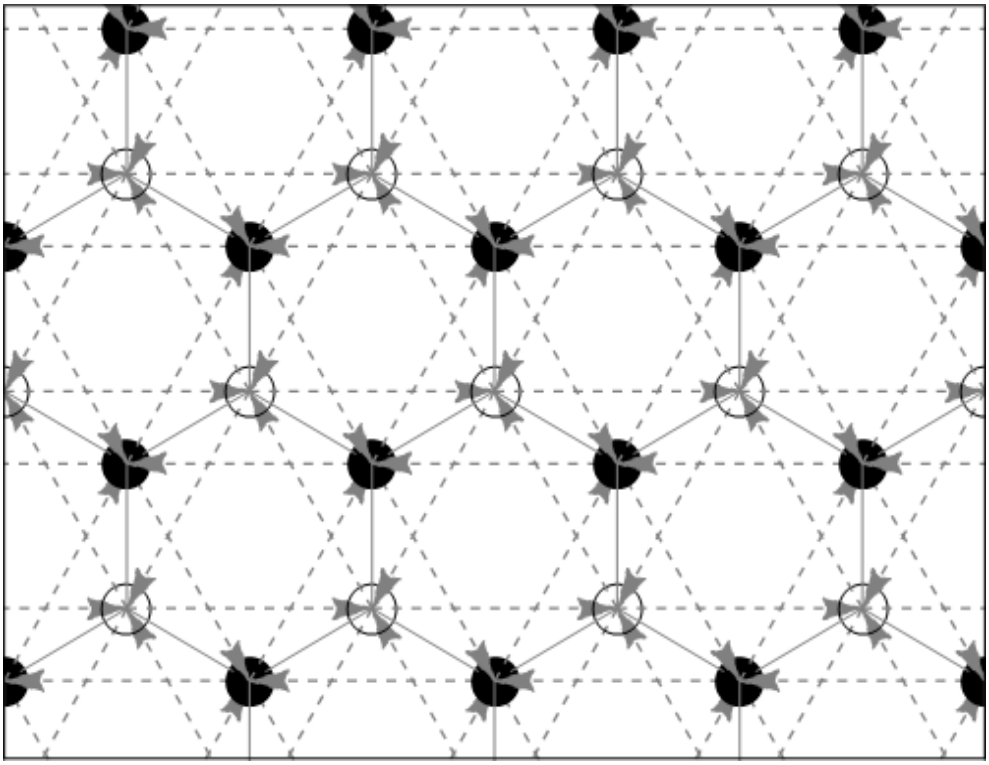

Figure 3.5: Honeycomb lattice. Next-Nearest-Neighbor hopping has phase $\phi$ when it happens along the direction of arrow and $-\phi$ otherwise.

Hamiltonian will have three A-to-A terms and three B-to-B, translated over the whole lattice:

$$\begin{aligned} H_{NNN} &= -t_1 e^{i\phi} \sum_i \left( a^+_{\vec{r}_i} a_{\vec{r}_i+\vec{v}_1} + a^+_{\vec{r}_i} a_{\vec{r}_i+\vec{v}_2} + a^+_{\vec{r}_i} a_{\vec{r}_i+\vec{v}_3} \right) \\ &\quad -t_1 e^{-i\phi} \sum_i \left( b^+_{\vec{r}_i} b_{\vec{r}_i+\vec{v}_1} + b^+_{\vec{r}_i} b_{\vec{r}_i+\vec{v}_2} + b^+_{\vec{r}_i} b_{\vec{r}_i+\vec{v}_3} \right) + h.c. \,, \end{aligned} \tag{3.24}$$

where $\vec{v}_1$ and $\vec{v}_2$ are the primitive translation vectors shown on Fig. 3.1 and $\vec{v}_3$ is the third primitive translation vector (linear combination of the first two). We can find explicit values for the components of $\vec{v}_3$ from Eq. 3.1 and Eq. 3.2:

$$\vec{v}_3 = -\vec{v}_1 - \vec{v}_2 = (-\frac{\sqrt{3}}{2}\, a, -\frac{3}{2}\, a). \tag{3.25}$$

By performing Fourier transformation, we obtain:

$$\begin{aligned} H_{NNN} &= -2t_1 \sum_{\vec{k}} a^+_{\vec{k}} a_{\vec{k}} \left( cos(\vec{k}\cdot\vec{v}_1 - \phi) + cos(\vec{k}\cdot\vec{v}_2 - \phi) + cos(\vec{k}\cdot\vec{v}_3 - \phi) \right) \\ &\quad -2t_1 \sum_{\vec{k}} b^+_{\vec{k}} b_{\vec{k}} \left( cos(\vec{k}\cdot\vec{v}_1 + \phi) + cos(\vec{k}\cdot\vec{v}_2 + \phi) + cos(\vec{k}\cdot\vec{v}_3 + \phi) \right). \end{aligned} \tag{3.26}$$

Then, in full Hamiltonian the off-diagonal terms from NN hopping (Eq. 3.11) will not change and we will get:

$$H = H_{NN} + H_{NNN} = \sum_{\vec{k}} (a^+_{\vec{k}} \quad b^+_{\vec{k}}) \begin{pmatrix} \mathcal{H}_{11}(\vec{k}) & \mathcal{H}_{12}(\vec{k}) \\ \mathcal{H}^*_{12}(\vec{k}) & \mathcal{H}_{22}(\vec{k}) \end{pmatrix} \begin{pmatrix} a_{\vec{k}} \\ b_{\vec{k}} \end{pmatrix}, \tag{3.27}$$

where

$$\mathcal{H}_{11}(\vec{k}) = -2t_1 \left( cos(\vec{k}\cdot\vec{v}_1 - \phi) + cos(\vec{k}\cdot\vec{v}_2 - \phi) + cos(\vec{k}\cdot\vec{v}_3 - \phi) \right), \tag{3.28}$$

$$\mathcal{H}_{22}(\vec{k}) = -2t_1 \left( cos(\vec{k}\cdot\vec{v}_1 + \phi) + cos(\vec{k}\cdot\vec{v}_2 + \phi) + cos(\vec{k}\cdot\vec{v}_3 + \phi) \right). \tag{3.29}$$

Using the definition of Pauli matrices 3.19, we can rewrite Hamiltonian as

$$\mathcal{H}(\vec{k}) = \mathcal{H}_0(\vec{k})\sigma^0 + \mathcal{H}_x(\vec{k})\sigma^x + \mathcal{H}_y(\vec{k})\sigma^y + \mathcal{H}_z(\vec{k})\sigma^z, \tag{3.30}$$

where

$$\mathcal{H}_0(\vec{k}) = -2t_1 cos(\phi) \left( cos(\vec{k}\cdot\vec{v}_1) + cos(\vec{k}\cdot\vec{v}_2) + cos(\vec{k}\cdot\vec{v}_3) \right), \tag{3.31}$$

$$\mathcal{H}_z(\vec{k}) = -2t_1 sin(\phi) \left( sin(\vec{k}\cdot\vec{v}_1) + sin(\vec{k}\cdot\vec{v}_2) + sin(\vec{k}\cdot\vec{v}_3) \right), \tag{3.32}$$

$$\mathcal{H}_x(\vec{k}) = -t \left( cos(\vec{k}\cdot\vec{e}_1) + cos(\vec{k}\cdot\vec{e}_2) + cos(\vec{k}\cdot\vec{e}_3) \right), \tag{3.33}$$

$$\mathcal{H}_y(\vec{k}) = -t \left( sin(\vec{k}\cdot\vec{e}_1) + sin(\vec{k}\cdot\vec{e}_2) + sin(\vec{k}\cdot\vec{e}_3) \right). \tag{3.34}$$

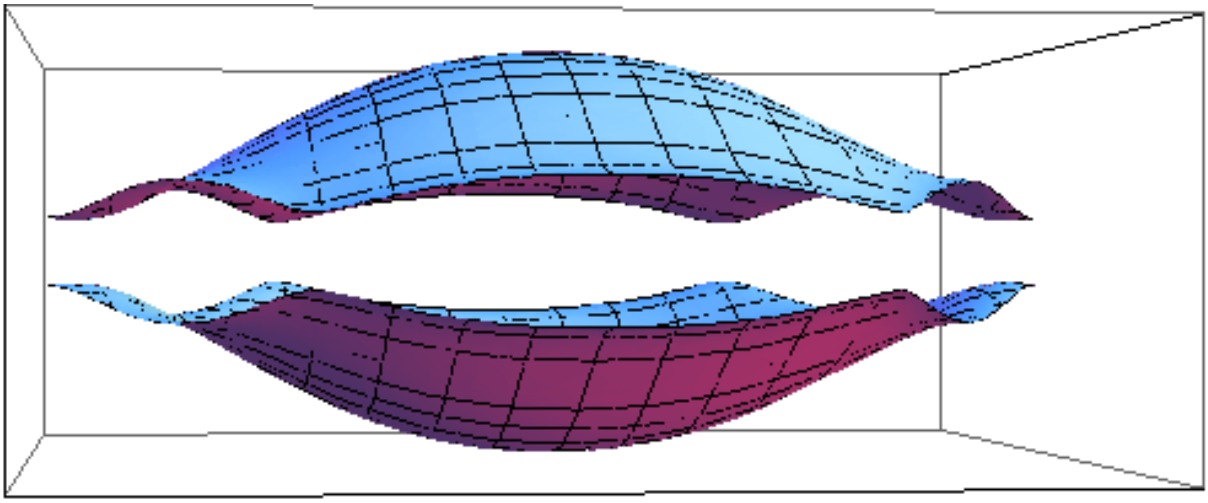

Figure 3.6: Energy as function of $k_x$ and $k_y$ in the first Brillouin Zone for $t_1 = 0.3t$, $\phi = \pi/2$. Bands never touch and the gap in energy between two bands is clearly visible.

Then we can find the energy as a function of the momentum for two bands. Using the fact that

$$\begin{aligned}(\mathcal{H}(\vec{k}) - \mathcal{H}_0(\vec{k})\,\sigma^0)^2 &= (\mathcal{H}_x(\vec{k})\sigma^x + \mathcal{H}_y(\vec{k})\sigma^y + \mathcal{H}_z(\vec{k})\sigma^z)^2 \\ &= \left(\mathcal{H}_x(\vec{k})^2 + \mathcal{H}_y(\vec{k})^2 + \mathcal{H}_z(\vec{k})^2\right)\sigma^0, \end{aligned} \tag{3.35}$$

we can write

$$\left(\epsilon_\pm(\vec{k}) - \mathcal{H}_0(\vec{k})\right)^2 = \mathcal{H}_x(\vec{k})^2 + \mathcal{H}_y(\vec{k})^2 + \mathcal{H}_z(\vec{k})^2. \tag{3.36}$$

Then we obtain:

$$\epsilon_\pm(\vec{k}) = \mathcal{H}_0(\vec{k}) \pm \sqrt{\mathcal{H}_x(\vec{k})^2 + \mathcal{H}_y(\vec{k})^2 + \mathcal{H}_z(\vec{k})^2}. \tag{3.37}$$

In the case of only NN hopping, Hamiltonian had only two parameters: $t$ and $a$. These parameters where setting the scale in energy and in momentum and not affecting the dispersion picture otherwise. Now we have two more parameters: $t_1$ and $\phi$. If we change them, dispersion picture can take very different forms. The two examples with random non-trivial values of $t_1$

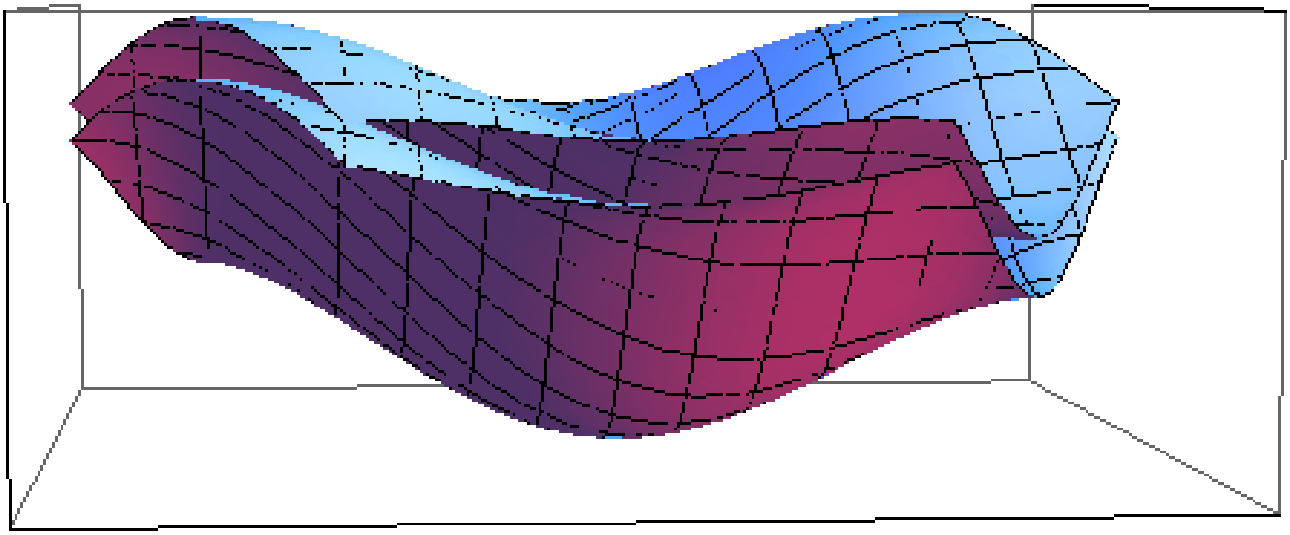

Figure 3.7: Energy as function of $k_x$ and $k_y$ in the first Brillouin Zone for $t_1 = t$, $\phi = \pi/8$. Bands can overlap in energy, but they never touch.

and $\phi$ are shown on Fig. 3.6 and 3.7. Then, if we put $t_1 = 0$, we get back to NN case (see Fig. 3.3 ). We see that for some values of parameters (as on Fig. 3.7) bands can overlap in energy, but in both cases of non-trivial $t_1$ and $\phi$ bands do not touch. In the case shown on Fog. 3.6 the sample will be an insulator, if Fermi energy is between the two bands and metal otherwise. In the case shown on Fig. 3.7 there are electron states at every energy and hence the sample will be metal, as it always has states at the Fermi energy.

Further in this chapter we will focus on the cases when two levels do not overlap, as on Fig. 3.6 in energy and the Fermi energy is between the two levels.

From Eq. 3.37 we see that the distance between the bands is increased by $\mathcal{H}_z$, compared to NN case. In NN case bands were only touching at the points $\pm\vec{k}_0$. Then, if $\mathcal{H}_z(\pm\vec{k}_0) \neq 0$, bands will not touch. From Eq. 3.32 we can get:

$$\mathcal{H}_z(\vec{k}_0) = -3\sqrt{3}\, t_1\, sin(\phi), \tag{3.38}$$

$$\mathcal{H}_z(-\vec{k}_0) = 3\sqrt{3}\, t_1\, sin(\phi). \tag{3.39}$$

Hence, if $t_1$ is not zero and $\phi$ is not equal to $\pi$ times an integer, bands will not touch.

## 3.4 Potential Energy

Now we will add the potential energy term to the Hamiltonian. In general, potential energy has the form

$$H_{pot} = \sum_i (V_{ai}\, a_i^+ a_i + V_{bi}\, b_i^+ b_i), \tag{3.40}$$

where $V_{ai}$ and $V_{bi}$ show how much energy it takes to put particle on one particular site of lattice. Since we don't want to break translational symmetry, we will consider only potentials independent on $i$. However, if we put $V$ same for A and B sublattices, it will be equivalent to changing the the zero of energy and will not make any physical changes to the system. Using this freedom to choose the reference frame in energy, we can pick zero so that $V_a = V$ and $V_b = -V$, where $V$ is one new parameter of the system. Hence

$$H_{pot} = \sum_i (V\, a_i^+ a_i - V\, b_i^+ b_i), \tag{3.41}$$

or in momentum space

$$H_{pot} = V \sum_{\vec{k}} (a_{\vec{k}}^+ \quad b_{\vec{k}}^+)\, \sigma^z \begin{pmatrix} a_{\vec{k}} \\ b_{\vec{k}} \end{pmatrix}. \tag{3.42}$$

Therefore, potential energy gives us term similar to $\mathcal{H}(\vec{k})$ (see Eq. 3.32), but now it is independent of the momentum. If we only consider the NN-hopping and potential energy, the two bands in the model will not touch for any non-zero $V$. In the case when we have both the NNN hopping and the potential energy terms, system can have very different properties depending on values of parameters. In order to understand the behavior of Haldane model at different relative weight of parameters, we need to study the wavefunctions in the system.

## 3.5 Wavefunctions

Until the discovery of quantum Hall effect, condensed matter physicists mostly focused on finding physically observable quantities such as the energy spectrum and the magnitude of wavefunctions. But, as we saw in Sec. 2.3, non-observable quantities like phase of wavefunctions or Berry connection are also important. In case of quantum Hall effect we saw that Hall conductivity can only be non-zero in insulator, if Berry connection has singularity.

Now, we will study the wavefunctions of Haldane model. All the pieces of this model: potential energy, NN hopping and NNN hopping can be put together in the form

$$\mathcal{H}(k) = \mathcal{H}_0(k)\sigma^0 + \mathcal{H}_x(k)\sigma^x + \mathcal{H}_y k)\sigma^y + \mathcal{H}_z(k)\sigma^z, \tag{3.43}$$

where $\mathcal{H}_z$ will now include the potential energy and all other terms will be same as in Eq. 3.45. Energy, as function of $\mathcal{H}_i$ has the same form as in Eq. 3.37:

$$\epsilon_\pm(\vec{k}) = \mathcal{H}_0(\vec{k}) \pm \sqrt{\mathcal{H}_x(\vec{k})^2 + \mathcal{H}_y(\vec{k})^2 + \mathcal{H}_z(\vec{k})^2} = \mathcal{H}_0(\vec{k}) \pm |\vec{\mathcal{H}}(\vec{k})|. \tag{3.44}$$

Now, we can find the eigenfunctions of Hamiltonian. We will now focus on the lower band:

$$u_-(\vec{k}) = \frac{1}{N(\vec{k})} \begin{pmatrix} \mathcal{H}_z(\vec{k}) - |\vec{\mathcal{H}}(\vec{k})| \\ \mathcal{H}_x(\vec{k}) + i\mathcal{H}_y(\vec{k}) \end{pmatrix}, \tag{3.45}$$

where $N(\vec{k})$ is the normalization factor for the particular $\vec{k}$.

If, for some $\vec{k}$, $\mathcal{H}_x = \mathcal{H}_y = 0$ and $\mathcal{H}_z > 0$, this wavefunction becomes singular. In the case of no potential energy, positive $t_1$ and $0 \leq \phi \leq \pi$ such point exists - it is $-\vec{k}_0$. At this point

$$u_-(\vec{k}) = \frac{1}{N(\vec{k})} \begin{pmatrix} 0 \\ 0 \end{pmatrix}. \tag{3.46}$$

There is another way to write down the eigenstates of Hamiltonian, which can be obtained from the Eq. 3.45 by changing the phase of wavefunctions:

$$u'(\vec{k}) = \frac{1}{N(\vec{k})} \begin{pmatrix} \mathcal{H}_z(\vec{k}) - |\vec{\mathcal{H}}(\vec{k})| \\ \mathcal{H}_x(\vec{k}) + i\mathcal{H}_y(\vec{k}) \end{pmatrix} \cdot \frac{\frac{\mathcal{H}_(\vec{k}) + |\vec{\mathcal{H}}(\vec{k})|}{\mathcal{H}_x(\vec{k}) + i\mathcal{H}_y(\vec{k})}}{|\frac{\mathcal{H}_(\vec{k}) + |\vec{\mathcal{H}}(\vec{k})|}{\mathcal{H}_x(\vec{k}) + i\mathcal{H}_y(\vec{k})}|} = \frac{1}{N'(\vec{k})} \begin{pmatrix} -\mathcal{H}_x(\vec{k}) + i\mathcal{H}_y(\vec{k}) \\ \mathcal{H}_z(\vec{k}) + |\vec{\mathcal{H}}(\vec{k})| \end{pmatrix}. \tag{3.47}$$

This second form is not singular, when $\mathcal{H}_x = \mathcal{H}_y = 0$ and $\mathcal{H}_z > 0$, but it is singular, when $\mathcal{H}_x = \mathcal{H}_y = 0$ and $\mathcal{H}_z < 0$. And we have such conditions at the $\vec{k}_0$ point of the Hamiltonian without potential energy. Therefore in order to have regular wavefunctions, we have to brake first BZ into two regions and use different wavefunctions in two regions.

By changing the value $V$ of potential energy, we can get from the case when $\mathcal{H}_z$ is negative at both corners of the BZ $\vec{k}_0$ and $-\vec{k}_0$ (big negative V), to the case when signs of $\mathcal{H}_z$ at two corners are opposite (V=0) to the case when $\mathcal{H}_z$ is positive at both corners of the BZ $\vec{k}_0$ and $-\vec{k}_0$ (big positive V). In the middle case we cannot choose one wavefunction, and hence material will be Topological insulator. In both side cases, however, we can choose one wavefunction for whole BZ and hence material will be a normal insulator. It is important to notice, that on the edges between these three insulators $\mathcal{H}_z$ is zero in one of the corners and hence system is not an insulator at such values of parameters. This is similar to the quantum Hall effect case, where we had to go through metallic state to get from one insulating state to another.

## 3.6 Edge states

In the example of the quantum Hall effect we saw that even when the bulk of the system consists of localized electron states, there could be delocalized states on the edge. In the case of Haldane model, since we have the Hamiltonian of the system, we can directly study the case when the lattice has boundaries.

The calculation we did in previous sections of this chapter relied on the translational invariance of the sample, when we changed basis from the real space to the momentum representation. Now we will consider the sample, that has two parallel boundaries along the $y$ axis and is infinite along $x$ axis. Such sample will still have translational invariance (for the translation by the integer multiple of primitive translation vector $v_1$, Eq. 3.1 ) in the $x$ direction. But translation along $y$ axis will not leave boundary in place and hence will not be a symmetry of the model any more. This means we can not use the $k_y$ to label the eigenstates of Hamiltonian.

We will consider the distance between the boundaries such that there are $2N$ pairs of sites ($N$ of sublattice A and $N$ of sublattice B) between the boundaries, not counting the sites that can be obtained by translation along $x$ axis of the previously counted ones. Since the translation along $x$ is still a symmetry of Hamiltonian, we can use $k_x$ to label eigenstates of Hamiltonian. But since we have $2N$ sites in vertical direction, there will be $2N$ states with each value of $k_x$.

In order to find the dispersion in this model we can use the same Fourier transformation as we did for infinite case( see Eqs. 3.8, 3.9), but only along $x$ axis. Then for the case of only nearest neighbors we will obtain from the Hamiltonian Eq. 3.4:

$$\begin{aligned} H_{NN} &= -t \sum_{k_x,r_y} \Bigg( a^+_{k_x,r_y}(b_{k_x,r_y+a} + b_{k_x,r_y-\frac{a}{2}} e^{i\sqrt{3}k_x a/2} + b_{k_x,r_y-\frac{a}{2}} e^{-i\sqrt{3}k_x a/2}) \\ &\quad + (b^+_{k_x,r_y+a} + b^+_{k_x,r_y-\frac{a}{2}} e^{-i\sqrt{3}k_x a/2} + b^+_{k_x,r_y-\frac{a}{2}} e^{i\sqrt{3}k_x a/2}) a_{k_x,r_y} \Bigg). \end{aligned} \tag{3.48}$$

Considering that bottom edge along the $x$ passes above the line of $B$ sites and below the line of $A$ sites, we can rewrite Hamiltonian as

$$\begin{aligned} H_{NN} &= -t \sum_{k_x} \sum_{n=2}^{N} \Bigg( a^+_{k_x,n}(b_{k_x,n} + b_{k_x,n-1} \cdot 2cos(\frac{\sqrt{3}k_x a}{2})) \\ &\quad + (b^+_{k_x,n} + b^+_{k_x,n-1} \cdot 2cos(\frac{\sqrt{3}k_x a}{2})) a_{k_x,n} \Bigg) - t \sum_{k_x} (a^+_{k_x,1} b_{k_x,1} + b^+_{k_x,1} a_{k_x,1}) \end{aligned} \tag{3.49}$$

We now can diagonalize the Hamiltonian numerically with respect to index $n$, treating $k_x$ as a parameter. The results as functions of $k_x$ are shown on Figs. 3.8a and 3.8b for $N = 5$ and $N = 20$ respectively. The dispersion of the infinite sample is shown on Fig. 3.8c for comparison.

From the three plots on Fig. 3.8 we can see that as $N$ grows, the dispersion picture of energy versus $k_x$ approaches the projection of the translation invariant case ($E = E(k_x, k_y)$) onto the $E - k_x$ plane.

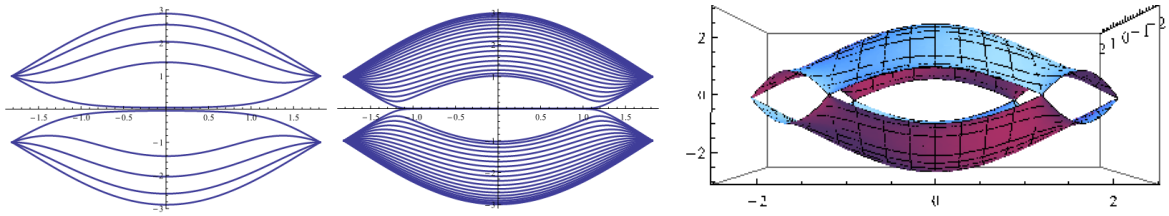

(a) N=5 (b) N=20 (c) infinite N (no boundaries)

Figure 3.8: Energy as function of $k_x$ in the NN Haldane Model for different number of sites in $y$ direction: (a) 2N=10 sites, (b) 2N=40 sites, (c) no boundary

But, while most of the states in the finite cases are fitting the projection of the infinite case, there are two states in each finite case, that have close to zero energy for all $k_x$ between $-k_0$ and $k_0$. As $N$ grows, the energy of these two states reaches zero closer to $\pm k_0$. Since these states do not correspond to any states in the infinite case, we can conclude that these are the edge states.

Now we can include the NNN hopping term in Hamiltonian. on the same lattice of width $2N$ it will take form

$$H = H_{NN} + H_{NNN} \tag{3.50}$$

with

$$\begin{aligned} & H_{NNN} = \\ = \; & -t_1 \sum_{k_x} \sum_{n=2}^{N-1} \Bigg( a^+_{k_x,n} \left[ 2cos(\phi - \sqrt{3}k_x a) a_{k_x,n} + 2cos(\phi + \frac{\sqrt{3}k_x a}{2})(a_{k_x,n+1} + a_{k_x,n-1}) \right] \\ & + b^+_{k_x,n} \left[ 2cos(-\phi - \sqrt{3}k_x a) b_{k_x,n} + 2cos(-\phi + \frac{\sqrt{3}k_x a}{2})(b_{k_x,n+1} + b_{k_x,n-1}) \right] \Bigg) \\ & - \sum_{k_x} \Big( 2cos(\phi - \sqrt{3}k_x a)(a^+_{k_x,1} a_{k_x,1} + a^+_{k_x,N} a_{k_x,N}) \\ & + 2cos(-\phi - \sqrt{3}k_x a)(b^+_{k_x,1} b_{k_x,1} + b^+_{k_x,N} b_{k_x,N}) \Big). \end{aligned} \tag{3.51}$$

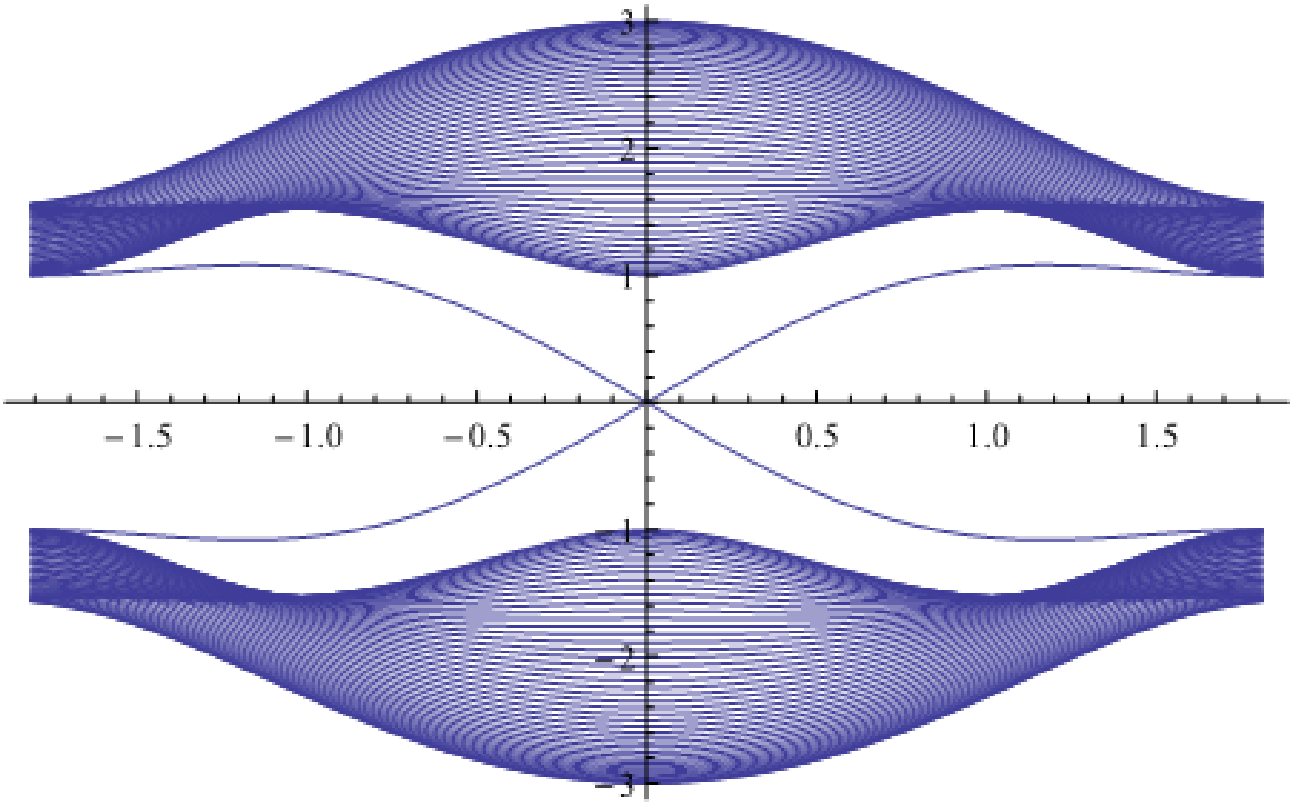


Figure 3.9: Energy as function of $k_x$ in the NNN Haldane Model for $t_1 = 0.3t$, $\phi = \pi/8$, with $2N = 100$ sites in $y$ direction.

In order to compare with the Fig. 3.6, we will chose same parameters: $t_1 = 0.3t$ and $\phi = \pi/2$. Diagonalizing the Hamiltonian with both $H_{NN}$ and $H_{NNN}$ numerically for each value of $k_x$, we obtain the dispersion as function of $k_x$, shown on Fig. 3.9. For such values of $t_1$ and $\phi$ in the case of infinite sample we had a gap between the two levels and when Fermi energy is zero, the sample was an insulator. Now we see on Fig. 3.9 that similarly to NN model, there are two states in the finite size model, that are not matching any states of infinite case. We can once again, same as for NN model, conclude, that these are the edge states of the NNN model. These two states, as functions of $k_x$, connect the two bulks of states below and above zero energy. Hence, for Fermi energy equal to zero, or any other Fermi energy between two

levels of infinite case, each of two edge states will be intersecting the Fermi energy level at some $k_x$. Therefore, we will have only two states, with two specific values of wave vector, on the Fermi surface.

We have already shown in section 3.5 that at such values of parameters Haldane model will describe not an ordinary insulator, but a topological insulator. Now we see that this model has edge states at the Fermi level. This means the edge of the sample will be able to conduct current. This is very similar to the quantum Hall effect, where states on the edge are not localized and hence we can as well conclude (even despite the fact that we used only a quasi-classical approximation to study them), that edge of quantum Hall effect is conducting.

We can trace the similarity between the edge of QHE and the edge of Haldane model even further. In the QHE all the electron states on the edge were chiral - able move only in one direction and with fixed velocity. In the Haldane model we can find the group velocity of excitations on the edge as

$$v_x = \frac{d\omega}{dk_x} = \frac{dE}{\hbar dk_x}. \tag{3.52}$$

Since we have two symmetrical lines crossing Fermi energy, we will have two opposite values of velocity. This could correspond to the chiral edge states, if on each edge electrons can move only in one direction, or to the ordinary metallic states, if electrons on each edge can move in both directions. In order to distinguish between these two possibilities we can use the numerical diagonalization of Hamiltonian Eq. 3.50. Taking the eigenfunctions $\psi(N, k_x)$ and $\psi(N+1, k_x)$ corresponding to the two energy levels that cross at zero energy on Fig. 3.8b, we plot the probability amplitude distribution of these wavefunctions versus $k_x$ and $n$ on Fig. 3.10.

From Fig. 3.10 we see that each of the states is concentrated near one edge. This proves that the electrons on each edge can move only in one direction and their states are chiral.

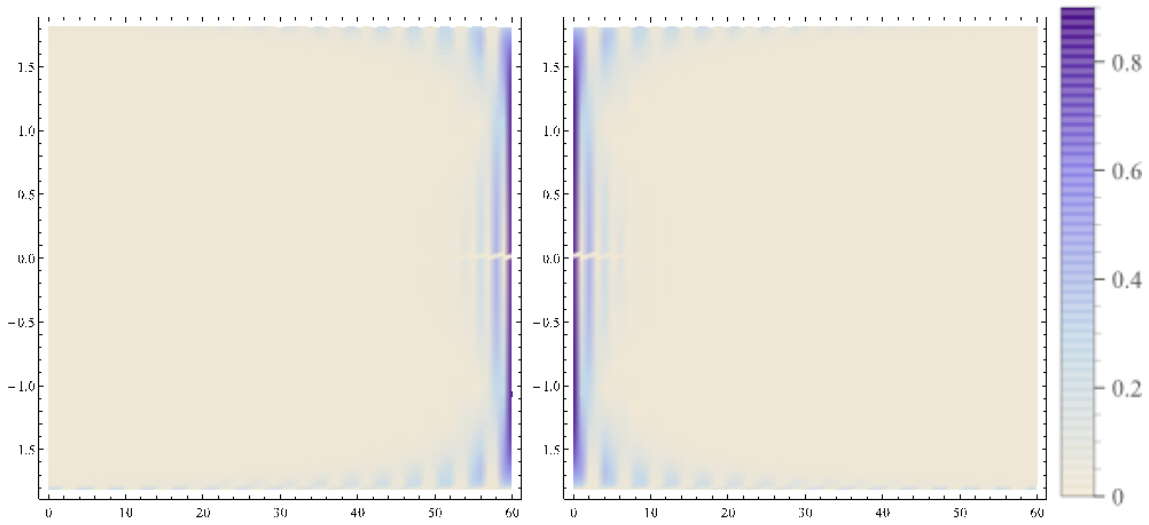


(a) top edge state (b) bottom edge state

Figure 3.10: Probability distribution of the edge states in Haldane model in the TI state, plotted as function of $k_x$ (vertical) and $n$ (horizontal); (a) top edge state: amplitude is non-zero only for n close to $2N$ (b) bottom edge state: amplitude is non-zero only for n close to 1

# Chapter 4

# Weyl metals

## 4.1 Introduction

In the chapter 3 we saw on the example of the graphene, that the presence of touching bands in the dispersion can lead to non-trivial topology of the material in the momentum space. In the case of Graphene the touching of the bands requires the fine tuning of the Hamiltonian: $\mathcal{H}_z(\pm\vec{k}_0)$ in Eq. 3.43 has to be exactly equal to zero for band to touch. At the same time, small changes in the $\mathcal{H}_x(\vec{k})$ and $\mathcal{H}_y(\vec{k})$ terms can only shift the position of the band touching points in momentum space, but can not remove them. Such sensitivity of the model to the $\mathcal{H}_z(\vec{k})$ term appeared due to the fact that model is two-dimensional and hence there is no $z$ component possible in $\vec{k}_0$ to absorb the changes in Hamiltonian. This lead to the theoretical idea that in three-dimensional material band touching points are not sensitive to small changes in Hamiltonian. Hence the presence of band touching in 3D material can lead to the existence of topologically protected properties of material.

The existence of band touching points in the dispersion of the 3D materials has been first predicted by Herring in 1937 [21]. But only after the discovery of graphene the band touching points started drawing attention. The first specific models of materials, $A_2Ir_2O_7$ and $Y_2Ir_2O_7$,

that should have the touching bands, were proposed in 2011 [8, 9]. Each of these materials was expected to have 24 band touching points at the same energy. Later the material, constructed of multiple layers of two different insulators, was proposed [10]. The latter material was much more complicated to fabricate, but it was expected to have only two band touching points.

Due to the similarity of the dispersion near the band touching points to the dispersion of Weyl fermions in high energy physics, all the material that have such points were named Weyl metals. Since the similarity to the Weyl fermions and the undoped graphene becomes the closest when Fermi energy level exactly matches the band touching points, such specific case was studied the most. In this specific case there the Fermi surface is reduced to the set of points in momentum space and hence material can not be called a metal. Therefore the materials that have band touching points at the Fermi energy were named Weyl semimetals. The points where two bands touch are consequently called Weyl nodes.

Since the big number of the band touching points makes the theoretical study of the properties of the materials very complicated, we will consider only the model with the minimal possible number of points [10].

## 4.2 Multilayer model

The multilayer heterostructure proposed in [10] is built of alternating thin layers of normal insulator (NI) and topological insulator (TI). Each layer of TI has a gap for all the bulk states, but it has gapless excitations on the both (top and bottom) 2D edges. Then, if an edge of another layer of TI is located close to it, the tunneling of the excitation between two 2D edges will occur. This will effectively allow the gapless excitations to move in all three directions.

The corresponding effective Hamiltonian for such model is

$$\begin{aligned} H &= \sum_{\vec{k}_\perp,i,j} \Bigg( v_F \tau^z (\hat{z} \times \vec{\sigma}) \cdot \vec{k}_\perp \delta_{i,j} + m\sigma^z \delta_{i,j} + \Delta_S \tau^x \delta_{i,j} \\ &\quad + \frac{1}{2}\Delta_D \tau^+ \delta_{i,j+1} + \frac{1}{2}\Delta_D \tau^- \delta_{i,j-1} \Bigg) \end{aligned} \tag{4.1}$$

In this Hamiltonian the first term describes the 2D Dirac fermions on the two surfaces of the TI (see Eq. 3.23), $v_F$ is the Fermi velocity of the Dirac fermions, $\vec{k}_\perp$ is the 2D momentum in the plane of TI surface, $\tau^i$ are the Pauli matrices that connect states on the two surfaces of TI. The indexes $i$ and $j$ label the layer of TI. The second term describes the energy splitting between spin up and spin down states. Such splitting can appear in the presence of the external magnetic field, or can be induced by doping of each layer of TI by magnetic impurities [22]. The $\Delta_S$ term describes the tunneling between two surfaces of same TI layer. The $\Delta_D$ terms describe the tunneling between the surfaces of two nearest layers of TI. The choice of signs for $\Delta_S$ and $\Delta_D$ does not affect the properties of the system and hence we can choose them both to be positive without the loss of generality.

Performing the Fourier transformation along the $x$ axis, we obtain the Hamiltonian in 3D momentum space:

$$H = \sum_{\vec{k}} \left( v_F \tau^z (\hat{z} \times \vec{\sigma}) \cdot \vec{k} + m\sigma^z + \Delta_S \tau^x + \frac{1}{2}\Delta_D \tau^+ e^{ik_z d} + \frac{1}{2}\Delta_D \tau^- e^{-ik_z d} \right). \tag{4.2}$$

### 4.2.1 Zero doping case

The parameters $m$, $\Delta_S$ and $\Delta_D$ in Hamiltonian Eq. 4.2 can be adjusted by changing the density of doping, the thickness of TI and thickness of NI layers respectively. We will start by considering the undoped case, or $m = 0$. In this case we can diagonalize Eq. 4.2 and obtain

$$\epsilon^2_{\vec{k}\pm} = v_F^2(k_x^2 + k_y^2) + \Delta^2(k_z), \tag{4.3}$$

where

$$\Delta(k_z) = \sqrt{\Delta_S^2 + \Delta_D^2 + 2\Delta_S\Delta_D cos(k_z d)}. \tag{4.4}$$

Here $d$ is the period in the direction across the layers ($z$), it is equal to the distance between the bottom edges of two consecutive TI layers. When $\Delta_S$ and $\Delta_D$ are not equal in magnitude, $\Delta(k_z)$ will be always positive and bands will not be touching (Fig. 4.1a). But if $\Delta_S$ and$\Delta_D$ are equal in magnitude ,bands will touch (Fig. 4.1b) and since each band is double degenerate, the dispersion near the node will take the for of the Dirac fermion:

$$\epsilon^2_{\vec{k}\pm} = v_F^2(k_x^2 + k_y^2) + \tilde{v}_F^2 k_z^2, \tag{4.5}$$

where $\tilde{v}_F = d\sqrt{\Delta_S\Delta_D}$.

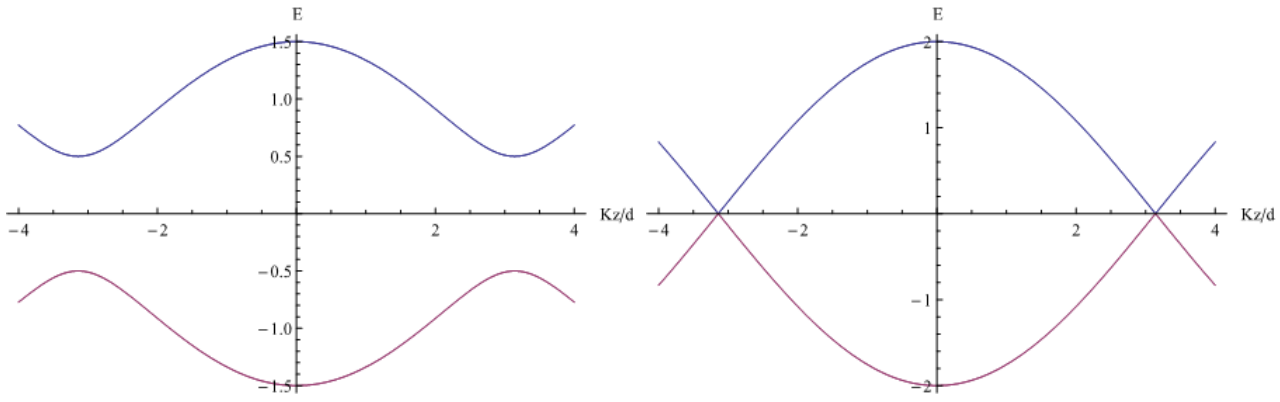


(a) $\Delta_S = \Delta_D/2$ (b) $\Delta_S = \Delta_D$

Figure 4.1: Energy as function of $k_z$ for $k_x = k_y = 0$ in the undoped case. (a) gapped case,$\Delta_S = \Delta_D/2$; (b) gapless case, $\Delta_S = \Delta_D$

The band described by Eq. 4.5 are double degenerate and hence, when they touch at $\Delta_S = \Delta_D$, they form Dirac node (or two Weyl nodes at the same position in the momentum space). The effective Hamiltonian in the proximity of Dirac point takes form

$$\mathcal{H}(\vec{k}) = v_F\tau^z(\hat{z} \times \vec{\sigma}) \cdot \vec{k} + \tilde{v}_F\tau^y k_z. \tag{4.6}$$

Therefore, there are four bands touching in one point and the effective Hamiltonian in the neighborhood of the node allows many more types of perturbations, compared to two by two Hamiltonian describing a Weyl node neighborhood. This leads to the topological instability of the node - small changes in parameters, such as value of $\Delta_S$ deviating from the value of $\Delta_D$ can make it disappear.

### 4.2.2 Non-zero doping case

In the case, when $m \neq 0$, diagonalizing the Hamiltonian leads to the band dispersion

$$\epsilon^2_{\vec{k}\pm} = v_F^2(k_x^2 + k_y^2) + (m \pm \Delta(k_z))^2. \tag{4.7}$$

In this dispersion two bands (corresponding to "+" index, when $m > 0$ or to "-" when $m < 0$) never reach the zero energy, while the other two bands reach zero at the points $(0, 0, \frac{\pi}{d} \pm k_0)$, where

$$k_0 = \frac{1}{d} cos^{-1}\left(1 - \frac{m^2 - (\Delta_S - \Delta_D)^2}{2\Delta_S\Delta_D}\right). \tag{4.8}$$

These two points exist as long as

$$(\Delta_S - \Delta_D)^2 < m^2 < (\Delta_S + \Delta_D)^2. \tag{4.9}$$

For such values of $m$ we have two Weyl nodes are separated in the momentum space. The example form of the band dispersion for specific values of $m$, $\Delta_S$ and $\Delta_D$, that satisfy the condition Eq. 4.9 is shown on Fig. 4.2.

The effective Hamiltonian in the neighborhood of each point can be transformed by the unitary transformation to the form

$$\mathcal{H}(\vec{k}) = v_F k_x \sigma^x + v_F k_y \sigma^y + \tilde{v}_F k_z \sigma^z. \tag{4.10}$$

Since this Hamiltonian is two by two matrix and it has to be Hermitian, all the possible perturbations are proportional to $\sigma^i$ and hence they either shift the position of $k_0$, if $i \in x, y, z$

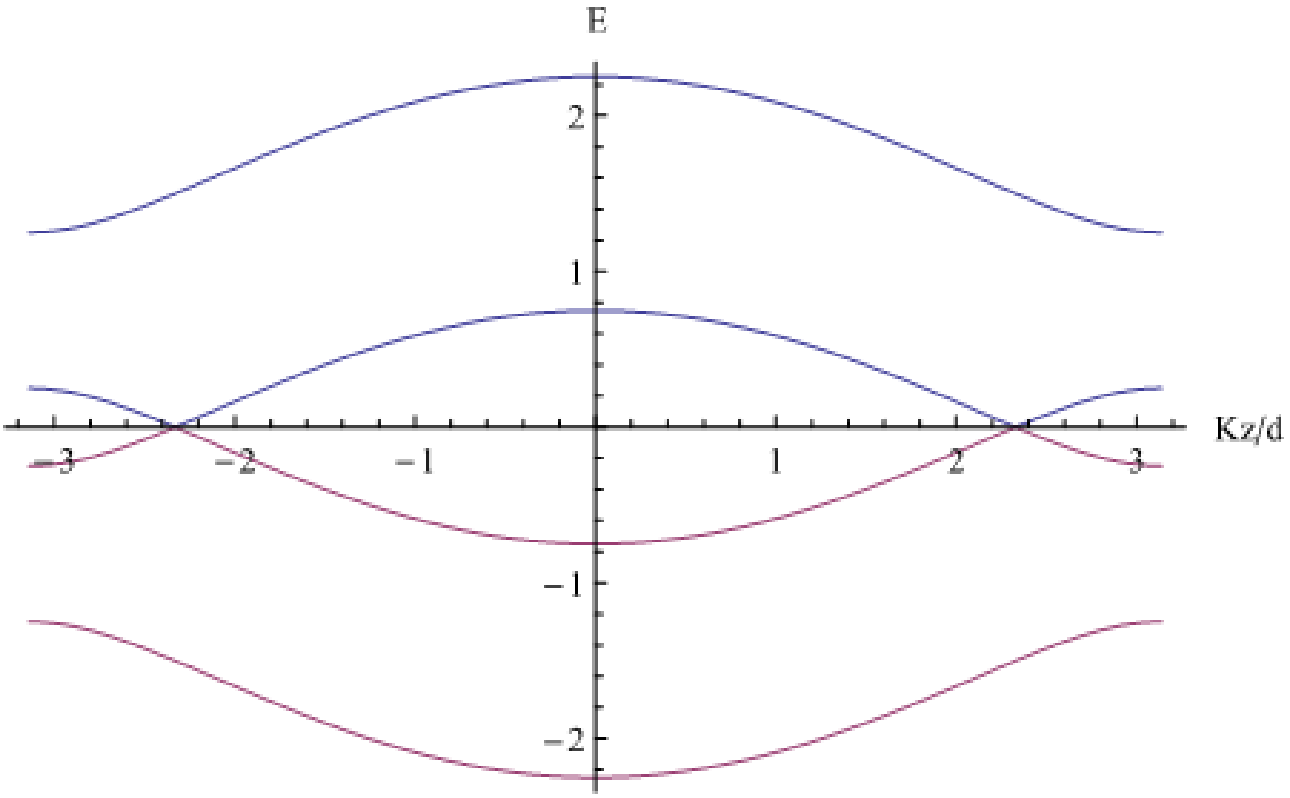


Figure 4.2: Energy as function of $k_z$ for $k_x = k_y = 0$ in the doped case for the values of parameters $\Delta_S = \Delta_D/2$, $m = \frac{\Delta_S+\Delta_D}{2}$ .

or shift the Fermi level relatively to the node, when $i = 0$. Therefore, the Weyl nodes are topologically stable as long as they are separated by finite distance in momentum space.

### 4.2.3 Berry curvature

In the chapter 2 we the existence of non-zero flux of Berry curvature through the close surface is a sign of non-trivial topology of the momentum space. In the case of doped 3D Weyl metal ( here we consider the case of $E_F \neq 0$) the Fermi surface consists of two disconnected closed surfaces, surrounding two Weyl nodes. Since most of the properties of metal are defined by the states at the Fermi surface, we will study the flux of Berry curvature trough the Fermi surface.

If the $E_F > 0$ is not far from zero so that we can still use the linear approximation of the Hamiltonian around the Weyl nodes, the Fermi surface will consist of two ellipsoids, or spheres if $v_F = \tilde{v}_F$. Then we can find the exact expression for the wavefunction of corresponding band of Hamiltonian 4.10. After that, using the definition of Berry curvature Eqs. 2.14-2.18 we can calculate the Berry curvature. If we rescale the $k_z$ so that $v_F = \tilde{v}_F$ to make the Fermi surface spherical, the Berry curvature as function of rescaled momentum, will take the symmetric form.

$$\vec{\Omega}(\vec{k} \pm (\frac{\pi}{d} - k_0)\hat{z}) = \pm\frac{\vec{k}}{2k^3}. \tag{4.11}$$

The flux of Berry curvature calculated for one of the Fermi spheres will give us an integer Chern number, same as in the QHE Eq. 2.25

$$C = \frac{1}{2\pi}\int \vec{\Omega}(\vec{k}) \cdot d\vec{S} = \pm 1. \tag{4.12}$$

Here we calculated the flux in the simplest geometry of the Fermi surface, but since Berry connection $\vec{\mathcal{A}}(\vec{k})$ is a regular function of $\vec{k}$ everywhere except the Weyl nodes, the flux will be same for each closed part of Fermi surface. It will not change with changing of parameters $E_F$, $m$, $\Delta_S$ and $\Delta_D$, as long as two separated Weyl nodes exist and Fermi energy forms two separate Fermi surfaces. For the higher $E_F$, when Fermi surface becomes connected we will have only one closed surface enclosing two Weyl nodes with corresponding Chern number $C = 1 + (-1) = 0$.

### 4.2.4 Edge states

Since we started considering the Weyl semimetal model from the Hamiltonian Eq. 4.1, without introducing corresponding lattice model in real space, we can not directly calculate the dispersion in the finite sample as we did for graphene in Sec. 3.6. But, if we only consider the two touching bands, the effective Hamiltonian for them can be written in the same form as for graphene Eq. 3.43. This means we can use the results from studying the graphene edge states.

If we consider the multilayer material, stacked along the $z$ direction to be limited along the $y$ direction, the momentum components $k_x$ and $k_z$ will still be the good quantum numbers and

hence Hamiltonian will be block-diagonal with $k_x$ and $k_z$ being just the parameters in each block.

Then we can consider $k_z$ as parameter and once again look at the infinite sample case. For $k_z = \frac{\pi}{d} \pm k_0$, the Hamiltonian will be the same as for the graphene with only nearest neighbors interaction - gapless. For all the values of $-\frac{\pi}{d}+k_0 < k_z < \frac{\pi}{d}-k_0$ the Hamiltonian will be same as for graphene with the NNN interaction - gapped TI. For all other values of $k_z$ Hamiltonian will be same as for the graphene with potential energy term dominating over the NNN interaction term - gapped NI.

From section 3.6 we know that graphene has gapless chiral edge states when it is in gapped TI phase. These states have energy equal zero for $k_x = 0$ (see fig. 3.9). Hence we can conclude that the finite sample of 3D Weyl semimetal will have the chiral edge states at the Fermi energy $E_F = 0$ for each value of momentum $k_z$ between the two Weyl nodes. This means that the Fermi surface in the doped Weyl semimetal is a line (a straight line in the considered model). This line in $k_x - k_z$ plane is formed by the states of both positive and negative chirality, but same as in graphene, these states will be localied on opposite surfaces of the sample and hence on each surface there will be the states of one chirality.

## 4.3 Experimental observation

Despite the fact that the iridates and the multilayer heterostructures were the first proposals for the Weyl semimentals realization, the existence of Weyl semimetal phase in them was not confirmed experimentally yet. However, in the other material - Tantalum Arsenide (TaAs) the distinctive features of Weyl semimetal were recently observed using the angle-resolved photoemission spectroscopy (ARPES) by two independent groups [12, 13].

The ARPES experiment is conducted by sending the photons at the surface of material with sufficient amount of energy to rip the electrons from the surface. The initial energy and momentum of the photon are controlled and the energy and momentum of outgoing electrons

are measured. With such data one can use the conservation laws to find the energy and the momentum which electron had while it was at the surface of material.

The theoretical (tight binding model with spin-orbit coupling) predicts for TaAs 24 Weyl nodes at the same energy level. Both experimental groups [12, 13] where able to detect not only gapless states at the location of the Weyl nodes, but also the lines of surface states that connect pairs of Weyl nodes in momentum space and all have energy equal to the $E_F$. Since these lines form a Fermi surface of the material and since they were not straight on the experiment, these lines were named Fermi arcs. The existence of Fermi arcs was predicted by the theoretical models of Weyl semimetal. In the simplest model we considered above we obtained the straight line due to the presence of particle-hole symmetry in initial Hamiltonian. Such one-dimensional Fermi surfaces, that have end points, were never observed in any other 3D material, or theoretically predicted for any material. Hence this observation confirms the existence of Weyl semimetal phase in TaAs.

# Chapter 5

# Density response in Weyl metals

In this chapter we study the behavior of Weyl metal in the presence of the external magnetic field. We use the two node model of Weyl metal, reviewed in chapter 4. First we derive the corrections to the compressibility of the material and to the plasmon frequency caused by the magnetic field. We show that these corrections are nonanalytic functions of the magnetic field. Then we show that existence of two separate nodes of dispersion does not lead to the emergence of any excitation modes other than plasmon excitations.

## 5.1 Introduction

Weyl semimetals is a new class of Dirac materials, which attracted a lot of interest recently, following several theoretical proposals for their realization [8, 9, 10, 11]. The following theoretical prediction [23, 24, 25] and experimental observation of the very closely related *Dirac semimetals* [26, 27, 28] paved the way for the experimental observation of Weyl semimetals and in last few year two different types of Weyl semimentals were discovered [12, 13, 14].

Many of the unique physical properties of Weyl semimetals may be regarded as being distinct consequences of a common underlying phenomenon, the chiral anomaly [29, 30, 31, 32, 33, 34,

35, 36, 37]. Chiral anomaly [38, 39], first discovered in the particle physics context, manifests in anomalous nonconservation of the particle number of particular chirality in the presence of an external electromagnetic field. It is a purely quantum-mechanical phenomenon which plays an important role in the modern understanding of topologically-nontrivial phases of matter in general [40, 41, 42].

In the context of Weyl semimetals, an important problem is to identify experimentally measurable phenomena, which can be attributed unambiguously to chiral anomaly. There are several proposals in the literature, involving either anomalous magnetoresistance, [31, 34], coupling between collective modes, [43] or nonlocal transport [44]. In this thesis we focus on manifestations of chiral anomaly in density response of *Weyl metals*, which encompass both Weyl semimetals and doped Weyl semimetals, in which the Fermi energy is not too far from the Weyl nodes (what "not too far" means precisely will be explained below). We find that the density response of Weyl metals in an external magnetic field exhibits universal features, which are unique to Weyl metals, and may be regarded as yet another manifestation of chiral anomaly. In particular we find that Weyl metals, placed in an external magnetic field, possess a nonanalytic correction to the electronic compressibility and the plasma frequency, proportional to the magnitude of the magnetic field. We argue that this is a distinguishing smoking-gun feature of Weyl metals.

A necessary condition for the existence of a Weyl semimetal is the violation of either inversion or time reversal symmetry. This removes the Kramers degeneracy, which would otherwise preclude band touching points between pairs of nondegenerate bands. We will focus specifically on the case of broken time reversal symmetry, i.e. a magnetic Weyl metal. However, some of our results are in fact universal and independent of the specific realization of Weyl semimetal.

The rest of the chapter is organized as follows. In section 5.2 we review the properties of electron gas in the solid. In section 5.3 we present a general expected picture of density response in a ferromagnetic metal based on symmetry considerations. In section 5.4 we consider a specific simple model of a Weyl metal, based on a magnetically doped topological insulator

heterostructure. We demonstrate explicitly that the density response of a Weyl metal, at least at low doping levels away from the nodal Weyl semimetal, is expected to be qualitatively different from that of a regular ferromagnetic metal, discussed in section 5.3. In section 5.5 we find the plasmon collective mode frequencies of a Weyl metal in a magnetic field, explicitly considering both the cases of a clean and dirty Weyl metal. We conclude the chapter with a brief discussion of our results in section 5.6.

## 5.2 Random Phase Approximation for the electron gas

In this section we will review the application of Quantum Field Theory methods in Condensed Matter physics [45]. Here we will consider the example of the Coulomb gas in the solid. This will allow us to introduce all the methods we need to derive the properties of the Weyl metals in following sections of this chapter and also this will give us the opportunity to compare the properties of the electron gas in ordinary metal to those we will obtain for the Weyl metal.

We will start by considering N electrons, moving in homogeneous positively charged background, interacting with each other by the Coulomb force. The Hamiltonian can be written as

$$\hat{H} = \sum_{i=1}^{N} \frac{\hat{\vec{p}}_i^{\,2}}{2m} + \sum_{i<j} \frac{e^2}{|\hat{\vec{r}}_i - \hat{\vec{r}}_j|}, \tag{5.1}$$

where $\hat{\vec{p}}_i$ and $\hat{\vec{r}}_i$ are momentum and coordinate operators of i-th electron.

Next, we define the density operator:

$$\hat{\rho}(\vec{r}) = \sum_{i=1}^{N} \delta(\vec{r} - \vec{r}_i), \tag{5.2}$$

where $\delta(\vec{r})$ is the Dirac's delta function.

Then we can find the density operator in the momentum representation by performing the

Fourier transformation:

$$\hat{\rho}(\vec{k}) = \int d\vec{r} e^{-i\vec{k}\cdot\vec{r}} \hat{\rho}(\vec{r}) = \sum_{j=1}^{N} e^{-i\vec{k}\cdot\vec{r}_j}. \tag{5.3}$$

The interaction term in Hamiltonian can be expressed in terms of $\hat{\rho}(\vec{k})$ as well. In order to do that, we first find the Fourier decomposition of the Coulomb potential:

$$\int d\vec{r} e^{-i\vec{k}\cdot\vec{r}} \left(\frac{e^2}{r}\right) = \frac{4\pi e^2}{\vec{q}^{\,2}}, \tag{5.4}$$

$$\frac{e^2}{r} = \frac{1}{V} \sum_{q} \frac{4\pi e^2 e^{i\vec{q}\cdot\vec{r}}}{\vec{q}^{\,2}}, \tag{5.5}$$

where $V$ is the volume of the sample. We will consider the simplest shape of the sample - the cube with the side length $L$ with the periodic boundary conditions. Then, $V = L^3$. Periodic boundary conditions demand that the wave vector $\vec{q}$ is quantized:

$$\vec{q} = \frac{2\pi}{L}(n_x, n_y, n_z), \tag{5.6}$$

where $n_x$, $n_y$ and $n_z$ are integers. Since there is only one allowed value of $\vec{q}$ per volume $V_k = \left(\frac{2\pi}{L}\right)^3$ in wave vector space, we can transform summation over $\vec{q}$ into integration, assuming number of states is big:

$$\sum_{\vec{q}} = \left(\frac{L}{2\pi}\right)^3 \int d^3\vec{q} = V \int \frac{d^3\vec{q}}{(2\pi)^3}. \tag{5.7}$$

The term in, Eq. 5.4, corresponding to $\vec{q} = \vec{0}$ diverges, when we send $L$ to infinity.. But, since we have positively charged background, the static ($\vec{q} = \vec{0}$) term in Coulomb interaction should be zero, since numbers of protons and electrons in the sample are same. Having this cancellation in mind, we will omit the $\vec{q} = \vec{0}$ term in the sum over $\vec{q}$ in Eq. 5.5:. Then we can

rewrite the Coulomb potential term of Hamiltonian:

$$\begin{aligned}\sum_{i<j}\frac{e^2}{|\hat{\vec{r}}_i-\hat{\vec{r}}_j|} &= \sum_{i<j}\frac{1}{V}\sum_{\vec{q}\neq\vec{0}}\frac{4\pi e^2}{\vec{q}^{\,2}}e^{i\vec{q}\cdot(\hat{\vec{r}}_i-\hat{\vec{r}}_j)} \\ &= \frac{1}{V}\sum_{\vec{q}\neq\vec{0}}\frac{4\pi e^2}{\vec{q}^{\,2}}\left(\frac{1}{2}\sum_i e^{i\vec{q}\cdot\hat{\vec{r}}_i}\sum_j e^{-i\vec{q}\cdot\hat{\vec{r}}_j}-\frac{N}{2}\right) \\ &= \frac{1}{V}\sum_{\vec{q}\neq\vec{0}}\frac{2\pi e^2}{\vec{q}^{\,2}}\left(\hat{\rho}(\vec{q})\hat{\rho}(-\vec{q})-N\right). \end{aligned} \tag{5.8}$$

Using the second quantization notations, we can rewrite Hamiltonian as

$$\begin{aligned}\hat{H} &= \int d^3\vec{r}\sum_\sigma \hat{\psi}^+_\sigma(\vec{r})\left(-\frac{\hbar^2}{2m}\vec{\nabla}^2-\mu\right)\hat{\psi}_\sigma(\vec{r}) \\ &+\frac{1}{V}\sum_{\vec{q}\neq\vec{0}}\frac{2\pi e^2}{\vec{q}^{\,2}}\left(\hat{\rho}(\vec{q})\hat{\rho}(-\vec{q})-N\right), \end{aligned} \tag{5.9}$$

where $\sigma$ labels the spin states and takes values "+" and "-". Density operator includes electrons with all spins, hence

$$\hat{\rho}(\vec{r}) = \sum_\sigma \hat{\psi}^+_\sigma(\vec{r})\hat{\psi}_\sigma(\vec{r}). \tag{5.10}$$

In order to transform first term into the momentum representation, we rewrite field operators as

$$\hat{\psi}_\sigma(\vec{r}) = \frac{1}{\sqrt{V}}\sum_{\vec{k}} e^{i\vec{k}\cdot\vec{r}}\hat{a}_{\vec{k}\,\sigma}, \tag{5.11}$$

$$\hat{\psi}^+_\sigma(\vec{r}) = \frac{1}{\sqrt{V}}\sum_{\vec{k}} e^{-i\vec{k}\cdot\vec{r}}\hat{a}^+_{\vec{k}\,\sigma}. \tag{5.12}$$

Using Eqs. 5.11 and 5.12, we can rewrite the density operator in Fourier components of the field operators:

$$\hat{\rho}(\vec{q}) = \sum_{\vec{k},\sigma}\hat{a}^+_{\vec{k}\,\sigma}\hat{a}_{\vec{k}+\vec{q}\,\sigma}. \tag{5.13}$$

Now we can write all part of Hamiltonian in terms of the operators $C$:

$$\hat{H} = \sum_{\vec{k},\sigma} \left( \frac{\hbar^2 \vec{k}^{\,2}}{2m} - \mu \right) \hat{a}^+_{\vec{k}\,\sigma} \hat{a}_{\vec{k}\,\sigma} + \frac{1}{V} \sum_{\vec{q}\neq\vec{0}} \frac{2\pi e^2}{\vec{q}^{\,2}} \left( \sum_{\vec{k},\vec{k'},\sigma,\sigma'} (\hat{a}^+_{\vec{k}\,\sigma} \hat{a}_{\vec{k}+\vec{q}\,\sigma} \hat{a}^+_{\vec{k'}\,\sigma'} \hat{a}_{\vec{k'}-\vec{q}\,\sigma'}) - N \right). \quad (5.14)$$

The last term here is not an operator and gives only a constant shift of energy scale, hence we can get rid of it by redefining the zero of energy.

Next, we want to use the path integral formalism to derive the properties of the system. But it is well known, that path integrals can be performed exactly only for quadratic functions of operators. In all other cases one has to use some small parameter expansion around the quadratic case. Our Hamiltonian contains quadratic term, that comes from the kinetic energy and the fourth power term, that comes from Coulomb interaction. Hence, the use of path integral formalism can only be helpful if the Coulomb interaction contribution to Hamiltonian is much smaller than the kinetic energy contribution.

In order to estimate the contributions of kinetic and potential energy to Hamiltonian we will consider that the average distance between electrons is $d$. Then

$$V = \frac{4\pi r^3}{3} N, \quad (5.15)$$

where $r = d/2$ - is the radius of the volume where we, on average, find one electron.

The Heisenberg uncertainty principle tells us that

$$\Delta r_x \Delta p_x \geq \hbar/2. \quad (5.16)$$

The kinetic energy will be minimal, if all the electrons have even $\Delta r_x \sim d$. Then the energy per one electron is

$$E_k = \frac{\vec{p}_i^{\,2}}{2m} \geq \frac{(\hbar/2)^2}{2m(d/2)^2} = \frac{\hbar^2}{2md^2}. \quad (5.17)$$

The potential energy for one electron is

$$E_C \sim \frac{e^2}{d}, \quad (5.18)$$

if we don't take into account the numeric prefactor, that arises from the summation over all other electrons.

Now we can compare the two contributions:

$$r_s = \frac{E_C}{E_k} \leq \frac{me^2}{\hbar^2} d = \frac{d}{r_B}, \tag{5.19}$$

where $r_B$ is the Bohr radius. The dimensionless parameter $r_s$ shows us if the path integral approach will give a converging expansion. If $r_s \ll 1$, we can expect that expanding in powers of $e$ and calculating only few terms in the path integral will give us a good approximation of the solution.

Therefore, in the case when density of electrons is big, $r_s \ll 1$ and we can use the path integrals. We start by writing the partition function for our system:

$$Z = \int \mathcal{D}\bar{\psi}\mathcal{D}\psi e^{-S}. \tag{5.20}$$

For the rest of this chapter we will use the units where $\hbar = c = 1$, then the action $S$ can be written as

$$\begin{aligned} S \;&= \int_0^\beta d\tau \Bigg( \int d^3\vec{r} \sum_\sigma \bar{\psi}(\vec{r},\tau) \left[ \partial_\tau - \frac{\vec{\nabla}^2}{2m} - \mu \right] \psi_\sigma(\vec{r},\tau) \\ &\quad + \frac{1}{V} \sum_{\vec{q}\neq\vec{0}} \frac{2\pi e^2}{\vec{q}^{\,2}} \left[ \rho(\vec{q},\tau)\rho(-\vec{q},\tau) - N \right] \Bigg). \end{aligned} \tag{5.21}$$

Since the second term in the action has the fourth power, when expressed in electron creation and annihilation operators, we can not calculate the path partition function Eq. 5.20 directly. This is why we introduce a new field and use the Stratonovich-Hubbard identity:

$$\begin{aligned} exp \;&\left( - \int_0^\beta d\tau \frac{1}{V} \sum_{\vec{q}\neq\vec{0}} \frac{2\pi e^2}{\vec{q}^{\,2}} \left[ \rho(\vec{q},\tau)\rho(-\vec{q},\tau) - N \right] \right) \\ = \;& \int \mathcal{D}\phi(\vec{q},\tau) exp \Bigg( - \frac{1}{8\pi} \int_0^\beta d\tau \sum_{\vec{q}\neq\vec{0}} \vec{q}^{\,2} \phi(\vec{q},\tau)\phi(-\vec{q},\tau) \\ & - \int_0^\beta d\tau \frac{ie}{2\sqrt{V}} \sum_{\vec{q}\neq\vec{0}} \left[ \phi(\vec{q},\tau)\rho(-\vec{q},\tau) + \rho(\vec{q},\tau)\phi(-\vec{q},\tau) \right] \Bigg). \end{aligned} \tag{5.22}$$

This identity allows us to substitute the fourth power term in action by the interaction with the auxiliary field $\phi$. Since $\rho(\vec{r})$ was real valued, in momentum representation it has to satisfy $\rho^*(\vec{q}) = \rho(-\vec{q})$ and the same way $\phi^*(\vec{q}) = \phi(-\vec{q})$.

Using the Eq. 5.22, we can rewrite the partitition function Eq. 5.20 as

$$Z = \int \mathcal{D}\bar{\psi}\mathcal{D}\psi\mathcal{D}\phi e^{-S(\bar{\psi},\psi,\phi)}, \tag{5.23}$$

where

$$S(\bar{\psi},\psi,\phi) = \int_0^\beta d\tau \int d^3r \left( \frac{1}{8\pi}(\vec{\nabla}(\vec{r},\tau))^2 \right.$$
$$\left. + \sum_\sigma \bar{\psi}_\sigma(\vec{r},\tau) \left[ \partial_\tau - \frac{1}{2m}\vec{\nabla}^2 - \mu + ie\phi(\vec{r},\tau) \right] \psi_\sigma(\vec{r},\tau) \right) - \frac{N}{V} \sum_{\vec{q}\neq\vec{0}} \frac{2\pi e^2}{\vec{q}^{\,2}}. \tag{5.24}$$

The last term in Eq. 5.24 does not have any field operators in it and hence We will label it

$$-\frac{N}{V} \sum_{\vec{q}\neq\vec{0}} \frac{2\pi e^2}{\vec{q}^{\,2}} = C \tag{5.25}$$

to shorten the notations. Since the action Eq. 5.24 is now quadratic in $\bar{\psi}$ and $\psi$, the path integration over this variables is Gaussian and can be formally performed. Then we find:

$$Z = \int \mathcal{D}\phi exp\left( -\int_0^\beta d\tau \int d^3\vec{r} \frac{(\vec{\nabla}\phi)^2}{8\pi} + C \right) \times \left( det\left[ \partial_\tau - \frac{\vec{\nabla}^2}{2m} - \mu + ie\phi(\vec{r},\tau) \right] \right)^2. \tag{5.26}$$

The determinant in Eq. 5.26 appears because the Eq. 5.24 is the quadratic form of the vector $\psi_\sigma(\vec{r},\tau)$ and hence the operator in square brackets in Eq. 5.26 has all the pairs of $(\vec{r},\tau)$ as its indexes. Determinant in Eq. 5.26 is squared, because index $\sigma$ in Eq. 5.24 has two values and hence there are effectively two identical quadratic forms in Eq. 5.24.

Since the determinant in Eq. 5.26 contains the differential operators, we can use the fact that determinant does not depend on basis and perform the Fourier transformation from basis $(\vec{r},\tau)$ to the basis $(\vec{q},\omega_n)$. Since operators $\bar{\psi}$ and $\psi$ are fermions, $\omega_n = \frac{(2n+1)\pi}{\beta}$ are the Matsubara

frequencies of fermions and $n$ is an integer number. For the Fourier transformation of the field $\phi$ we get:

$$\phi(\vec{r},\tau) = \frac{1}{\sqrt{\beta V}} \sum_{\vec{q},\omega_l} e^{-i\omega_l\tau + i\vec{q}\cdot\vec{r}} \phi(\vec{q},\omega_l), \tag{5.27}$$

where

$$\omega_l = \frac{2\pi l}{\beta} \tag{5.28}$$

are the Matsubara frequencies of bosons and $l$ is an integer number.

Now we can write the determinant from Eq. 5.26 in the new basis:

$$\begin{aligned} &det\left(\left[\partial_\tau - \frac{\vec{\nabla}^2}{2m} - \mu + ie\phi(\vec{r},\tau)\right]_{(\vec{k},\omega_n),(\vec{k}',\omega_m)}\right) \\ &= det\left(\left[-i\omega_n + \frac{\vec{k}^{\,2}}{2m} - \mu\right]\delta_{\vec{k},\vec{k}'}\delta_{\omega_n,\omega_m} + \frac{ie}{\sqrt{\beta V}}\phi(\vec{k}-\vec{k}',\omega_n-\omega_m)\right). \end{aligned} \tag{5.29}$$

Using the multi-index $k = (\vec{k},\omega_n)$, we can write matrix elements of Eq. 5.29 in the following form:

$$M_{k,k'} = (M_0)_{k,k'} + (M_1)_{k,k'} = -G_0^{-1}(k)\delta_{k,k'} + \frac{ie}{\sqrt{\beta V}}\phi(k-k'), \tag{5.30}$$

where $G_0(k)$ is the Green function of the free fermions, given by

$$G_0(k) = G_0(\vec{k},\omega_n) = \frac{1}{i\omega_n - \epsilon_{\vec{k}}}. \tag{5.31}$$

And $\epsilon_{\vec{k}}$ is the kinetic energy minus the chemical potential:

$$\epsilon_{\vec{k}} = \frac{\vec{k}^{\,2}}{2m} - \mu. \tag{5.32}$$

By defining the effective action

$$S_{eff}(\phi) = \int_0^\beta d\tau \int d^3\vec{r} \frac{(\vec{\nabla}\phi(\vec{r},\tau))^2}{8\pi} - 2\ ln\ det\ M + C, \tag{5.33}$$

we can put all the terms in Eq. 5.26 into one exponent:

$$Z = \int \mathcal{D}\phi \; e^{-S_{eff}(\phi)}. \tag{5.34}$$

Since the matrices $M$, $M_0$ and $M_1$ are Hermitian, we can use the matrix identities

$$\begin{aligned} &ln\ det\ A = Tr\ ln\ A, \\ &Tr(AB) = TrA + TrB. \end{aligned} \tag{5.35}$$

This allows us to write

$$\begin{aligned} ln\ det\ M &= Tr\ ln\ M = Tr\ ln(M_0 + M_1) \\ &= Tr\ ln(-G_0^{-1} + M_1) = Tr\ ln((-G_0^{-1})(1 - G_0 M_1)) \\ &= Tr\ ln(-G_0^{-1}) + Tr\ ln(1 - G_0 M_1). \end{aligned} \tag{5.36}$$

The first term in Eq. 5.36 does not have any field operators in it, same as the term Eq. 5.25 and hence it will give one more constant contribution to the action, which we can name $C_1$:

$$Z = \int \mathcal{D}\phi \; exp\left( - \int_0^\beta d\tau \left[ \frac{(\vec{\nabla}\phi)^2}{8\pi} + 2\ Tr\ ln(1 - G_0 M_1) \right] + C + C_1 \right). \tag{5.37}$$

Since terms $C$ and $C_1$ give only an extra constant factor after the integration, trowing away this factor is equivalent to the shift of energy scale and hence does not affect the properties of the system. Therefore we will drop the constants $C$ and $C_1$. Then we finally get

$$Z = \int \mathcal{D}\phi \; exp\left( - \int_0^\beta d\tau \left[ \frac{(\vec{\nabla}\phi)^2}{8\pi} + 2\ Tr\ ln(1 - G_0 M_1) \right] \right). \tag{5.38}$$

The scalar bosonic field $\phi$ in Eq. 5.38, that mediates the electromagnetic interaction between the electrons, is the same as the the scalar electromagnetic potential $\Phi$ introduced in chapter 2.

We now have the partition function written in terms of path integral over the electromagnetic potential $\phi$ only. The effective action, aside from quadratic in $\phi$ term, contains as well the $\phi$

operator under the logarithm, hence we can not simplify it any further exactly and we have to use the approximation of weak interaction. As it was discussed at the beginning of this section, such approximation is valid when $r_s \ll 1$ (see Eq. 5.19). Since interaction term has the factor of $e$, expanding expression in powers of $r_s$ is equivalent to expanding in powers of $e$. Hence, we will use $e$ as small parameter. For the logarithmic term we can use the Taylor expansion

$$ln(1-x) = -\sum_{n=1}^{\infty} \frac{x^n}{n} \tag{5.39}$$

and write

$$ln(1-G_0M_1) = -\sum_{n=1}^{\infty} \frac{(G_0M_1)^n}{n}. \tag{5.40}$$

In the lowest, the first, order in $e$ we get:

$$Tr\ G_0M_1 \ = \sum_{k,k'} (G_0)_{k,k'}(M_1)_{k',k} = \sum_k G_0(k)(M_1)_{k,k} = \sum_k G_0(k) \left( \frac{ie\ \phi(0)}{\sqrt{\beta V}} \right). \tag{5.41}$$

When we introduced the field $\phi$ in Eq. 5.22, we excluded the $\vec{q} = \vec{0}$ term, because of the total charge of the sample being zero. Hence, we have to put $\phi(0) = 0$. Then the whole first order contribution (Eq. 5.41 ) is zero.

In the second order we get:

$$\begin{aligned} \tfrac{1}{2}Tr(G_0M_1)^2 \ &= \frac{1}{2} \sum_{k,k'} G_0(k)(M_1)_{k,k'} G_0(k')(M_1)_{k',k} \\ &= \frac{1}{2} \sum_{q,k} G_0(k)(M_1)_{k,k+q} G_0(k+q)(M_1)_{k+q,k} \\ &= -\frac{e^2}{2\beta V} \sum_q \left( \sum_k G_0(k)G_0(k+q) \right) \phi(q)\phi(-q). \end{aligned} \tag{5.42}$$

If we define the polarization function

$$\Pi(q) = \frac{2}{\beta V} \sum_k G_0(k)G_0(k+q), \tag{5.43}$$

the effective action from Eq. 5.38 can be written as

$$S_{eff} = \sum_q \left( \frac{\vec{q}^{\,2}}{8\pi} - \frac{1}{2} e^2 \Pi(q) \right) \phi(q)\phi(-q) + O(e^4)\phi^4. \tag{5.44}$$

Since the initial interaction was proportional to $e^2$, all the odd powers in expansion cancel out and hence the second non-zero term in expansion contains the forth power of $e$.

Since we are considering $r_s \ll 1$, we will neglect all the terms of power higher than two. This approximation is called Random Phase Approximation and is justified for high density of electrons. With such approximation action becomes quadratic and does not contain any off-diagonal terms, connecting different values of $q$. Then we can directly read the inverse of Green function for the potential $\phi$ from Eq. 5.44:

$$D^{-1}(q) = \frac{\vec{q}^{\,2}}{4\pi} - e^2 \Pi(q). \tag{5.45}$$

The difference by factor of two here appears, because sum in Eq. 5.44 runs trough each value of $q$ twice.

Now we need to calculate the polarization function $\Pi(q)$. Substituting Eq. 5.31 into Eq. 5.43, we get

$$\Pi(\vec{q}, \omega_l) = \frac{2}{\beta V} \sum_{\vec{k}, \omega_n} \frac{1}{i\omega_l + i\omega_n - \epsilon_{\vec{k}+\vec{q}}} \cdot \frac{1}{i\omega_n - \epsilon_{\vec{k}}}. \tag{5.46}$$

After performing the summation over the frequencies, we obtain

$$\Pi(\vec{q}, \omega_l) = \frac{2}{V} \sum_{\vec{k}} \frac{f(\epsilon_{\vec{k}}) - f(\epsilon_{\vec{k}+\vec{q}})}{i\omega_l + \epsilon_{\vec{k}} - \epsilon_{\vec{k}+\vec{q}}}, \tag{5.47}$$

where $f(\epsilon)$ is the Fermi distribution

$$f(x) = \frac{1}{e^{\beta x} + 1}. \tag{5.48}$$

Summation over $\vec{k}$ can not be done analytically in general case, hence we will consider only the case when $\vec{q}$ is much smaller than $k_F$. Then all the Fermi distributions can be expanded in

powers of $\vec{q}$ and we obtain in the first order:

$$\Pi(\vec{q},\omega_l) = -2\rho_0 \left(1 - \frac{\omega_l}{v_F|\vec{q}|} \tan^{-1}\left[\frac{v_F|\vec{q}|}{\omega_l}\right]\right), \tag{5.49}$$

where

$$v_F = \frac{k_F}{m} \tag{5.50}$$

$$\rho_0 = \frac{2mk_F}{(2\pi)^2} \tag{5.51}$$

are the Fermi velocity and the density of states at Fermi surface.

The polarization function $\Pi(\vec{q},\omega_l)$ describes the correction, compared with non-interacting system, to the propagation of excitations with energy $\omega_l$ and wave vector $\vec{q}$. We now can consider the limiting cases of $\Pi(\vec{q},\omega_l)$: the static case, when $|\omega_l| << v_F|\vec{q}|$ and the dynamic case, when $|\omega_l| >> v_F|\vec{q}|$. In the first case, when the frequency is small in comparison with $v_F|\vec{q}|$, we can use the approximation $tan^{-1}x \approx \frac{\pi}{2}\ sign\ (x)$ and obtain

$$\Pi(\vec{q},\omega_l) \approx -2\rho_0(1 - \frac{\pi|\omega_l|}{2v_F|\vec{q}|}). \tag{5.52}$$

The Green function of field $\phi$ takes form

$$D(\vec{q},\omega_l) \approx \frac{4\pi}{\vec{q}^{\,2} + 8\pi e^2\rho_0(1 - \frac{\pi|\omega_l|}{2v_F|\vec{q}|})}. \tag{5.53}$$

Using the analytical continuation of this function in the upper half plane we can obtain the retarded Green function. In order to do that we substitute $i\omega_l$ by $\omega + i\delta$, where $\delta$ is small positive number, and then send $\delta$ to zero. Then we get:

$$D^R(\vec{q},\omega) \approx \frac{4\pi}{\vec{q}^{\,2} + 8\pi e^2\rho_0(1 + \frac{i\pi\omega}{2v_F|\vec{q}|})}. \tag{5.54}$$

The imaginary term here represents the damping of the excitations with corresponding frequency and wave vector.

In the stationary case when $\omega = 0$

$$D^R(\vec{q}, 0) = D(\vec{q}, 0) = \frac{4\pi}{\vec{q}^{\,2} + \lambda^{-2}}, \tag{5.55}$$

where $\lambda = (8\pi e^2 \rho_0)^{-1/2}$ is the characteristic length of the interaction. If we use the Fourier transformation, in real space we obtain

$$D^R(\vec{r}, 0) = D(\vec{r}, 0) = \frac{e^{-|\vec{r}|/\lambda}}{|\vec{r}|}. \tag{5.56}$$

Hence, in the case of stationary charge, Coulomb force does not decay polynomially as in empty space, but is damped exponentially as the distance exceeds the characteristic length $\lambda$. This effect is know as the screening of the potential and can be expected even in the classical model of the solid: If we place a point charge in the material, opposite charges around will move closer to it, alike charges will move further away. At some length scale $\lambda$ this will even out the inhomogeneity in charge distribution. Beyond this scale the region will appear neutral and there will be no Coulomb force. Due to this screening interpretation, $\lambda$ is also called the screening length.

Let's now consider the case of other limit - when frequency $\omega_l$ is much bigger $v_F|\vec{q}|$. In this case we can use $tan^{-1}x \approx x - \frac{x^3}{3}$ and write

$$\Pi(\vec{q}, \omega_l) \approx -\frac{2\ \rho_0\ v_F^2\ \vec{q}^{\,2}}{3\ \omega_l}. \tag{5.57}$$

Using the relation

$$\rho_0 v_F^2 = \frac{3N}{2mV}, \tag{5.58}$$

we can write

$$D(\vec{q}, \omega_l) \approx \frac{4\pi}{\vec{q}^{\,2}(1 + \omega_p^2/\omega_l^2)}, \tag{5.59}$$

where

$$\omega_p = \sqrt{\frac{4\pi N e^2}{mV}}. \tag{5.60}$$

Similarly to Eq. 5.54 we can write the retarded Green function in the dynamic case as

$$D^R(\vec{q},\omega) \approx \frac{4\pi}{\vec{q}^{\,2}(1-\omega_p^2/\omega^2)}. \tag{5.61}$$

The right hand side of Eq. 5.61 diverges, when $\vec{q}=\vec{0}$ and $\omega=\omega_p$, which corresponds to the undamped collective excitations in the system. Such excitations are called plasma oscillations and hence their frequency $\omega_p$ is called plasma frequency.

## 5.3 Density response of a ferromagnetic metal in an external magnetic field

We will begin with a simple symmetry-based picture of the density response of a ferromagnetic metal, placed in an external magnetic field. For simplicity of the presentation we will focus here only on the orbital effect of the external field. We will however discuss the effects of the Zeeman splitting separately in the discussion section.

Suppose we have a ferromagnetic metal with a uniform and time-independent magnetization along the $z$-direction. Let us also apply an external magnetic field in the $z$-direction $\vec{B}=B\hat{z}$, where $B$ can be either positive or negative and use the Landau gauge $\vec{A}=xB\hat{y}$. We will assume that the magnetic field can have a smooth temporal and spatial variation.

First, we integrate out electron variables as it was done in section 5.2 to obtain an effective action for the electromagnetic field, which encodes the electromagnetic response of the metal. To the first order in the magnetic field, this action will have the following general form

$$\begin{aligned} S = \sum_{\vec{q},i\Omega} \Bigg[ & \left(\frac{\vec{q}^{\,2}}{8\pi} - \frac{e^2}{2}\Pi_0(\vec{q},i\Omega)\right)\varphi(\vec{q},i\Omega)\varphi(-\vec{q},-i\Omega) \\ - & \frac{e^2}{2}\Pi_1(\vec{q},i\Omega)\varphi(\vec{q},i\Omega)q_x A_y(-\vec{q},-i\Omega) \\ - & \frac{e^2 B}{2}\,\Pi_2(\vec{q},i\Omega)\varphi(\vec{q},i\Omega)\varphi(-\vec{q},-i\Omega)+\ldots\Bigg], \end{aligned} \tag{5.62}$$

where $\varphi(\vec{q}, i\Omega)$ is the scalar electromagnetic potential. The first term in Eq. 5.62 describes the standard electronic polarization processes in the absence of the external magnetic field Eq. 5.44. The second and third terms couple density and magnetic responses, which is allowed by symmetry in any magnetic material. In particular, the second term, which may be regarded as a three-dimensional (3D) generalization of the Chern-Simons term, describes the anomalous Hall response, written in Landau gauge. The last term in Eq. 5.62 may be thought of as a magnetic field-induced correction to the electronic compressibility of the ferromagnet. Indeed, let us consider the static limits of the $\Pi_1(\vec{q}, i\Omega)$ and $\Pi_2(\vec{q}, i\Omega)$ response functions. We have

$$\sigma_{xy}^{II} = \lim_{\vec{q}\to 0} \lim_{i\Omega\to 0} e^2 \Pi_1(\vec{q}, i\Omega) = e \left(\frac{\partial N}{\partial B}\right)_\mu , \tag{5.63}$$

and

$$\frac{\partial \kappa}{\partial B} = \lim_{\vec{q}\to 0} \lim_{i\Omega\to 0} \Pi_2(\vec{q}, i\Omega) = \frac{\partial^2 N}{\partial \mu \partial B} = \frac{1}{e} \frac{\partial \sigma_{xy}^{II}}{\partial \mu}. \tag{5.64}$$

Here $\sigma_{xy}^{II}$ is a thermodynamic equilibrium part of the anomalous Hall conductivity [46] and $\kappa$ is the electronic compressibility. The last relation can be viewed as simply a derivative of the Streda formula for the Hall conductivity Eq. 5.63 with respect to the chemical potential. Thus any ferromagnetic metal has a linear in magnetic field correction to its compressibility, which is proportional to the derivative of the equilibrium part of its intrinsic anomalous Hall conductivity with respect to the chemical potential. This is very closely related to what has been described as "Berry phase correction to the electron density of states in solids" by Xiao, Shi and Niu, [47] and can be argued to be present in any ferromagnetic metal, based only on symmetry considerations. In this chapter we will argue that a Weyl metal is distinguished from an ordinary ferromagnetic metal by the *absence* of such a linear in magnetic field correction to the compressibility. Instead, there is a nonanalytic correction to the compressibility, proportional to the *magnitude* of the magnetic field and which can be associated with the Weyl nodes. The analytic linear in the field correction appears only when the Fermi energy is sufficiently far from the Weyl nodes. In the following section we will demonstrate this explicitly for a simple model of a Weyl semimetal in a magnetically doped multilayer heterostructure, introduced by Burkov [10].

## 5.4 Density response in a Weyl metal

We start from the model of a Weyl semimetal in a heterostructure, made of alternating layers of topological (TI) and ordinary (NI) insulators, doped with a sufficient concentration of magnetic impurities to produce a ferromagnetic state [10].

If we modify the momentum operator in Eq. 4.2 to include the external magnetic field, the Hamiltonian will take the following form

$$\mathcal{H}(k_z) = v_F \tau^z (\hat{z} \times \vec{\sigma}) \cdot \left( -i\vec{\nabla} + e\vec{A} \right) + \hat{\Delta}(k_z) + b\sigma^z, \tag{5.65}$$

where $\hat{\Delta}(k_z) = \Delta_S \tau^x + \frac{1}{2}(\Delta_D \tau^+ e^{ik_z d} + H.c.)$ is the interlayer tunneling operator, partially diagonalized by Fourier transform with respect to the layer index and $k_z$ is the corresponding component of the crystal momentum, defined in the first Brillouin zone (BZ) $(-\pi/d, \pi/d)$ of the multilayer superlattice. The $\vec{\sigma}$ Pauli matrices act on the real spin degrees of freedom while the $\vec{\tau}$ ones act on the pseudospin degrees of freedom, describing the top and bottom surfaces in the TI layers. $b$ is the spin splitting due to magnetized impurities and $\vec{A}$ is the vector potential of the externally applied magnetic field. And we are using the units in which $\hbar = c = 1$. Finally, we will neglect the Zeeman spin splitting due to the field, but will consider its effects in the Discussion section.

After the canonical transformation $\sigma^\pm \to \tau^z \sigma^\pm$, $\tau^\pm \to \sigma^z \tau^\pm$, the Hamiltonian takes the form in which the spin and pseudospin degrees of freedom decouple

$$\mathcal{H}(k_z) = v_F (\hat{z} \times \vec{\sigma}) \cdot \left( -i\vec{\nabla} + e\vec{A} \right) + [b + \hat{\Delta}(k_z)]\sigma^z. \tag{5.66}$$

The tunneling operator can now be diagonalized separately from the rest of the Hamiltonian, which gives

$$\mathcal{H}_t(k_z) = v_F (\hat{z} \times \vec{\sigma}) \cdot \left( -i\vec{\nabla} + e\vec{A} \right) + m_t(k_z)\sigma^z. \tag{5.67}$$

Here $t = \pm$ labels the two distinct eigenvalues of the tunneling operator $t\Delta(k_z)$, where $\Delta(k_z) = \sqrt{\Delta_S^2 + \Delta_D^2 + 2\Delta_S \Delta_D \cos(k_z d)}$, and $m_t(k_z) = b + t\Delta(k_z)$. The corresponding eigenvectors of

the tunneling operator are given by

$$|u^t_{k_z}\rangle = \frac{1}{\sqrt{2}}\left(1, t\frac{\Delta_S + \Delta_D e^{-ik_z d}}{\Delta(k_z)}\right). \tag{5.68}$$

The two-component spinor $|u^t_{k_z}\rangle$ is a vector in the $\tau$-pseudospin space. To diagonalize the remaining Hamiltonian, we orient the external magnetic field in the growth direction ($\hat{z}$), and pick the Landau gauge $\vec{A} = xB\hat{y}$. In the present model, this allows for a full analytic solution for the Landau levels. Our results are not restricted to this special orientation of the magnetic field, however. For the continuity of presentation, we defer the discussion of effect of the orientation of the field on our results until Section 5.6. It is then easily shown [48] that the eigenstates of $\mathcal{H}_t(k_z)$ have the following form

$$|n, k_y, k_z, s, t\rangle = v^{st}_{nk_z\uparrow}|n-1, k_y, \uparrow\rangle + v^{st}_{nk_z\downarrow}|n, k_y, \downarrow\rangle, \tag{5.69}$$

if $B > 0$ and the $\uparrow$ and $\downarrow$ are interchanged if $B < 0$. Here

$$\langle\vec{r}|n, k_y, \sigma\rangle = \phi_{nk_y}(\vec{r})|\sigma\rangle, \tag{5.70}$$

and $\phi_{n,k_y}(\vec{r})$ are the Landau gauge orbital wavefunctions. $s = \pm$ labels the electron-like and hole-like sets of Landau levels

$$\epsilon_{nst}(k_z) = s\sqrt{2\omega_B^2 n + m_t^2(k_z)} = s\epsilon_{nt}(k_z), n \geq 1, \tag{5.71}$$

and the corresponding eigenvectors $|v^{st}_n\rangle$ are given by

$$|v^{st}_{nk_z}\rangle = \frac{1}{\sqrt{2}}\left(\sqrt{1 + s\frac{m_t(k_z)}{\epsilon_{nt}(k_z)}}, -is\sqrt{1 - s\frac{m_t(k_z)}{\epsilon_{nt}(k_z)}}\right), \tag{5.72}$$

where $|v^{st}_{nk_z}\rangle$ is a vector in the $\sigma$-pseudospin space.

The $n = 0$ Landau level is anomalous, as it is the only Landau level that does not consist of two symmetric electron and hole-like partners. Its energy eigenvalues are given by

$$\epsilon_{0t}(k_z) = -m_t(k_z)\text{sign}(B) \tag{5.73}$$

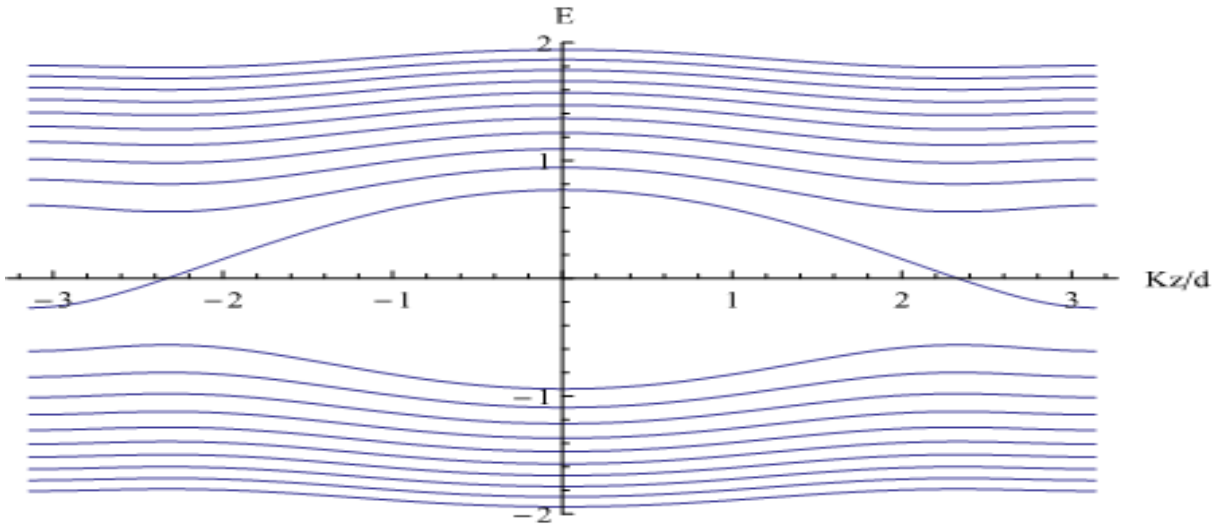


Figure 5.1: Energy as function of $k_z$ for the Weyl metal in external magnetic field. All the Landau level up to $n = 10$ are shown. On this example $\Delta_S = 1/2\Delta_D$,$b = 0.75\Delta_D$, $\omega_B = 0.4\Delta_D$, $B_z > 0$.

and

$$|v_0^t\rangle = (0, 1), \tag{5.74}$$

when $B > 0$ and

$$|v_0^t\rangle = (1, 0), \tag{5.75}$$

when $B < 0$.

All the levels up to $n = 10$ are show at Fig. 5.1.

The dependence of the energy of the $n = 0$ Landau levels on the sign of the magnetic field in Eq. 5.73 is important and will play a significant role in what follows. To simplify the notation we can introduce a composite index $a = (s, t)$ and a tensor product eigenvector

$$|z_{nk_z}^a\rangle = |v_{nk_z}^a\rangle \otimes |u_{k_z}^a\rangle. \tag{5.76}$$

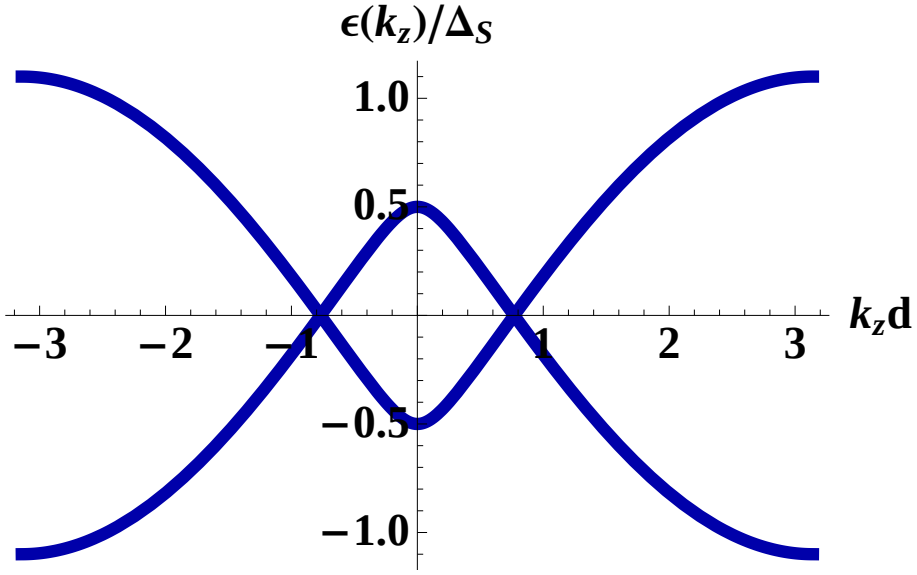


Figure 5.2: Plot of the band edges along the $z$-direction in momentum space for the two bands that touch at the Weyl nodes in the absence of the magnetic field.

We can now evaluate the density response. It is convenient to use the Landau level basis, introduced above, for this calculation and take the magnetic field to be static and uniform from the start. Integrating out electron variables in the presence of a fluctuating scalar potential $\varphi$, which mediates Coulomb interactions between the electrons, we obtain the following Matsubara action for $\varphi(\vec{q}, i\Omega)$:

$$S = \frac{1}{2}\sum_{\vec{q},i\Omega}\left[\frac{\vec{q}^{\,2}}{4\pi} - e^2\Pi(\vec{q}, i\Omega)\right]\varphi(\vec{q}, i\Omega)\varphi(-\vec{q}, -i\Omega), \tag{5.77}$$

where the response function $\Pi(\vec{q}, i\Omega)$ is given by

$$\begin{aligned}\Pi(\vec{q}, i\Omega) &= \frac{1}{2\pi\ell_B^2 L_z}\sum_{n,a,a',k_z}|\langle z^a_{nk_z+q}|z^{a'}_{nk_z}\rangle|^2 \\ &\times \frac{n_F[\xi_{na'}(k_z)] - n_F[\xi_{na}(k_z+q)]}{i\Omega + \xi_{na'}(k_z) - \xi_{na}(k_z+q)},\end{aligned} \tag{5.78}$$

where $\ell_B = 1/\sqrt{e|B|}$ is the magnetic length. We have assumed here that $\vec{q} = q\hat{z}$, i.e. we are interested only in the collective modes, propagating along the direction of the magnetic field,

since only in this case does one get an anomalous contribution to the density response. In this case Landau levels with different indices $n$ are not mixed in Eq. 5.78. Furthermore, it is easy to convince oneself that only $a = a'$ contributions are important in determining collective mode dispersions, at least for small values of $q$. In this case, we can take $\langle z^a_{nk_z+q} | z^a_{nk_z} \rangle \approx 1$ and Eq. 5.78 simplifies to

$$\Pi(\vec{q}, i\Omega) = \frac{1}{2\pi\ell_B^2 L_z} \sum_{n,s,t,k_z} \frac{n_F[\xi_{nst}(k_z)] - n_F[\xi_{nst}(k_z+q)]}{i\Omega + \xi_{nst}(k_z) - \xi_{nst}(k_z+q)}. \tag{5.79}$$

It is convenient to explicitly separate contributions from the anomalous $n = 0$ Landau levels and the rest. We obtain:

$$\Pi(\vec{q}, i\Omega) = \Pi_0(\vec{q}, i\Omega) + \Pi_1(\vec{q}, i\Omega), \tag{5.80}$$

where

$$\Pi_0(\vec{q}, i\Omega) = \frac{1}{2\pi\ell_B^2 L_z} \sum_{t,k_z} \frac{n_F[\xi_{0t}(k_z)] - n_F[\xi_{0t}(k_z+q)]}{i\Omega + \xi_{0t}(k_z) - \xi_{0t}(k_z+q)}, \tag{5.81}$$

is the contribution of the two $n = 0$ Landau levels and

$$\begin{aligned} \Pi_1(\vec{q}, i\Omega) &= \frac{1}{2\pi\ell_B^2 L_z} \sum_{n\geq 1,s,t,k_z} \\ &\times \frac{n_F[\xi_{nst}(k_z)] - n_F[\xi_{nst}(k_z+q)]}{i\Omega + \xi_{nst}(k_z) - \xi_{nst}(k_z+q)}. \end{aligned} \tag{5.82}$$

Note that the contribution of the $n = 0$ Landau levels exist only in the presence of the magnetic field and vanishes when $B \to 0$. On the other hand, $\Pi_1(\vec{q}, i\Omega)$ does not vanish when $B \to 0$, with the leading correction to the $B = 0$ result going as $B^2$. At low magnetic fields we can then assume that the leading $B$-dependence of the density response function is contained entirely in $\Pi_0(\vec{q}, i\Omega)$, while $\Pi_1(\vec{q}, i\Omega)$ gives the $B = 0$ limit of the density response function.

Let us then focus on the field-dependent part, i.e. $\Pi_0(\vec{q}, i\Omega)$. Expanding both the numerator

and the denominator of Eq. 5.81 to first order in $q$, we obtain

$$\begin{aligned}\Pi_0(\vec{q}, i\Omega) &= \frac{1}{2\pi\ell_B^2}\int_{-\pi/d}^{\pi/d}\frac{dk_z}{2\pi}\delta[-m_t(k_z)\mathrm{sign}(B)-\epsilon_F] \\ &\times \frac{\frac{dm_t(k_z)}{dk_z}\mathrm{sign}(B)q}{i\Omega+\frac{dm_t(k_z)}{dk_z}\mathrm{sign}(B)q}.\end{aligned} \tag{5.83}$$

Let us restrict ourselves to the most interesting situation, when the Fermi level is not far from the Weyl nodes and crosses only the $t=-$ Landau level. The values of $k_z$, at which the crossing occurs are given by the solutions of the equation

$$\Delta(k_z) = b + \epsilon_F \mathrm{sign}(B). \tag{5.84}$$

The dependence on the sign of the magnetic field will thus enter into the final results only through their dependence on the Fermi energy. Eq. 5.84 has two solutions, which are given by $k_z^{\pm} = \pi/d \pm k_0$, where

$$k_0 = \frac{1}{d}\arccos\left[\frac{\Delta_S^2+\Delta_D^2-(b+\epsilon_F\mathrm{sign}(B))^2}{2\Delta_S\Delta_D}\right]. \tag{5.85}$$

This solution exists as long as

$$b_{c1} \le b + \epsilon_F\mathrm{sign}(B) \le b_{c2}, \tag{5.86}$$

where

$$b_{c1} = |\Delta_S - \Delta_D|, \;\; b_{c2} = \Delta_S + \Delta_D. \tag{5.87}$$

Introducing the Fermi velocity in the $z$-direction, corresponding to the two crossing points above

$$\begin{aligned}\pm\tilde{v}_F &= \left.\frac{d\Delta(k_z)}{dk_z}\right|_{k_z=k_z^{\pm}} = \pm\frac{d}{2[b+\epsilon_F\mathrm{sign}(B)]} \\ &\times \sqrt{[(b+\epsilon_F\mathrm{sign}(B))^2-b_{c1}^2][b_{c2}^2-(b+\epsilon_F\mathrm{sign}(B))^2]},\end{aligned} \tag{5.88}$$

we finally obtain

$$\Pi_0(\vec{q}, i\Omega) = -\frac{1}{2\pi^2 \tilde{v}_F \ell_B^2} \frac{\tilde{v}_F^2 q^2}{(i\Omega)^2 - \tilde{v}_F^2 q^2}. \tag{5.89}$$

The dependence on the magnetic field enters through $\tilde{v}_F$, which depends on sign(B), and through the magnetic length, which depends on $|B|$.

Let us note the following very important property of Eq. 5.89. Suppose the Fermi level is located not too far from the Weyl nodes, namely the following conditions are satisfied

$$b_{c1} \ll b + \epsilon_F \text{sign}(B) \ll b_{c2}. \tag{5.90}$$

In this limit, the Fermi velocity becomes

$$\tilde{v}_F \approx \frac{d}{2}(\Delta_S + \Delta_D), \tag{5.91}$$

i.e. the dependence on the Fermi energy, and, therefore, on the sign of the magnetic field, drops out. Physically this means that the Fermi level is close enough to the Weyl nodes, so that the spectrum is to a good approximation linear and thus Fermi velocity is independent of the Fermi energy. In this limit, the dependence of the density response function on the magnetic field is thus nonanalytic ($\propto |B|$) and is the same as when the Fermi level coincides with the Weyl nodes, i.e. $\epsilon_F = 0$. It is not surprising that the $B$-dependence is nonanalytic at $\epsilon_F = 0$. However, the fact that the nonanalytic ($\propto |B|$) correction to the electronic compressibility dominates the analytic one for a finite range of $\epsilon_F$ near the location of the nodes, is surprising and unexpected. This smoking-gun feature is unique to doped Weyl semimetals, and can be used for their experimental identification. This is one of our main results.

Let us now explore in more detail the connection between the above result for the density response, and the anomalous Hall conductivity of a doped Weyl semimetal, more specifically its non-Fermi-surface part $\sigma_{xy}^{II}$. An explicit expression for $\sigma_{xy}^{II}$ was derived by Burkov [49]:

$$\begin{aligned} \sigma_{xy}^{II} &= \frac{e^2}{8\pi^2} \sum_t \int_{-\pi/d}^{\pi/d} dk_z \ \text{sign}[m_t(k_z)] \\ &\times \left[\Theta(\epsilon_F + |m_t(k_z)|) - \Theta(\epsilon_F - |m_t(k_z)|)\right]. \end{aligned} \tag{5.92}$$

Differentiating this expression with respect to the Fermi energy and assuming $\epsilon_F > 0$ for simplicity [$\sigma^{II}_{xy}(\epsilon_F)$ is an even function of $\epsilon_F$], we obtain

$$\frac{\partial \sigma^{II}_{xy}}{\partial \epsilon_F} = -\frac{e^2}{8\pi^2} \sum_t \int_{-\pi/d}^{\pi/d} dk_z \text{sign}[m_t(k_z)] \delta(\epsilon_F - |m_t(k_z)). \tag{5.93}$$

Just as before, let us assume $\epsilon_F$ is not far from the Weyl nodes. In this case, as above, only the $t = -$ Landau level contributes to the integral in Eq. 5.93. To evaluate the integral we need to solve the equation

$$|b - \Delta(k_z)| = \epsilon_F. \tag{5.94}$$

This has two pairs of solutions, corresponding to $\Delta(k_z) = b \pm \epsilon_F$. Thus we obtain

$$\begin{aligned} \frac{\partial \sigma^{II}_{xy}}{\partial \epsilon_F} &= -\frac{e^2}{8\pi^2} \int_{-\pi/d}^{\pi/d} dk_z \\ &\times \left[\delta(\Delta(k_z) - b + \epsilon_F) - \delta(\Delta(k_z) - b - \epsilon_F)\right] \\ &= \frac{e^2}{4\pi^2} \left(1/\tilde{v}_{F+} - 1/\tilde{v}_{F-}\right), \end{aligned} \tag{5.95}$$

where

$$\tilde{v}_{F\pm} = \frac{d}{2(b \pm \epsilon_F)} \sqrt{[(b \pm \epsilon_F)^2 - b_{c1}^2][b_{c2}^2 - (b \pm \epsilon_F)^2]}, \tag{5.96}$$

coincide with the Fermi velocities, corresponding to the positive or negative sign($B$) in Eq. 5.88 (note that the Hall conductivity itself is evaluated at zero field).

Now let us go back to Eq. 5.89 for the density response function. Let us consider its static limit, i.e. take the limits $\Omega \to 0$ and $q \to 0$ in such a way that $\Omega/v_F q \to 0$. In this case we obtain

$$\kappa = \kappa_0 + \Pi_0(0,0) = \kappa_0 + \frac{1}{2\pi^2 \tilde{v}_F \ell_B^2} = \kappa_0 + \frac{e|B|}{2\pi^2 \tilde{v}_F}, \tag{5.97}$$

where $\kappa_0 \propto \epsilon_F^2$ is the electronic compressibility in the absence of the magnetic field. We can now separate the compressibility into two parts, symmetric and antisymmetric with respect to changing the sign of the magnetic field. We obtain

$$\kappa_s = \kappa_0 + \frac{e|B|}{4\pi^2}(1/\tilde{v}_{F+} + 1/\tilde{v}_{F-}), \tag{5.98}$$

while

$$\kappa_a = \frac{eB}{4\pi^2}(1/\tilde{v}_{F+} - 1/\tilde{v}_{F-}). \tag{5.99}$$

An important difference between $\kappa_s$ and $\kappa_a$ is that while $\kappa_a$ is an analytic function of $B$, $\kappa_s$ is not. Comparing Eqs. 5.95 and 5.99, we obtain

$$\frac{\partial \kappa_a}{\partial B} = \frac{1}{e}\frac{\partial \sigma_{xy}^{II}}{\partial \mu}, \tag{5.100}$$

which coincides with Eq. 5.64. Thus the magnetic field derivative of the analytic *antisymmetric* part of the electronic compressibility is equal to the derivative of the non-Fermi-surface part of the anomalous Hall conductivity with respect to the chemical potential. Note that $\partial\kappa_a/\partial B$ vanishes exactly when $\epsilon_F = 0$, and approximately as long as the Fermi velocity is a constant, i.e. as long as the dispersion is linear to a good approximation.

The nonanalytic symmetric part of the magnetic field dependence of the compressibility, can in turn be expressed in terms of the derivative of $\sigma_{xy}^{II}$ with respect to the magnetization $b$, as

$$\frac{\partial \kappa_s}{\partial |B|} = \frac{1}{e}\frac{\partial \sigma_{xy}^{II}}{\partial b}, \tag{5.101}$$

which is also obtained directly from Eq. 5.92.

## 5.5 Plasmons in a Weyl metal

### 5.5.1 Plasmons in a clean Weyl metal

Let us now find the plasmon mode frequency as a function of the magnetic field. We will first consider the case of a clean Weyl metal, ignoring impurity scattering. The $B$-independent part of the density response function, i.e. the $B \to 0$ limit of $\Pi_1(\vec{q}, i\Omega)$, may be easily evaluated analytically when $\epsilon_F$ is small. In the dynamical limit $|\Omega| \gg v_F q$ one obtains

$$\Pi_1(\vec{q}, i\Omega) = \frac{\epsilon_F^2}{3\pi^2 v_F^2 \bar{v}_F}\frac{\bar{v}_F^2 q^2}{(i\Omega)^2} = \frac{2}{3}\kappa_0 \frac{\bar{v}_F^2 q^2}{(i\Omega)^2}, \tag{5.102}$$

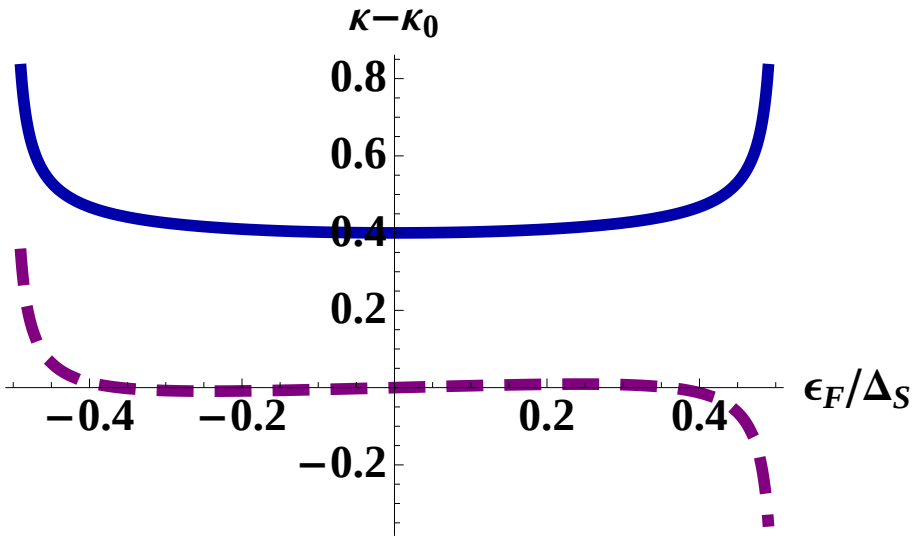


Figure 5.3: Symmetric (solid line) and antisymmetric (dashed line) parts of the correction to compressibility, $\kappa - \kappa_0$, in units of $1/2\pi\ell_B^2\Delta_S d$. The antisymmetric part is negligibly small compared to the symmetric part, while the symmetric part is only weakly dependent on the Fermi energy. The apparent divergences at $\epsilon_F/\Delta_S = \pm 0.5$ correspond to band-edge van Hove singularities.

where $\bar{v}_F = \tilde{v}_F(\epsilon_F = 0)$. The quadratic dependence of $\Pi_1(\vec{q}, i\Omega)$ on the Fermi energy reflects the energy dependence of the density of states near the Weyl nodes $g(\epsilon) \propto \epsilon^2$. Collective mode frequency is given by the solution of

$$\frac{\vec{q}^{\,2}}{4\pi} - e^2\Pi_0(\vec{q}, i\Omega \to \omega + i\eta) - e^2\Pi_1(\vec{q}, i\Omega \to \omega + i\eta) = 0. \tag{5.103}$$

Solving Eq. 5.103 we obtain the following expression for the plasmon frequency of a Weyl metal

$$\omega^2 = \frac{4e^2\bar{v}_F\epsilon_F^2}{3\pi v_F^2} + \frac{2e^3\tilde{v}_F|B|}{\pi}. \tag{5.104}$$

The first term is the square of the plasmon frequency of an ordinary metal with the density of states $g(\epsilon) \propto \epsilon^2$, while the second term contains the leading correction due to the magnetic

field. Note that for small $\epsilon_F \to 0$, Eq. (5.104) is valid for $e^2/v_F \ll 1$ only. Otherwise, the dielectric screening by higher Landau levels should in general be taken into account.

Just as in our discussion of the electronic compressibility before, the field-dependent contribution can be separated into a nonanalytic part, proportional to $|B|$, and an analytic part, proportional to $B$ as

$$\omega_s^2 = \frac{4e^2\bar{v}_F\epsilon_F^2}{3\pi v_F^2} + \frac{e^3|B|}{\pi}(\tilde{v}_{F+} + \tilde{v}_{F-}), \tag{5.105}$$

and

$$\omega_a^2 = \frac{e^3 B}{\pi}(\tilde{v}_{F+} - \tilde{v}_{F-}). \tag{5.106}$$

The antisymmetric part vanishes as long as the spectrum is linear. In this case the plasmon frequency of a Weyl metal contains a nonanalytic correction, proportional to the magnitude, but not the sign, of the applied field. As mentioned above, this should be regarded as a general property of a Weyl metal and its smoking-gun experimental signature.

### 5.5.2 The absence of "hydrodynamic" plasmon modes at low frequencies

In this subsection we will discuss the situation when there is a considerable impurity or electron-electron scattering present near each Weyl node, while the inter-node scattering may still be regarded as weak. In this case one can still think of well-defined nodes and safely regard the material a Weyl metal [50]. Specifically, we would like to see if there is a new type of collective mode with the oscillation frequency low compared to the intra-nodal momentum scattering rate, yet high compared to the typical inter-node scattering rate. We will show that if the Fermi level is such that it crosses multiple Landau levels, as can generically be expected at weak fields in a Weyl metal, the parameter regime for the existence of such a mode is essentially absent.

For simplicity, we will abandon our microscopic model of a Weyl metal here and consider a generic low-energy model of a Weyl metal with two nodes and two corresponding "valleys"

(we will refer to them by the ± chirality of the node), when the Fermi energy is away from the nodes. We will also use a semiclassical, instead of a fully microscopic approach.

We consider a plasmon mode, propagating along an external magnetic field, $\vec{B}$. The fluctuations of particle density in the ± valleys in such a density wave are connected with the current fluctuation via the continuity equation, which however contains an anomalous nonvanishing total divergence due to chiral anomaly. Neglecting the intervalley scattering for a moment, the continuity equation reads

$$\frac{\partial \rho_{\pm}}{\partial t} + \vec{\nabla} \cdot \vec{j}_{\pm} = \pm \frac{e^3}{4\pi^2} \vec{E} \cdot \vec{B}. \tag{5.107}$$

The equation for the current, flowing along the magnetic field, including the usual Drude contribution, but neglecting the diffusion current as we intend to consider the $\vec{q} \to 0$ limit, is given by

$$\vec{j}_{\pm} = \sigma_D \vec{E} \pm \frac{e^2}{4\pi^2} \mu_{\pm} \vec{B}, \tag{5.108}$$

where $\mu_{\pm}$ are the chemical potentials in the two valleys. An implicit assumption in Eq. 5.108 is that the intravalley impurity scattering is strong enough, so that each valley may be assumed to be in a quasi-equilibrium state at any given moment, characterized by the corresponding chemical potential $\mu_{\pm}$. The Drude conductivity, $\sigma_D$ is assumed to be isotropic for simplicity. The electric field entering Eq. 5.108 is produced by the total fluctuation in the local density

$$\vec{\nabla} \cdot \vec{E} = 4\pi(\rho_+ + \rho_-). \tag{5.109}$$

Finally, the fluctuations in the density in each valley are related to the fluctuations in the chemical potentials via the usual Thomas-Fermi relations

$$\rho_{\pm} = e g_B (\mu_{\pm} - \epsilon_F), \tag{5.110}$$

where $\epsilon_F$ is the value of the unperturbed Fermi level, and $g_B$ is the density of states at the unperturbed Fermi level (which depends on the magnetic field, hence the subscript). The

magnitude of the Drude conductivity, $\sigma_D$, and the density of states, entering Eqs. 5.108 and 5.110, depend on the magnitude of the magnetic field, and are determined by how many Landau levels are occupied for a given $B$. Introducing the Fermi velocity in a valley, $v_F$, evaluated at the unperturbed value of the chemical potential in that valley, we can distinguish two simple limits for $\sigma_D$ and $g_B$: That of a weak magnetic field, $\epsilon_F \gg v_F/\ell_B$, and strong magnetic field $\epsilon_F < v_F/\ell_B$. In the former case, $g_B = \epsilon_F^2/2\pi v_F^3$, and $\sigma_D \approx e^2\epsilon_F^2\tau_{\rm tr}/3v_F$ ($\tau_{tr}$ being the transport scattering time), while in the latter $g_B = 1/4\pi^2 v_F \ell_B^2$, $\sigma_D \to 0$.

Solving equations 5.107, 5.108, 5.109, and 5.110 simultaneously, we obtain the following equation for the plasmon frequency at zero wave vector

$$\omega^2 + 8\pi i\sigma_D\omega - \frac{8\pi B^2}{g_B}\left(\frac{e^2}{4\pi^2}\right)^2 = 0. \tag{5.111}$$

For $B = 0$, this equation has a purely imaginary solution $\omega = -8\pi i\sigma_D$ which corresponds to the Maxwell relaxation of charge fluctuations with a decrement determined by the total Drude conductivity in the two valleys, $2\sigma_D$. Solutions with a non-zero real part, corresponding to either overdamped or underdamped oscillations, appear for

$$\frac{8\pi B^2}{g_B}\left(\frac{e^2}{4\pi^2}\right)^2 > (4\pi\sigma_D)^2. \tag{5.112}$$

For large magnetic fields, such that $v_F/\ell_B \gtrsim \epsilon_F$, the inequality in Eq. 5.112 is clearly satisfied, and for $v_F/\ell_B \gg \epsilon_F$ we recover the result for the plasmon frequency, obtained in the previous subsection

$$\omega^2 = \frac{2e^2 v_F}{\pi\ell_B^2}. \tag{5.113}$$

In the opposite limit $v_F/\ell_B \lesssim \epsilon_F$, it is easy to see that Eq. 5.112 prohibits the existence of any propagating modes. Indeed, in the limit of weak magnetic fields, the expression for $\sigma_D$ is $\sigma_D \approx e^2\epsilon_F^2\tau_{\rm tr}/3v_F$, and it is easy to check that Eq. 5.112 yields a condition

$$\frac{v_F}{\ell_B} > \epsilon_F\sqrt{\epsilon_F\tau_{tr}}. \tag{5.114}$$

Such condition can be reconciled with the weak field one only for $\epsilon_F \tau_{tr} \ll 1$, which is hard to imagine to hold. Therefore, in the regime of weak magnetic fields only the usual plasmon mode exists, whose frequency is given by Eq. (5.104).

## 5.6 Discussion and Conclusions

We have so far restricted ourselves to considering only the orbital effect of the applied magnetic field. In reality, Zeeman effect is also present and can be expected to influence the results. Let us demonstrate that our conclusions are in fact unchanged even when the Zeeman effect is taken into account. Zeeman splitting adds a term $g\mu_B B$ to the magnetization-induced spin splitting $b$. Substituting this correction into Eq. 5.88 for the Fermi velocity as a function of $b$ and $\epsilon_F$, it is clear that the effect of this correction is equivalent to a shift of the Fermi energy by $g\mu_B|B|$. This has no effect on our results, as long as the Fermi velocity may be regarded as being independent from the Fermi energy. Thus our conclusions regarding the absence of an analytic linear-in-$B$ correction to the electronic compressibility of a Weyl metal are unchanged by adding the Zeeman splitting.

Another issue that has so far not been discussed is the dependence of our results on the orientation of the magnetic field relative to the magnetization. On symmetry grounds we expect that the linear in magnetic field correction to the compressibility, which is common in normal metallic ferromagnets, but is absent in Weyl metals, should be proportional to $\vec{B} \cdot \hat{m}$, where $\hat{m}$ is the unit vector in the direction of the spontaneous magnetization (ignoring any intrinsic anisotropy that the material may have in the absence of the magnetization). The nonanalytic correction, proportional to $|B|$, on the other hand, should depend on the direction of the magnetic field less strongly, only to the extent required by possible anisotropy of the band dispersion near the Weyl nodes.

The model of a Weyl metal we have explicitly considered in this thesis relies on broken time reversal symmetry to realize it. The second class of Weyl metals is realized when inversion

symmetry is broken instead. [51] In this realization of a Weyl metal, anomalous Hall effect and linear in magnetic field correction to compressibility are absent by symmetry. The leading analytic correction to compressibility in this case is proportional to $B^2$. [34] However, the nonanalytic $\sim |B|$ correction still exists. The presence of such a nonanalytic $\sim |B|$ correction to compressibility and to (square of) the plasmon frequency may thus be regarded as a *universal property of Weyl metals*, independent of the specific realization. This effect is especially striking when the Fermi level coincides with the Weyl nodes, i.e. $\epsilon_F = 0$ in our model. In this case, in the absence of magnetic field the Weyl semimetal is incompressible, since the density of states vanishes. However, when an external field is applied, there appears a finite compressibility, proportional to $|B|$ and the corresponding plasmon collective mode with frequency $\omega \sim \sqrt{|B|}$.

# Chapter 6

# Chiral spin liquid from magnetic Wannier states

In this chapter we present a mapping of a two-dimensional system of interacting bosons in a strong perpendicular magnetic field into an equivalent system of interacting bosons on the square lattice in the absence of the field. Starting from the mapping of the single particle states in the lowest Landau level, we derive the mapping of the Hamiltonians between the systems. This mapping allows us to identify the lattice models, the ground states of which have to be the gapped fractionalized quantum Hall liquids or gapless Bose metal states by construction.

## 6.1 Introduction

Following the remarkable discovery of topological insulators (TI), [52, 53] electronic structure topology has been understood to be a previously largely overlooked, but essential ingredient in our understanding of the phases of condensed matter. [54] One of the reasons nontrivial electronic structure topology is of significant importance is that it is a purely quantum-mechanical phenomenon, with no classical analogs, yet, in many cases, has observable manifestations on

macroscopic scale. This makes such phenomena not only interesting from the purely scientific viewpoint, but also potentially useful technologically.

Quantum mechanical nature of the electrons in solids may also manifest on macroscopic scales through the electron-electron interactions, well-known examples being the phenomena of magnetism and superconductivity. Perhaps particularly remarkable is the fractional quantum Hall effect (FQHE), where electrons effectively fractionalize and the low-energy quasiparticles are characterized by fractional quantum numbers and non-fermionic statistics. This amazing behavior is made possible by the interplay of the strong electron-electron interactions (kinetic energy being completely quenched by the magnetic field), and the nontrivial topology of the individual Landau levels.

An important question is whether such phenomena are unique to the system of two-dimensional electrons in a strong perpendicular magnetic field, or they are more general and may be found in other systems where both interactions and nontrivial electronic structure topology are present. This question was first raised in the seminal paper of Kalmeyer and Laughlin, [55] who pointed out strong similarities between the physics of FQHE and the resonating valence bond theory [56] of spin-liquid states in Mott insulators [57]. The interest in this issue was reinvigorated recently, after the discovery of TI, which demonstrated that nontrivial electronic structure topology is quite common among heavy-element compounds with strong spin-orbit interactions [58]. This gives one some hope that analogs of FQHE may be found in crystalline materials with nontrivial electronic structure topology in the absence of an external magnetic field (such a hypothetical material may be called a fractional Chern insulator).

There has by now been a significant amount of work on fractional Chern insulators, see Refs. [59, 60, 61, 62, 63, 64, 65, 66, 67, 68, 69, 70, 71, 72, 73, 74, 75, 76, 77, 78, 79, 80] for an incomplete list. Our purpose is to derive, somewhat in the spirit of the Kalmeyer and Laughlin paper, [55] a mapping between a model of interacting bosons in the lowest Landau level (LLL), and a lattice model of bosons in the absence of an external magnetic field (but with broken time reversal symmetry), with the lattice filling identical to the LLL filling factor.

By construction, the ground states of this lattice model are equivalent to the ground states of interacting bosons in the LLL, i.e. may be fractionalized liquids or Bose metals [81, 82] with broken time reversal symmetry at specific rational filling factors. While most of the calculations, presented below, may be carried out for a model of interacting electrons in the LLL just as well, we choose interacting bosons, having in mind potential realizations in magnetic systems, [57] or cold atoms in optical lattices [83]. Some work along these lines, but valid only at high boson filling factors, has already been done by Burkov [84] Here we present a more complete analysis, containing points related to the LLL topology, overlooked in Ref. [84], but crucially important at low boson filling factors, at which fractionalized liquid states are realized.

The rest of the chapter is organized as follows. In section 6.2 we introduce our model of interacting bosons in two dimensions (2D) in the presence of a strong perpendicular magnetic field, such that the LLL projection may be used. We introduce a magnetic Bloch and magnetic Wannier single particle basis in the LLL, following the procedure, first described by Rashba *et al.* [85] The advantage of this particular realization of the magnetic Wannier states is that they have the fastest possible decay rate for such states, $1/r^2$, in all directions, and have the full symmetry of the Bravais lattice [86]. In section6.3 we derive a representation of the density operator in the magnetic Bloch basis and point out some of its most important properties. Focusing on long-wavelength density modes, we perform a gradient expansion of the density operator and derive a simplified expression, valid in the long-wavelength limit. In section 6.4, using the results obtained in the previous sections, we rewrite the Hamiltonian of interacting bosons in the LLL in the magnetic Wannier basis, using the long-wavelength expressions for the density operators. We show that in this long-wavelength limit the Hamiltonian has a very simple form, consisting only of a few distinct (long-range) terms. This provides a mapping between the Hamiltonian of interacting bosons in the LLL and a lattice boson Hamiltonian, with no explicitly present external magnetic field (broken time reversal symmetry is still explicit, however, since some of the terms in the Hamiltonian are complex). We conclude in section 6.5 with a discussion of our results and a brief summary.

## 6.2 Magnetic Bloch and magnetic Wannier bases in the LLL

We start from a model of bosons of charge $-e$, interacting via some two-body interaction potential in 2D (to be specified in more detail below), in the presence of a perpendicular magnetic field $\vec{B} = B\hat{z}$. We will assume that the magnetic field is sufficiently strong, such that only states in the LLL can be occupied.

We will use the LLL basis of magnetic Wannier states, first introduced in Ref. [85]. The advantage of this particular realization of the magnetic Wannier states is that they have the fastest decay rate at long distances, compatible with the nontrivial LLL topology, which is $1/r^2$ [86]. They also are highly symmetric and allow, as will be demonstrated below, for the construction of Wannier Hamiltonians with the full symmetry of any 2D Bravais lattice.

To construct this basis, we adopt the symmetric gauge $\vec{A} = \frac{1}{2}\vec{B} \times \vec{r}$, and start from the zero-angular-momentum symmetric gauge orbital in the LLL

$$c_0(\vec{r}) = \frac{1}{\sqrt{2\pi\ell^2}} e^{-\frac{r^2}{4\ell^2}}, \tag{6.1}$$

where $\ell = \sqrt{c/eB}$ is the magnetic length and will use the $\hbar = 1$ units throughout. We then construct an overcomplete basis of the LLL orbitals by translating the $c_0(\vec{r})$ orbital, localized at the origin, to sites of any 2D Bravais lattice with unit cell area $2\pi\ell^2$. We will focus on the simplest case of the square lattice henceforth and show that the geometry of lattice is unimportant in the discussion below. We obtain

$$\begin{aligned} c_{\vec{m}}(\vec{r}) &= T_{m_x\vec{a}_x} T_{m_y\vec{a}_y} c_0(\vec{r}) \\ &= \frac{(-1)^{m_x m_y}}{\sqrt{2\pi\ell^2}} e^{-\frac{(\vec{r}-\vec{r}_{\vec{m}})^2}{4\ell^2} + \frac{i}{2\ell^2}\hat{z}\cdot(\vec{r}\times\vec{r}_{\vec{m}})}. \end{aligned} \tag{6.2}$$

Here

$$T_{\vec{R}} = e^{-i\vec{R}\cdot\left(\vec{p} - \frac{e}{c}\vec{A}\right)}, \tag{6.3}$$

is the magnetic translation operator in the symmetric gauge, $\vec{a}_{x,y} = a\hat{x}, a\hat{y}$ are the primitive translation vectors of the square lattice with the lattice constant $a = \sqrt{2\pi\ell^2}$, and $\vec{m} = (m_x, m_y)$ is a vector with integer components, labeling the lattice sites.

The set of functions $c_{\vec{m}}(\vec{r})$ is overcomplete by exactly one state, which is a consequence of the Perelomov identity [87]

$$\sum_{\vec{m}} (-1)^{m_x+m_y} c_{\vec{m}}(\vec{r}) = 0. \tag{6.4}$$

This property plays an important role in what follows.

The magnetic Bloch states may now be constructed as linear combinations of the LLL orbitals $c_{\vec{m}}(\vec{r})$ as

$$\begin{aligned} \Psi_{\vec{k}}(\vec{r}) &= \frac{1}{\sqrt{N\nu(\vec{k})}} \sum_{\vec{m}} c_{\vec{m}}(\vec{r}) e^{i\vec{k}\cdot\vec{r}_{\vec{m}}} \\ &= \sqrt{\frac{2}{a^2 N\nu(\vec{k})}} e^{-\frac{\pi}{2a^2}\vec{r}^{\,2}} e^{-\frac{a^2}{2\pi}\left[k_y + \frac{\pi}{a^2}(x-iy)\right]^2} \\ &\times \theta_3\left(\frac{k_+ a}{2}, e^{-\pi}\right) \theta_3\left(\frac{k_- a}{2} - \frac{i\pi}{a}(x-iy), e^{-\pi}\right). \end{aligned} \tag{6.5}$$

where $k_+$ and $k_-$ are the complex coordinates $z$ and $\bar{z}$ analogs in momentum space: $k_\pm = k_x \pm i k_y$, $N = L_x L_y / 2\pi\ell^2$ is the number of the magnetic flux quanta, contained in the sample area $L_x L_y$, $\theta_3(z,q)$ are Jacobi theta functions and $\nu(\vec{k})$ is needed to normalize the Bloch function to unity in the sample volume. Explicitly, the normalization factor is given by

$$\begin{aligned} \nu(\vec{k}) &= \sum_{\vec{m}} (-1)^{m_x m_y} e^{-\frac{\vec{r}_{\vec{m}}^{\,2}}{4\ell^2}} e^{i\vec{k}\cdot\vec{r}_{\vec{m}}} \\ &= \sqrt{2} e^{-\frac{k_y^2 a^2}{2\pi}} \theta_3\left(\frac{k_+ a}{2}, e^{-\pi}\right) \theta_3\left(\frac{k_- a}{2}, e^{-\pi}\right). \end{aligned} \tag{6.6}$$

The probability density, corresponding to a magnetic Bloch state, $|\Psi_{\vec{k}}(\vec{r})|^2$, has the form of a square Abrikosov vortex lattice, as shown in Fig. 6.1.

The function $\nu(\vec{k})$ is non-negative everywhere in the first Brillouin zone (BZ). As immediately follows from the Perelomov identity, Eq. 6.4, $\nu(\vec{k})$ vanishes at the BZ corner $\vec{k}_0 = (\pi/a, \pi/a)$, $\nu(\vec{k}_0) = 0$ , see Fig. 6.2.

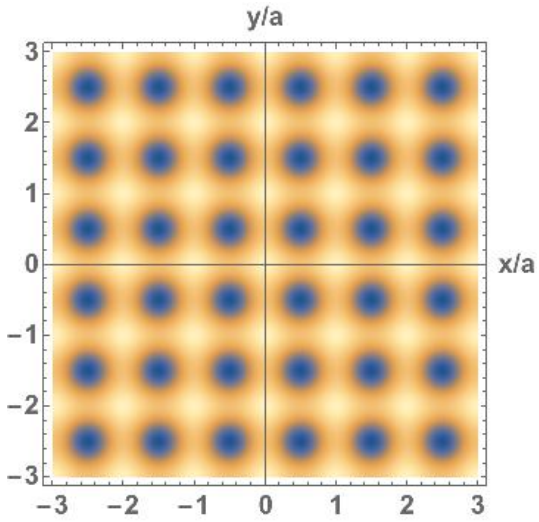


Figure 6.1: Plot of $|\Psi_{\vec{k}}(\vec{r})|^2$ for $\vec{k} = 0$. In general $|\Psi_{\vec{k}}(\vec{r})|^2$ has the form of a square Abrikosov vortex lattice, shifted with respect to the lattice, shown in the figure, by the vector $\ell^2 \hat{z} \times \vec{k}$.

Near $\vec{k}_0$, $\nu(\vec{k})$ behaves as

$$\nu(\vec{k}_0 + \vec{k}) \approx \frac{\gamma}{2} \vec{k}^{\,2} a^2, \tag{6.7}$$

where

$$\gamma = -\frac{1}{2a} \sum_{\vec{m}} (-1)^{m_x + m_y} c_{\vec{m}}(0) \vec{r}^{\,2}_{\vec{m}}, \tag{6.8}$$

is a positive constant of order unity. We will use the above results extensively later.

The quantum geometry of the magnetic Bloch states, defined by Eq. 6.5, turns out to be closely connected to the properties of the function $\nu(\vec{k})$. Defining a "periodic part" of the Bloch function in the standard way as (it is periodic, but with respect to the magnetic translations, not ordinary ones) $u_{\vec{k}}(\vec{r}) = e^{-i\vec{k}\cdot\vec{r}} \Psi_{\vec{k}}(\vec{r})$, and evaluating the Berry connection $\vec{\mathcal{A}}(\vec{k}) = -i \langle u_{\vec{k}} | \vec{\nabla}_{\vec{k}} | u_{\vec{k}} \rangle$, we obtain

$$\vec{\mathcal{A}}(\vec{k}) = \frac{1}{2} (\hat{z} \times \vec{\nabla}_{\vec{k}}) \ln[\nu(\vec{k})]. \tag{6.9}$$

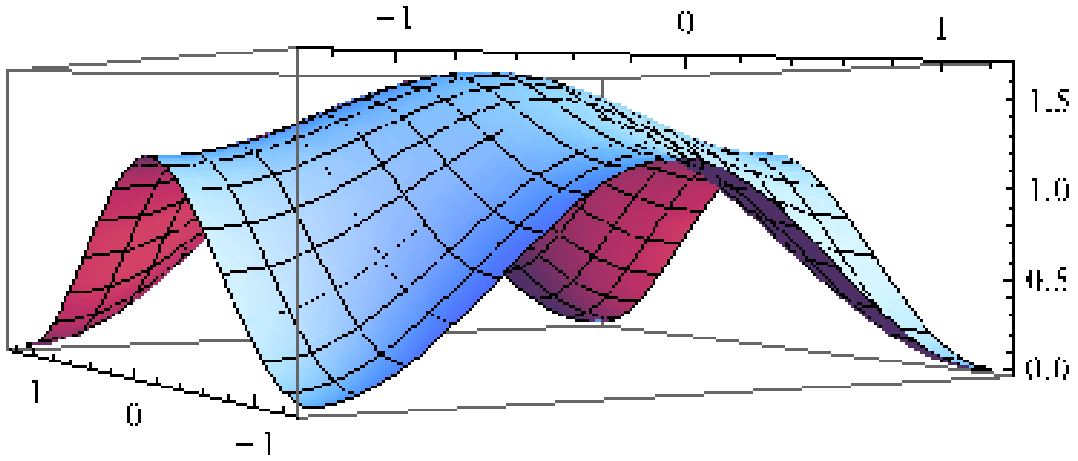


Figure 6.2: Normalization factor $\nu(\vec{k})$ of the Bloch states as function of $k_x$ and $k_y$ in the First Brillouin zone.

This may be particularly easily evaluated near the BZ corners. In this case, using Eq. 6.7, we obtain

$$\vec{\mathcal{A}}(\vec{k}_0 + \vec{k}) \approx \frac{\hat{z} \times \vec{k}}{\vec{k}^{\,2}}. \tag{6.10}$$

This expression is singular when $\vec{k} \to 0$, which expresses the impossibility of choosing a smooth gauge for the Bloch functions in the LLL, due to the nonzero Chern number, which we will calculate below. The BZ corner is where a "Dirac string" must enter the first BZ, to ensure that the circulation of the Berry connection around the BZ boundary is equal to $2\pi$. Evaluating the $z$-component of the Berry curvature, we obtain

$$\Omega_z(\vec{k}) = \vec{\nabla}_{\vec{k}} \times \vec{\mathcal{A}}(\vec{k}) = \frac{1}{2}\vec{\nabla}^{\,2}_{\vec{k}} \ln[\nu(\vec{k})] = -\frac{a^2}{2\pi}, \tag{6.11}$$

which follows immediately from Eq. 6.6. The integral of $\Omega_z(\vec{k})$ over the BZ then gives the nontrivial Chern number of the LLL, as it was expected:

$$C = \frac{1}{2\pi}\int_{-\pi/a}^{\pi/a} dk_x dk_y \Omega_z(\vec{k}) = -1. \tag{6.12}$$

This result may also be obtained using the expression Eq. 6.10 for the Berry connection near the BZ corners. If we evaluate the circulation of the Berry connection around the firs BZ boundary, it is clear that, due to the periodicity of the function $\nu(\vec{k})$ in the first BZ, only the singular points at the BZ corners will actually contribute to the circulation, see Fig. 6.3. Using the Eq. 6.10, one obtains

$$\oint_{\partial BZ} \vec{\mathcal{A}}(\vec{k}) \cdot d\vec{k} = -2\pi, \tag{6.13}$$

which is equivalent to Eq. 6.12.

The magnetic Wannier states are related to the Bloch states in the standard way

$$\Phi_{\vec{m}}(\vec{r}) = \frac{1}{\sqrt{N}} \sum_{\vec{k}} \Psi_{\vec{k}}(\vec{r}) e^{-i\vec{k}\cdot\vec{r}_{\vec{m}}}. \tag{6.14}$$

It is straightforward to show [85] that the divergence of the normalization factor of the Bloch wavefunction at the BZ corner

$$\frac{1}{\sqrt{\nu(\vec{k}_0 + \vec{k})}} \sim \frac{1}{k}, \tag{6.15}$$

leads to power-law $1/r^2$ tail in the long-distance decay of the Wannier states $\Phi_{\vec{m}}(\vec{r})$. Nonetheless, the functions $\Phi_{\vec{m}}(\vec{r})$ form a complete orthonormal set of states, since the Bloch function $\Psi_{\vec{k}_0}(\vec{r})$ is still well-defined, the singularity, in the form of a momentum-space vortex, only existing in its phase

$$\Psi_{\vec{k}_0+\vec{k}}(\vec{r}) = \frac{ie^{i\phi_{\vec{k}}}}{\sqrt{2N\gamma}} \sum_{\vec{m}} (-1)^{m_x+m_y} (m_x - im_y) c_{\vec{m}}(\vec{r}), \tag{6.16}$$

where $\vec{k} \to 0$ and $\phi_{\vec{k}}$ is the azimuthal angle of the vector $\vec{k}$. This phase singularity is again a consequence of the Dirac string, as in Eq. 6.10. Since the functions $\Phi_{\vec{m}}(\vec{r})$ form a complete orthonormal set of states, the question of the LLL Hamiltonian in the magnetic Wannier basis is also well-defined.

## 6.3 Density operator in the magnetic Bloch and Wannier bases

In this section we will construct the density operator in the Bloch and Wannier bases, introduced in the previous section. As is well-known, the peculiar algebra (Girvin-MacDonald-Platzman, or GMP algebra) [88] of the LLL-projected density operator plays a crucial role in the appearance of the fractional quantum Hall liquid states in the LLL. It is thus important to understand how this algebra is realized when the density operator is written in the magnetic Bloch and Wannier bases.

Evaluating the Fourier transform of the LLL-projected density operator, one obtains

$$\begin{aligned} \varrho(\vec{q}) &= \int d^2r \Psi^+(\vec{r})\Psi(\vec{r})e^{-i\vec{q}\cdot\vec{r}} \\ &= e^{-\frac{q^2a^2}{4\pi}} \sum_{\vec{k}} \frac{\nu\left(\vec{k}+\frac{\vec{q}}{2}-\frac{i}{2}\hat{z}\times\vec{q}\right)}{\sqrt{\nu(\vec{k}+\vec{q})\nu(\vec{k})}} b^+_{\vec{k}} b_{\vec{k}+\vec{q}}. \end{aligned} \tag{6.17}$$

This expression may be simplified further either using Jacobi theta function identities or invoking properties of the Bloch functions $\Psi_{\vec{k}}(\vec{r})$. We will take the second route as it is more transparent.

The property of the Bloch functions we will use is that they are fully determined, up to a $\vec{k}$-dependent phase factor, by their zeros, which form a square Abrikosov vortex lattice with the lattice constant $a$, as shown in Fig. 6.1. Mathematically, this statement may be expressed in the form of the following relation [84]

$$\Psi_{\vec{k}+\vec{q}}(\vec{r}) = e^{i\gamma(\vec{k}+\vec{q},\vec{k})} e^{\frac{i}{2}\vec{q}\cdot\vec{r}} \Psi_{\vec{k}}(\vec{r}-\ell^2\hat{z}\times\vec{q}), \tag{6.18}$$

where $e^{i\vec{q}\cdot\vec{r}/2}$ is an Aharonov-Bohm phase factor and

$$\begin{aligned} e^{i\gamma(\vec{k}+\vec{q},\vec{k})} &= \int d^2r \Psi_{\vec{k}+\vec{q}}(\vec{r})\Psi^*_{\vec{k}}(\vec{r}-\ell^2\hat{z}\times\vec{q}) e^{-\frac{i}{2}\vec{q}\cdot\vec{r}} \\ &= e^{-\frac{q^2a^2}{8\pi}} \frac{\nu\left(\vec{k}+\frac{\vec{q}}{2}-\frac{i}{2}\hat{z}\times\vec{q}\right)}{\sqrt{\nu(\vec{k}+\vec{q})\nu(\vec{k})}}. \end{aligned} \tag{6.19}$$

This immediately gives

$$\gamma(\vec{k}+\vec{q},\vec{k}) = \mathrm{Im}\ln\nu\left(\vec{k}+\frac{\vec{q}}{2}-\frac{i}{2}\hat{z}\times\vec{q}\right), \tag{6.20}$$

or, equivalently

$$\frac{\nu\left(\vec{k}+\frac{\vec{q}}{2}-\frac{i}{2}\hat{z}\times\vec{q}\right)}{\sqrt{\nu(\vec{k}+\vec{q})\nu(\vec{k})}} = e^{\frac{q^2a^2}{8\pi}}e^{i\mathrm{Im}\ln\nu\left(\vec{k}+\frac{\vec{q}}{2}-\frac{i}{2}\hat{z}\times\vec{q}\right)}. \tag{6.21}$$

The physical meaning of the phase $\gamma(\vec{k}+\vec{q},\vec{k})$ is the momentum-space Berry phase, accumulated upon adiabatic evolution of the Bloch state from $\vec{k}$ to $\vec{k}+\vec{q}$ (strictly speaking, a path in the first BZ needs to be specified for this identification to be precise, but this will not be necessary for our purposes).

Thus we finally obtain the following expression for the density operator

$$\varrho(\vec{q}) = e^{-\frac{q^2a^2}{8\pi}}\sum_{\vec{k}} e^{i\gamma(\vec{k}+\vec{q},\vec{k})}b^{+}_{\vec{k}}b_{\vec{k}+\vec{q}} \equiv e^{-\frac{q^2a^2}{8\pi}}\,\bar{\varrho}(\vec{q}). \tag{6.22}$$

Using Eqs. 6.11 and 6.18 it is straightforward to show that the density operators $\bar{\varrho}(\vec{q})$ satisfy the GMP algebra

$$[\bar{\varrho}(\vec{q}),\bar{\varrho}(\vec{q}')] = -2i\sin\left[\frac{a^2}{4\pi}\hat{z}\cdot(\vec{q}\times\vec{q}')\right]\bar{\varrho}(\vec{q}+\vec{q}'), \tag{6.23}$$

as we expected.

To make further progress we will assume that $q\,a$ may be taken to be small, i.e. only the long-wavelength density modes are of interest to us. This might, perhaps, be justified using renormalization-group-type arguments, although it is not easy in the present case, as we are interested in gapped fractionalized liquid phases with short correlation length. We will thus take a more simple-minded approach here and assume the interparticle interaction potential has a long, but finite, range $\xi \gg a$. Contribution of the density modes with $q > 1/\xi$ is then suppressed naturally, without renormalization. This also gives us a natural small parameter $a/\xi$, which we will use to control our theory. Extensive earlier studies of the FQHE in finite-width

quantum well systems [89] indicate that $\xi$ may be safely taken to be as long as 10 magnetic lengths.

Taking $q\,a \ll 1$, the Berry phase given by Eq. 6.20 is an analytic function of $\vec{q}$ everywhere, except in a circular patch of radius $1/\xi \ll 1/a$ around the BZ corner, see Fig. 6.3. This is again a consequence of the Dirac string, entering the BZ at the corner. Let us analyze the behavior of $\gamma(\vec{k}+\vec{q},\vec{k})$ near the BZ corner $\vec{k}=\vec{k}_0$ in detail. Using Eq. 6.7, one obtains

$$\mathrm{Im}\ln\nu\left(\vec{k}_0+\vec{k}+\frac{\vec{q}}{2}-\frac{i}{2}\hat{z}\times\vec{q}\right)\approx tan^{-1}\frac{(\hat{z}\times\vec{k})\cdot\vec{q}}{\vec{k}^2+\vec{k}\cdot\vec{q}}. \tag{6.24}$$

The meaning of Eq. 6.24 is simply the azimuthal angle between the directions of the vector $\vec{k}+\vec{q}$ and vector $\vec{k}$. This may be viewed as a direct consequence of Eq. 6.16. Outside of the BZ corner patch, where $q<k$, this gives

$$\begin{aligned}&\mathrm{Im}\ln\nu\left(\vec{k}_0+\vec{k}+\frac{\vec{q}}{2}-\frac{i}{2}\hat{z}\times\vec{q}\right)\\ \approx\ &\frac{\hat{z}\times\vec{k}}{\vec{k}^2}\cdot\vec{q}\approx\vec{\mathcal{A}}(\vec{k}_0+\vec{k})\cdot\vec{q},\end{aligned} \tag{6.25}$$

The above discussion makes it clear that, in general, $\bar{\varrho}(\vec{q})$ is a nonanalytic function of $\vec{q}$ in the vicinity of $\vec{q}=0$ and thus may not be expanded in Taylor series with respect to $\vec{q}$. However, as will be seen below, the nonanalyticity appears explicitly only when one goes beyond the first order in $\vec{q}$, or, in other words, $\vec{\nabla}\bar{\varrho}(\vec{q}\to 0)$ is finite, even though all the higher gradients are not. Thus, the gradient expansion of $\bar{\varrho}(\vec{q})$ does exist, if it is restricted to terms of up to first order in $qa$, or $a/\xi$. Expanding to only this order, we thus obtain

$$\bar{\varrho}(\vec{q})\approx\sum_{\vec{k}}e^{i\vec{A}(\vec{k})\cdot\vec{q}}b^{+}_{\vec{k}}b_{\vec{k}+\vec{q}}\approx\sum_{\vec{k}}\left[1+i\vec{\mathcal{A}}(\vec{k})\cdot\vec{q}\right]b^{+}_{\vec{k}}b_{\vec{k}+\vec{q}}. \tag{6.26}$$

This is an expression for the LLL-projected density operator to leading nontrivial order in the small parameter $a/\xi$.

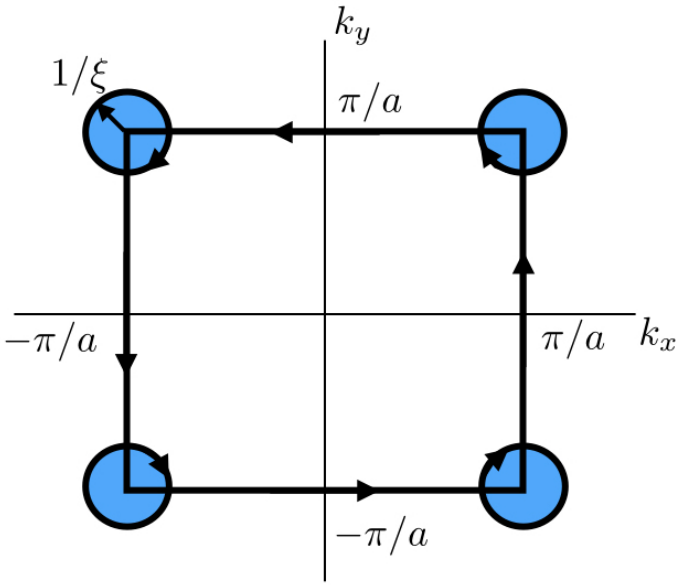


Figure 6.3: First Brillouin zone with corner patches shown by shaded circles of radius $1/\xi$. Circulation of the Berry connection vector around the BZ boundary, excluding the corners, as shown by arrows, gives the Chern number $C = -1$.

## 6.4 LLL Hamiltonian in the magnetic Wannier basis

We now rewrite Eq. 6.26 in the magnetic Wannier basis using

$$b^+_{\vec{k}} = \frac{1}{\sqrt{N}} \sum_{\vec{m}} b^+_{\vec{m}} e^{i\vec{k}\cdot\vec{r}_{\vec{m}}}. \tag{6.27}$$

One obtains

$$\begin{aligned} \bar{\varrho}(\vec{q}) &= \sum_{\vec{m}} e^{-i\vec{q}\cdot\vec{r}_{\vec{m}}} b^+_{\vec{m}} b_{\vec{m}} \\ + \quad & \frac{i}{N} \sum_{\vec{m}\vec{m}'} \sum_{\vec{k}} \vec{\mathcal{A}}(\vec{k}) \cdot \vec{q} e^{i\vec{k}\cdot(\vec{r}_{\vec{m}} - \vec{r}_{\vec{m}'})} e^{-i\vec{q}\cdot\vec{r}_{\vec{m}'}} b^+_{\vec{m}} b_{\vec{m}'}. \end{aligned} \tag{6.28}$$

Even though the Berry connection $\vec{A}(\vec{k})$ is singular in the limit $\vec{k} \to \vec{k}_0$ due to the presence of the Dirac string, the integral over $\vec{k}$ in Eq. 6.28 still converges (but divergent terms will

appear if expansion to higher orders in $\vec{q}$ is attempted). However, due to the divergence of the Berry connection, the main contribution to the integral over $\vec{k}$ at long distances, i.e. when $|\vec{r}_{\vec{m}} - \vec{r}_{\vec{m}'}| \gg a$, comes from the vicinity of the BZ corner. This also makes sense physically since, as discussed at the end of Section 6.2, it is the contribution of vicinity of the BZ corner that leads to the $1/r^2$ tail of the Wannier function $\Phi_{\vec{m}}(\vec{r})$. In this case $\vec{\mathcal{A}}(\vec{k})$ may be approximated by Eq. 6.10 and the integral over $\vec{k}$ in Eq. 6.28 is then easily evaluated analytically. We obtain

$$\begin{aligned} \bar{\varrho}(\vec{q}) &= \sum_{\vec{m}} e^{-i\vec{q}\cdot\vec{r}_{\vec{m}}} b^+_{\vec{m}} b_{\vec{m}} - \frac{a^2}{2\pi} \sum_{\vec{m}\vec{m}'} \vec{q}\cdot \frac{\hat{z}\times(\vec{r}_{\vec{m}} - \vec{r}_{\vec{m}'})}{(\vec{r}_{\vec{m}} - \vec{r}_{\vec{m}'})^2} \\ \times \quad & e^{i\vec{k}_0\cdot(\vec{r}_{\vec{m}} - \vec{r}_{\vec{m}'})} e^{-i\vec{q}\cdot\vec{r}_{\vec{m}'}} b^+_{\vec{m}} b_{\vec{m}'}. \end{aligned} \tag{6.29}$$

The oscillating phase factor $e^{i\vec{k}_0\cdot(\vec{r}_{\vec{m}} - \vec{r}_{\vec{m}'})}$ may be eliminated by a gauge transformation of the boson creation and annihilation operators

$$b_{\vec{m}} e^{-i\vec{k}_0\cdot\vec{r}_{\vec{m}}} \to b_{\vec{m}}, \tag{6.30}$$

and we will ignore this factor henceforth.

The interacting-boson Hamiltonian, projected to the LLL, is given by

$$H = \frac{1}{2L_xL_y} \sum_{\vec{q}} U(\vec{q}) e^{-\frac{\vec{q}^2a^2}{4\pi}} \bar{\varrho}(\vec{q})\bar{\varrho}(-\vec{q}), \tag{6.31}$$

where $U(\vec{q})$ is the Fourier transform of the interparticle interaction potential. In accordance with the discussion above we take $U(\vec{q})$ to be negligible when $q > 1/\xi$ and equal to a constant $U(\vec{q}) = U\xi^2$ when $q < 1/\xi$, where $U$ has dimensions of energy. In this case the integral over $\vec{q}$ in Eq. 6.31 is easily done analytically. Restricting ourselves to only the terms of zeroth and first order in the small parameter $a/\xi$, we obtain $H = H_0 + H_1$, where

$$H_0 = U_0 \sum_{\vec{m}\vec{n}} \frac{\mathrm{J}_1(|\vec{r}_{\vec{m}} - \vec{r}_{\vec{n}}|/\xi)}{|\vec{r}_{\vec{m}} - \vec{r}_{\vec{n}}|/\xi} b^+_{\vec{m}} b_{\vec{m}} b^+_{\vec{n}} b_{\vec{n}}, \tag{6.32}$$

and

$$\begin{aligned} H_1 = i\frac{aU_1}{\xi} \sum_{\vec{m}\vec{m}'\vec{n}} \hat{z}\cdot \frac{a\,\xi\,(\vec{r}_{\vec{m}} - \vec{r}_{\vec{m}'})\times(\vec{r}_{\vec{m}'} - \vec{r}_{\vec{n}})}{|\vec{r}_{\vec{m}'} - \vec{r}_{\vec{n}}|^2 |\vec{r}_{\vec{m}} - \vec{r}_{\vec{m}'}|^2} \\ \times \quad \mathrm{J}_2(|\vec{r}_{\vec{m}'} - \vec{r}_{\vec{n}}|/\xi) b^+_{\vec{m}} b_{\vec{m}'} b^+_{\vec{n}} b_{\vec{n}}, \end{aligned} \tag{6.33}$$

where $J_{1,2}$ are Bessel functions of the corresponding order, $U_0 = U/4\pi$, and $U_1 = U/4\pi^2$. Eqs. 6.32 and 6.33 constitute the main result of this chapter.

It may be useful, especially for possible future numerical studies of this model, to extend it by introducing an ordinary kinetic energy term (hopping) for the bosons. Physically this may be achieved by adding an external potential, with exactly the same periodicity as the square lattice, formed by the magnetic Wannier state centers. This potential would introduce a boson hopping term of the form

$$H_2 = -t \sum_{\langle \vec{m}\vec{m}' \rangle} e^{i\vec{k}\cdot(\vec{r}_{\vec{m}} - \vec{r}_{\vec{m}'})} b^+_{\vec{m}} b_{\vec{m}'}. \tag{6.34}$$

Here hopping is assumed to be restricted to the nearest-neighbor pairs of sites, $t > 0$ and the phase factor $e^{i\vec{k}\cdot(\vec{r}_{\vec{m}} - \vec{r}_{\vec{m}'})}$ depends on the location of the Wannier orbital center within the unit cell of the physical square lattice. The ground states of $H_0$ correspond to the bosons condensing into one of the Bloch states $\Psi_{\vec{k}}(\vec{r})$ and forming an Abrikosov vortex lattice state. The value of $\vec{k}$ determines the location of the vortex cores of the Abrikosov lattice relative to the Wannier orbital centers.

The full Hamiltonian $H = H_0 + H_1 + H_2$ will then contain both an ordinary superfluid phase, when the $H_2$ term is dominant, and the fractionalized chiral liquid phases when $H_0 + H_1$ is dominant. This may be generalized even further by allowing the coupling constants $U_0$ and $U_1$ to be independent, which will also introduce ordinary Mott insulator phases with broken translational symmetry when $U_0 \gg t, U_1$.

## 6.5 Discussion and conclusions

In the previous sections we have derived, using a controlled expansion in the small parameter $a/\xi$, a magnetic Wannier state representation of interacting bosons in the LLL. This Hamiltonian describes interacting bosons on a square lattice (the lattice geometry does not play a role here, as discussed below). The magnetic field does not enter explicitly in this Hamiltonian, but

time reversal symmetry is still explicitly broken in the $H_1$ part of the Hamiltonian. The form of the $H_1$ term is a direct consequence of Eq. 6.26 and in this sense it may be regarded as a realization of the GMP algebra, satisfied by the LLL-projected density operators.

By construction, the ground states of the lattice Hamiltonian must be the same as the ground states of interacting bosons in the LLL, which include gapped fractionalized quantum Hall liquids at some rational filling fractions, e.g. at filling factor 1/2. In this sense, the Hamiltonian given by Eqs. 6.32, 6.33, 6.34 may be regarded as a parent Hamiltonian of chiral spin liquids (although time reversal symmetry is broken explicitly here). Chiral spin liquids have attracted considerable attention, [55, 90, 91, 92, 93, 94] particularly due to recent work demonstrating they may be realized in spin-1/2 antiferromagnets on the kagome lattice [91, 95, 96, 97, 98, 99, 100, 101]. While in our model time reversal symmetry is broken explicitly, it may still be a useful starting point for constructing models in which it is broken spontaneously.

The expression for the kinetic part of the Hamiltonian, Eq. 6.33, reveals several features, which are presumably important to achieve a chiral spin liquid. First, $H_1$ has the form of a correlated hopping Hamiltonian, where the boson hopping amplitude from site $\vec{m}$ to $\vec{m}'$ depends on the boson density at site $\vec{n}$. This reminds one, not accidentally, of flux attachment [102]. Second, both $H_0$ and $H_1$ terms are long-range, exhibiting power-law decay. This is a direct consequence of the long-range $1/r^2$ tail of the Wannier functions $\Phi_{\vec{m}}(\vec{r})$, which in turn is rooted in the nontrivial topology of the LLL. This feature is also shared with previous constructions of parent Hamiltonians for chiral spin liquids, [92, 94] employing mapping to the LLL in some form. The power law decay in Eqs. 6.32, 6.33 is the fastest possible for this type of construction, since we are using the Wannier states with the fastest possible decay rate in all directions.

In our construction of the magnetic Wannier basis we have chosen to place the Wannier orbitals on the sites of a square lattice. This choice is of course arbitrary: any 2D Bravais lattice would work just as well. This may appear strange since the lattice geometry naturally plays a crucial role within the prevailing paradigm in the search for quantum spin liquid physics, that of geometrically frustrated magnets. In our model, however, lattice geometry plays no role

at all due to the long range nature of the interactions. The choice of the square lattice was thus dictated only by its simplicity. Our construction, however, may be repeated on any 2D Bravais lattice and in long range limit it will lead to the identical results.

In conclusion, we have provided a derivation of a lattice Hamiltonian which, by construction, will have gapped fractionalized liquid ground states at certain rational filling fractional filling fractions, such as 1/2. The construction employs magnetic Wannier states, which are highly symmetric (the Hamiltonian has the full symmetry of the Bravais lattice used) and have the fastest possible decay rate, compatible with the nontrivial topology of the LLL, i.e. $1/r^2$. It would be interesting to confirm our construction by an explicit numerical solution of Eqs. 6.32, 6.33, 6.34.

# Chapter 7

# Conclusion

In this thesis we studied the two examples of the interacting systems with non-trivial topology of the states in the momentum space.

In the first part of the thesis, the simplest, two node model of Weyl metal in the presence of external magnetic field was considered. The dependence of the electronic compressibility and the plasmon excitations on the magnetic field were studied. We found that both the compressibility and the plasmon frequency obtain the nonanalytic corrections not only in the degenerate case of Weyl semimetal, when the Fermi surface is reduced to two points in momentum space, but also for the finite range of Fermi energy values around the node. This corrections depend only on the magnitude of the applied magnetic field, but do not depend on the angle between the external field and internal magnetization of the material. This result is consistent with the fact that average of the Berry curvature over the whole BZ is zero and hence there is no preferred direction in such material. But the leading term dependence on magnitude of the magnetic field is linear, while first analytic directionless term would be quadratic. We have also shown that the presence of two disconnected parts of Fermi surface in the momentum space does not lead to the emergence of any types of undamped excitations other than the plasmon excitations. Since Weyl metals were first experimentally observed only few years ago due to the subtlety of

recognizing such state of matter, our results can serve as another way of distinguishing Weyl metal from the ordinary one.

In the second part of the thesis the bosonic quantum Hall system and the bosonic lattice models. While most commonly the continuous models are obtained as small lattice spacing limit of the lattice models, the opposite direction mapping was considered here. Using the axial gauge in order to preserve the rotational symmetry, the mapping of the single particle states from the lowest Landau level to the lattice model was built. It was shown, that density operators on the lattice will obey the same Girvin-MacDonald-Platzman algebra as the density operators on the lowest Landau level. Since in this algebra operators do not commute even at the limit of small momentum, the Hamiltonian of the lattice system has to contain the small momentum or long-range terms. In the approximation of small momentum (long wavelength) the mapping of the interaction Hamiltonian in the magnetic field into the interaction Hamiltonian on the lattice was obtained. By construction, the time reversal symmetry of the lattice model was explicitly broken. In the absence of the external magnetic field symmetry was broken by the presence of complex-valued interaction terms in Hamiltonian. Since the mapping originates from the quantum Hall system, it allowed to identify the lattice Hamiltonians, ground states of which should be the gapped fractionalized quantum Hall liquids. It was also shown that the periodic potential, that can be crated by the ion lattice, in the quantum Hall systems is mapped into the the nearest neighbor hopping in the lattice model. Obtained mapping can be used to create lattice models of the continuous system, and hence it allows one to use all the numerical methods, that were developed on lattice, for the continuous systems.

# Bibliography


[1] I. Panfilov, A. A. Burkov, and D. A. Pesin Phys. Rev. B **89**, 245103 (2014).

[2] I. Panfilov, A. Patri, Kun Yang, and A. A. Burkov Phys. Rev. B **93**, 125126 (2016).

[3] P. Drude, Annalen der Physic **1**, 566 (1900).

[4] K.v. Klitzing, G. Dorda, M. Pepper, Phys. Rev. Lett. **45**, 494 (1980).

[5] R. B. Laughlin Phys. Rev. B **23** 5632 (1981).

[6] Pankratov, O.A.; Pakhomov, S.V.; Volkov, B.A. Solid State Communications. **61** (2): 93–96. (1987).

[7] König, Markus; Wiedmann, Steffen; Brüne, Christoph; Roth, Andreas; Buhmann, Hartmut; Molenkamp, Laurens W.; Qi, Xiao-Liang; Zhang, Shou-Cheng (2007-11-02). "Quantum Spin Hall Insulator State in HgTe Quantum Wells". Science. **318** (5851): 766–770.

[8] X. Wan, A.M. Turner, A. Vishwanath, and S.Y. Savrasov, Phys. Rev. B **83**, 205101 (2011).

[9] K.-Y. Yang, Y.-M. Lu, and Y. Ran, Phys. Rev. B **84**, 075129 (2011).

[10] A.A. Burkov and L. Balents, Phys. Rev. Lett. **107**, 127205 (2011).

[11] G. Xu, H.-M. Weng, Z.-J. Wang, X. Dai, and Z. Fang, Phys. Rev. Lett. **107**, 186806 (2011).

[12] S.-Y. Xu, I. Belopolski, N. Alidoust, M. Neupane, G. Bian, C. Zhang, R. Sankar, G. Chang, Z. Yuan, C.-C. Lee, S.- M. Huang, H. Zheng, J. Ma, D. S. Sanchez, B. Wang, A. Bansil, F. Chou, P. P. Shibayev, H. Lin, S. Jia, and M. Z. Hasan, Science **349**, 613 (2015).

[13] B. Q. Lv, H. M. Weng, B. B. Fu, X. P. Wang, H. Miao, J. Ma, P. Richard, X. C. Huang, L. X. Zhao, G. F. Chen, Z. Fang, X. Dai, T. Qian, and H. Ding, Phys. Rev. X **5**, 031013 (2015).

[14] L. Huang, T. M. McCormick, M. Ochi, Z. Zhao, M.- t. Suzuki, R. Arita, Y. Wu, D. Mou, H. Cao, J. Yan, N. Trivedi, and A. Kaminski, ArXiv e-prints (2016), arXiv:1603.06482 [cond-mat.mes-hall].

[15] D. C. Tsui, H. L. Stormer and A. C. Gossard, Phys. Rev. Lett. **48**, 1559 (1982).

[16] F.D.M. Haldane, Phys. Rev Lett. **93**, 206602 (2004).

[17] F.D.M. Haldane, Phys. Rev Lett. **61**, 2015 (1988).

[18] K. S. Novoselov, A. K. Geim, S. V. Morozov, D. Jiang, M. I. Katsnelson, I. V. Grigorieva, S. V. Dubonos, A. A. Firsov, Nature **438** 197 (2005).

[19] C. L. Kane and E. J. Mele, Phys. Rev. Lett. **95**, 146802 (2005).

[20] C. L. Kane and E. J. Mele, Phys. Rev. Lett. **95**, 226801 (2005).

[21] C. Herring, Phys. Rev. **52**, 365 (1937).

[22] R. Yu et al., Science **329**, 61 (2010).

[23] S.M. Young, S. Zaheer, J.C.Y. Teo, C.L. Kane, and E.J. Mele, Phys. Rev. Lett. **108**, 140405 (2012).

[24] Z.-J. Wang, Y. Sun, X.-Q. Chen, C. Franchini, G. Xu, H.-M. Weng, X. Dai, and Z. Fang, Phys. Rev. B **85**, 195320 (2012).

[25] Z.J. Wang, H.-M. Weng, Q.-S. Wu, X. Dai, and Z. Fang, Phys. Rev. B **88**, 125427 (2013).

[26] S. Borisenko, Q. Gibson, D. Evtushinsky, V. Zabolotnyy, B. Büchner, and R.J. Cava, arXiv:1309.7978 (unpublished).

[27] Z.K. Liu, B. Zhou, Z.J. Wang, H.M. Weng, D. Prabhakaran, S.-K. Mo, Y. Zhang, Z.X. Shen, Z. Fang, X. Dai, Z. Hussain, and Y.L. Chen, arXiv:1310.0391 (unpublished).

[28] M. Neupane, S.-Y. Xu, R. Sankar, N. Alidoust, G. Bian, C. Liu, I. Belopolski, T.-R. Chang, H.-T. Jeng, H. Lin, A. Bansil, F. Chou, and M.Z. Hasan, arXiv:1309.7892 (unpublished).

[29] H.B. Nielsen and M. Ninomiya, Phys. Lett. B **130**, 389 (1983).

[30] G.E. Volovik, *The Universe in a Helium Droplet* (Clarendon Press, Oxford, 2003); Lect. Notes Phys. **718**, 31 (2007).

[31] V. Aji, Phys. Rev. B **85**, 241101 (2012).

[32] D.T. Son and N. Yamamoto, Phys. Rev. Lett. **109**, 181602 (2012).

[33] A.A. Zyuzin and A.A. Burkov, Phys. Rev. B **86**, 115133 (2012).

[34] D.T. Son and B.Z. Spivak, Phys. Rev. B **88**, 104412 (2013).

[35] A.G. Grushin, Phys. Rev. D **86**, 045001 (2012).

[36] P. Goswami and S. Tewari, Phys Rev. B **88**, 245107 (2013).

[37] P. Hosur and X.-L. Qi, C. R. Physique **14**, 857 (2013).

[38] S. Adler, Phys. Rev. **177**, 2426 (1969).

[39] J.S. Bell and R. Jackiw, Nuovo Cimento **60A**, 4 (1969).

[40] S. Ryu, J.E. Moore, and A.W.W. Ludwig, Phys. Rev. B **85**, 045104 (2012).

[41] A. Furusaki, N. Nagaosa, K. Nomura, S. Ryu, and T. Takayanagi, arXiv:1211.0533 (unpublished).

[42] X.-G. Wen, arXiv:1303.1803 (unpublished).

[43] C.-X. Liu, P. Ye, X.-L. Qi, Phys. Rev. B **87**, 235306 (2013).

[44] S.A. Parameswaran, T. Grover, D.A. Abanin, D.A. Pesin, and A. Vishwanath, arXiv:1306.1234 (unpublished).

[45] N. Nagaosa, Quantum Field Theory in Condensed Matter Physics, Springer (1999).

[46] P. Streda, J. Phys. C **15**, L717 (1982).

[47] D. Xiao, J. Shi, and Q. Niu, Phys. Rev. Lett. **95**, 137204 (2005).

[48] A.A. Zyuzin, S. Wu, and A.A. Burkov, Phys. Rev. B **85**, 165110 (2012).

[49] A.A. Burkov, Phys. Rev. B **89**, 155104 (2014).

[50] Z. Huang, D.P. Arovas, and A.V. Balatsky, New J. Phys. **15**, 123019 (2013).

[51] G.B. Halasz and L. Balents, Phys. Rev. B **85**, 035103 (2012).

[52] M. Z. Hasan and C. L. Kane, Rev. Mod. Phys. **82**, 3045 (2010).

[53] X.-L. Qi and S.-C. Zhang, Rev. Mod. Phys. **83**, 1057 (2011).

[54] C.-K. Chiu, J. C. Y. Teo, A. P. Schnyder, and S. Ryu, ArXiv e-prints (2015), arXiv:1505.03535 [cond-mat.meshall].

[55] V. Kalmeyer and R. B. Laughlin, Phys. Rev. Lett. **59**, 2095 (1987).

[56] G. Baskaran, Z. Zou, and P. Anderson, Solid State Communications **63**, 973 (1987).

[57] L. Balents, Nature **464**, 199 (2010).

[58] D. Pesin and L. Balents, Nat Phys **6**, 376 (2010).

[59] D. N. Sheng, Z.-C. Gu, K. Sun, and L. Sheng, Nat Commun **2**, 389 (2011).

[60] T. Neupert, L. Santos, C. Chamon, and C. Mudry, Phys. Rev. Lett. **106**, 236804 (2011).

[61] N. Regnault and B. A. Bernevig, Phys. Rev. X **1**, 021014 (2011).

[62] K. Sun, Z. Gu, H. Katsura, and S. Das Sarma, Phys. Rev. Lett. **106**, 236803 (2011).

[63] E. Tang, J.-W. Mei, and X.-G.Wen, Phys. Rev. Lett. **106**, 236802 (2011).

[64] X. Hu, M. Kargarian, and G. A. Fiete, Phys. Rev. B **84**, 155116 (2011).

[65] S. A. Parameswaran, R. Roy, and S. L. Sondhi, Phys. Rev. B **85**, 241308 (2012).

[66] Y.-L. Wu, B. A. Bernevig, and N. Regnault, Phys. Rev. B **85**, 075116 (2012).

[67] Y.-F. Wang, H. Yao, Z.-C. Gu, C.-D. Gong, and D. N. Sheng, Phys. Rev. Lett. **108**, 126805 (2012).

[68] R. Roy, Phys. Rev. B **90**, 165139 (2014).

[69] J. W. F. Venderbos, S. Kourtis, J. van den Brink, and M. Daghofer, Phys. Rev. Lett. **108**, 126405 (2012).

[70] Y.-F. Wang, Z.-C. Gu, C.-D. Gong, and D. N. Sheng, Phys. Rev. Lett. **107**, 146803 (2011).

[71] T. Neupert, L. Santos, S. Ryu, C. Chamon, and C. Mudry, Phys. Rev. B **84**, 165107 (2011).

[72] G. Murthy and R. Shankar, Phys. Rev. B **86**, 195146 (2012).

[73] Y.-H.Wu, J. K. Jain, and K. Sun, Phys. Rev. B **86**, 165129 (2012).

[74] Z. Liu, E. J. Bergholtz, H. Fan, and A. M. Läuchli, Phys. Rev. Lett. **109**, 186805 (2012).

[75] A. G. Grushin, T. Neupert, C. Chamon, and C. Mudry, Phys. Rev. B **86**, 205125 (2012).

[76] X.-L. Qi, Phys. Rev. Lett. **107**, 126803 (2011).

[77] Y.-L. Wu, N. Regnault, and B. A. Bernevig, Phys. Rev. B **86**, 085129 (2012).

[78] T. Scaffidi and G. Möller, Phys. Rev. Lett. **109**, 246805 (2012).

[79] C.-M. Jian and X.-L. Qi, Phys. Rev. B **88**, 165134 (2013).

[80] M. Claassen, C. H. Lee, R. Thomale, X.-L. Qi, and T. P. Devereaux, Phys. Rev. Lett. **114**, 236802 (2015).

[81] O. I. Motrunich and M. P. A. Fisher, Phys. Rev. B **75**, 235116 (2007).

[82] D. N. Sheng, O. I. Motrunich, S. Trebst, E. Gull, and M. P. A. Fisher, Phys. Rev. B **78**, 054520 (2008).

[83] I. Bloch, Nat Phys **1**, 23 (2005).

[84] A. A. Burkov, Phys. Rev. B **81**, 125111 (2010).

[85] E. I. Rashba, L. E. Zhukov, and A. L. Efros, Phys. Rev. B **55**, 5306 (1997).

[86] D. J. Thouless, J. Phys. C: Solid State Phys. **17**, L325 (1984).

[87] A. M. Perelomov, Teor. Mat. Phys. **6**, 213 (1971).

[88] S. M. Girvin, A. H. MacDonald, and P. M. Platzman, Phys. Rev. B **33**, 2481 (1986).

[89] S. He, F. C. Zhang, X. C. Xie, and S. Das Sarma, Phys. Rev. B **42**, 11376 (1990).

[90] X. G. Wen, F. Wilczek, and A. Zee, Phys. Rev. B **39**, 11413 (1989).

[91] K. Yang, L. K. Warman, and S. M. Girvin, Phys. Rev. Lett. **70**, 2641 (1993).

[92] A. Seidel, H. Fu, D.-H. Lee, J. M. Leinaas, and J. Moore, Phys. Rev. Lett. **95**, 266405 (2005).

[93] H. Yao and S. A. Kivelson, Phys. Rev. Lett. **99**, 247203 (2007).

[94] D. F. Schroeter, E. Kapit, R. Thomale, and M. Greiter, Phys. Rev. Lett. **99**, 097202 (2007).

[95] B. Bauer, L. Cincio, B. P. Keller, M. Dol

, G. Vidal, S. Trebst, and A. W. W. Ludwig, Nat Commun **5**, 5137 (2014).

[96] Y.-C. He, D. N. Sheng, and Y. Chen, Phys. Rev. Lett. **112**, 137202 (2014).

[97] W. Zhu, S. S. Gong, and D. N. Sheng, Phys. Rev. B **92**, 014424 (2015).

[98] S.-S. Gong, W. Zhu, L. Balents, and D. N. Sheng, Phys. Rev. B **91**, 075112 (2015).

[99] Y.-C. He and Y. Chen, Phys. Rev. Lett. **114**, 037201 (2015).

[100] Y.-C. He, S. Bhattacharjee, F. Pollmann, and R. Moessner, Phys. Rev. Lett. **115**, 267209 (2015).

[101] S. Bieri, L. Messio, B. Bernu, and C. Lhuillier, Phys. Rev. B **92**, 060407 (2015).

[102] Y.-C. He, S. Bhattacharjee, R. Moessner, and F. Pollmann, Phys. Rev. Lett. **115**, 116803 (2015).